



Hui Yu (余晖), Ph.D.
Shanghai Typhoon Institute/CMA, Director.
WMO/WWRP Working Group on Tropical Meteorological Research,
Member
Tropical Cyclone Research and Review, Deputy-chief-editor

Research interests

Tropical cyclone track, intensity, and structure change

Tropical cyclone prediction techniques

Tropical cyclone climatology and disaster risk assessment

Email address: yuh@typhoon.org.cn

Tel: 86-21-54896309

THE SENIOR MANAGEMENT AND OPERATION COURSE ON TROPICAL CYCLONE MONITORING AND FORECASTING
(20 November to 1 December 2023, Guangzhou, China)

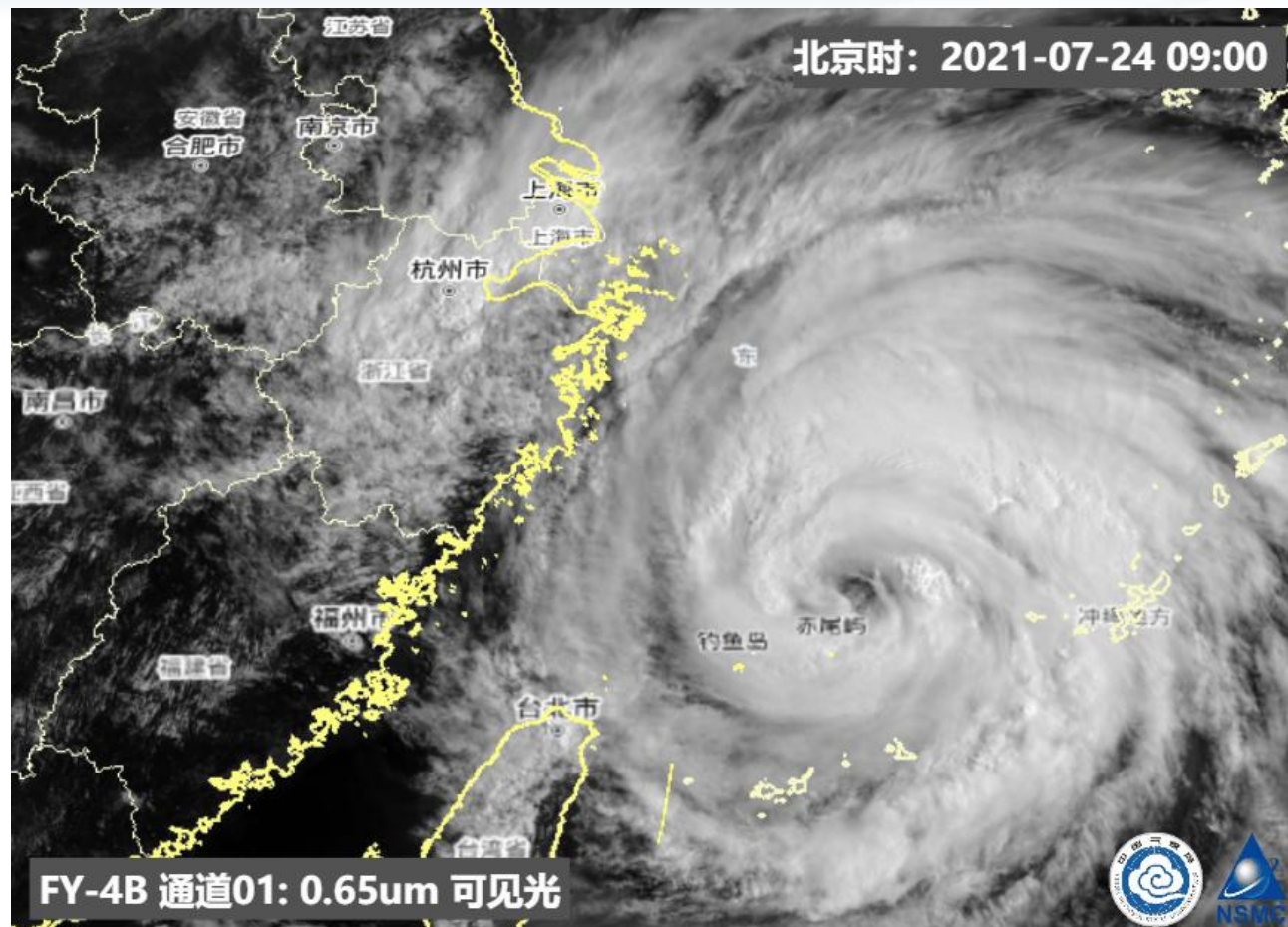
Tropical Cyclone Gale Monitoring and Forecasting Technology

Hui YU
Shanghai Typhoon Institute/CMA



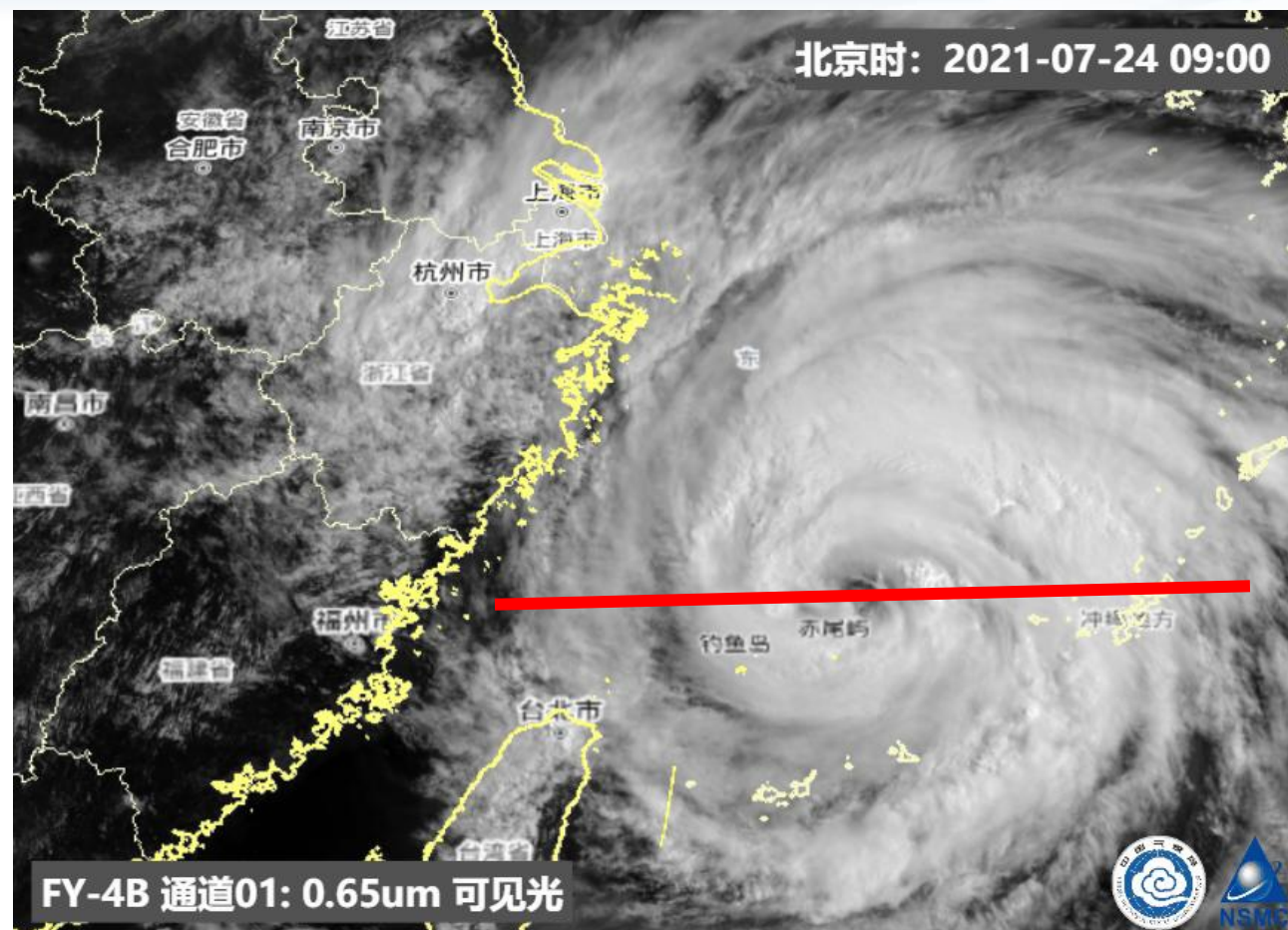
Outline

- **Surface wind structure of tropical cyclones and a parametric wind field model for tropical cyclones**
- **Tropical cyclone intensity and size estimation techniques based on satellite observations**
- **Tropical cyclone gale forecast techniques**



Vmax: 38m/s
Pmin: 965hPa

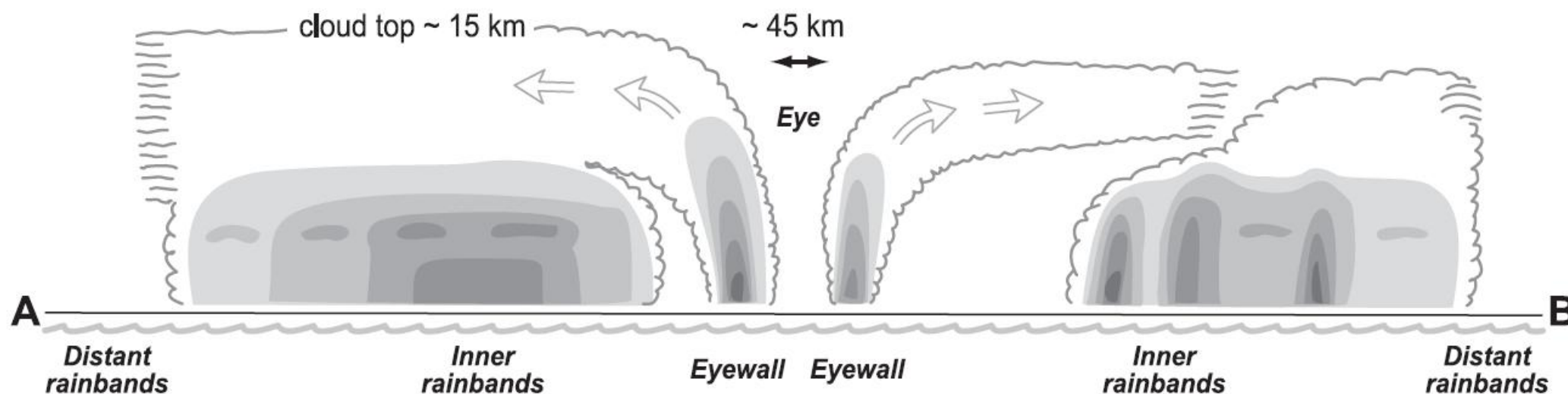
Visible image of typhoon In-fa (2021) from the satellite FengYun-4B, when the typhoon approached the coast of East China



Make a cross-section through the center of the typhoon as shown by this red line.

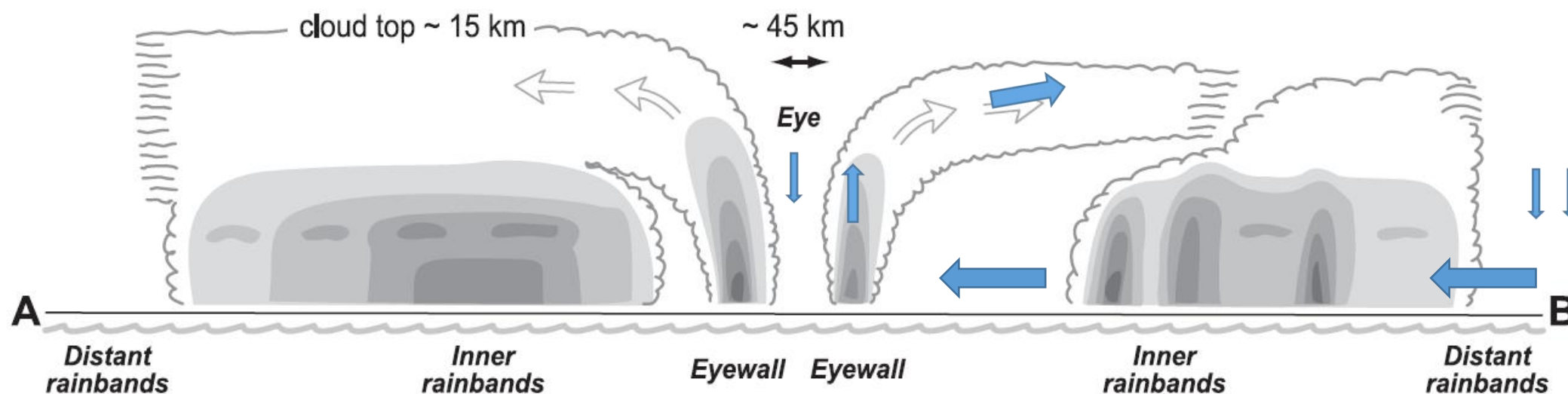
Visible image of typhoon In-fa (2021) from the satellite FengYun-4B, when the typhoon approached the coast of East China

Idealized vertical structure of a tropical cyclone

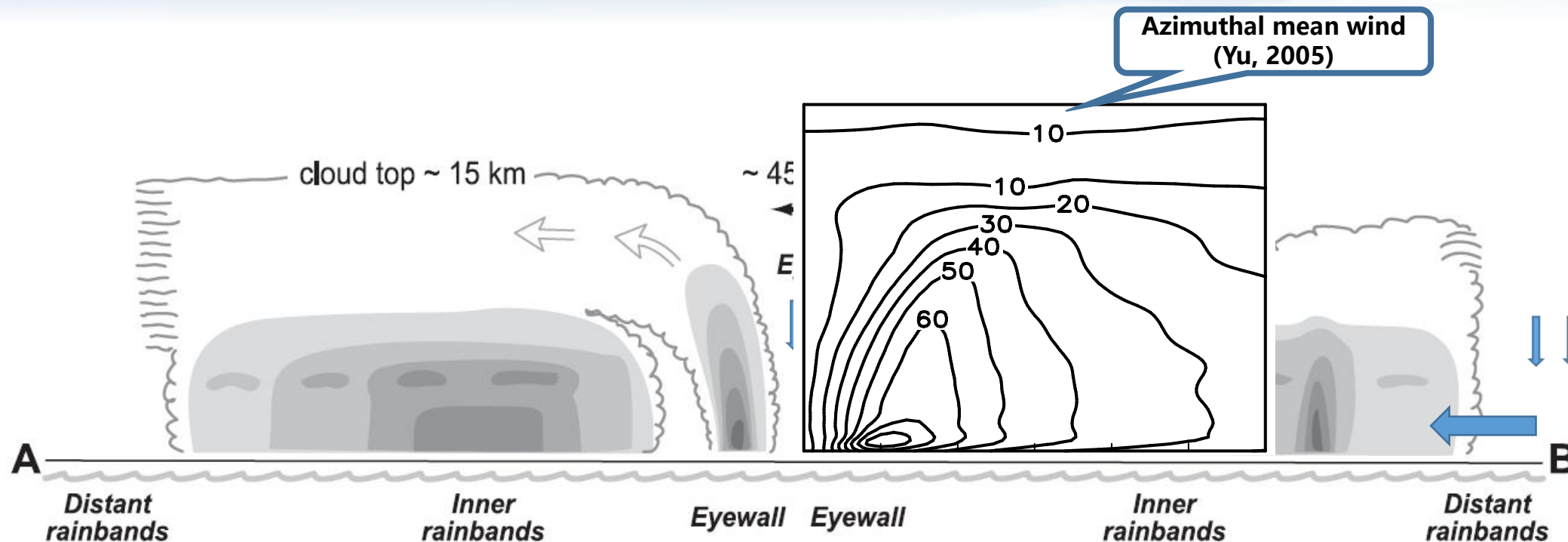


Scalloped region represents the cloud boundary of the convective features in a TC. The shading is for threshold values of 25, 30, 35, 37.5, 40, and 45 dBZ in radar reflectivity. The open arrows represent the flow of ice outward from the eyewall region. (Hence and Houze, 2012)

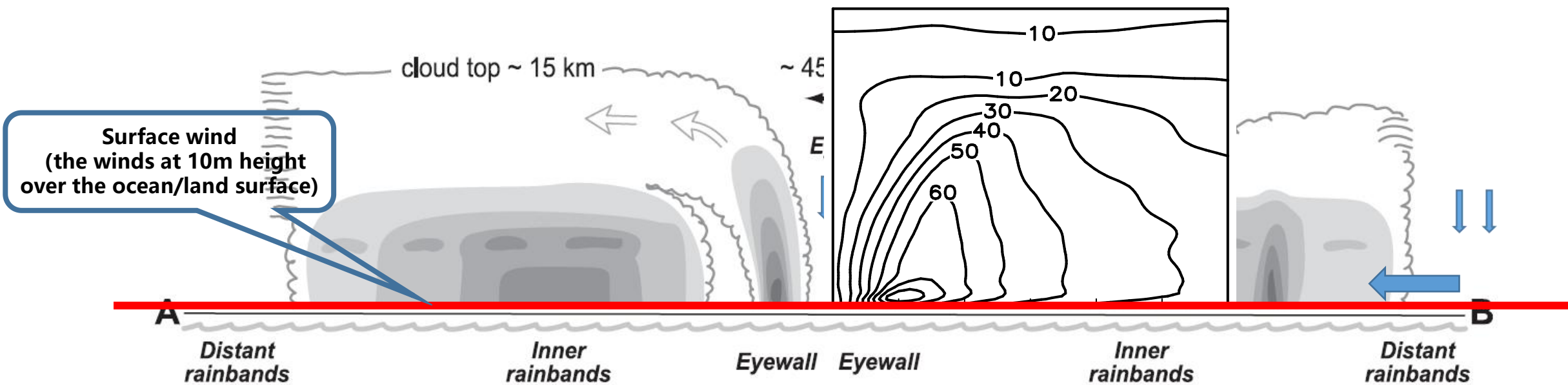
Idealized vertical structure of a tropical cyclone

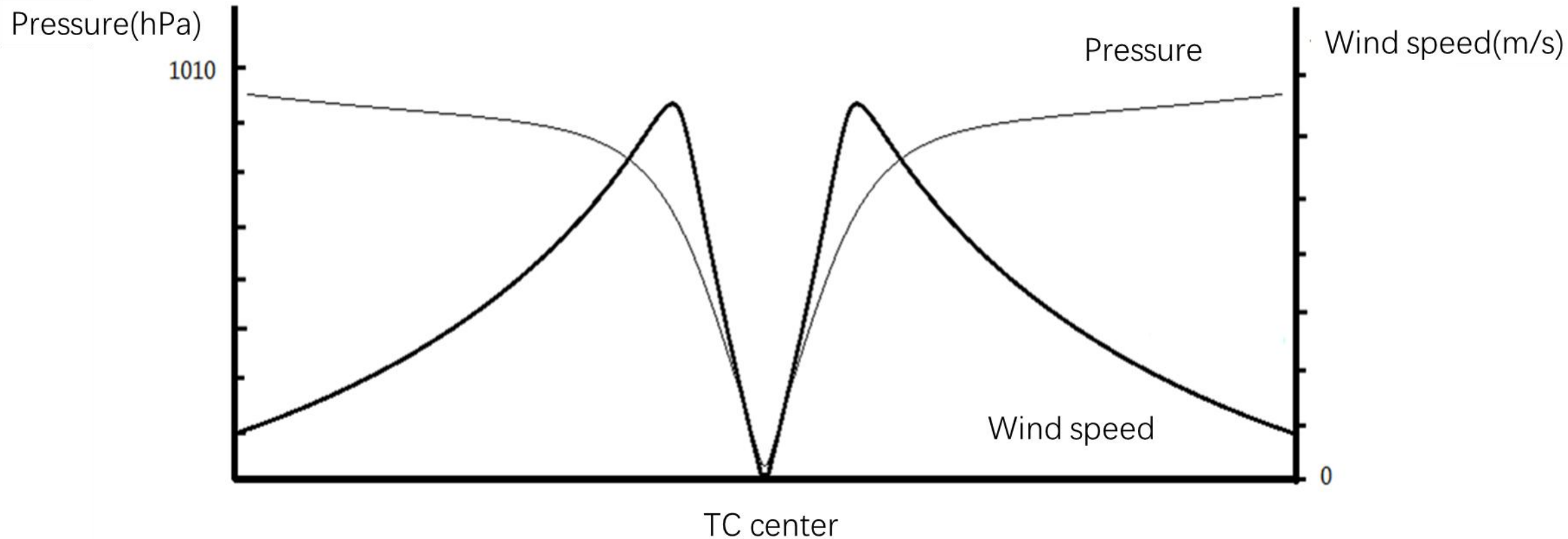


The convective features are accompanied by a vertical circulation with inflow at lower levels and outflow at upper levels. There are compensated descending motion of the air in both the eye region and also the outer region away from the center.

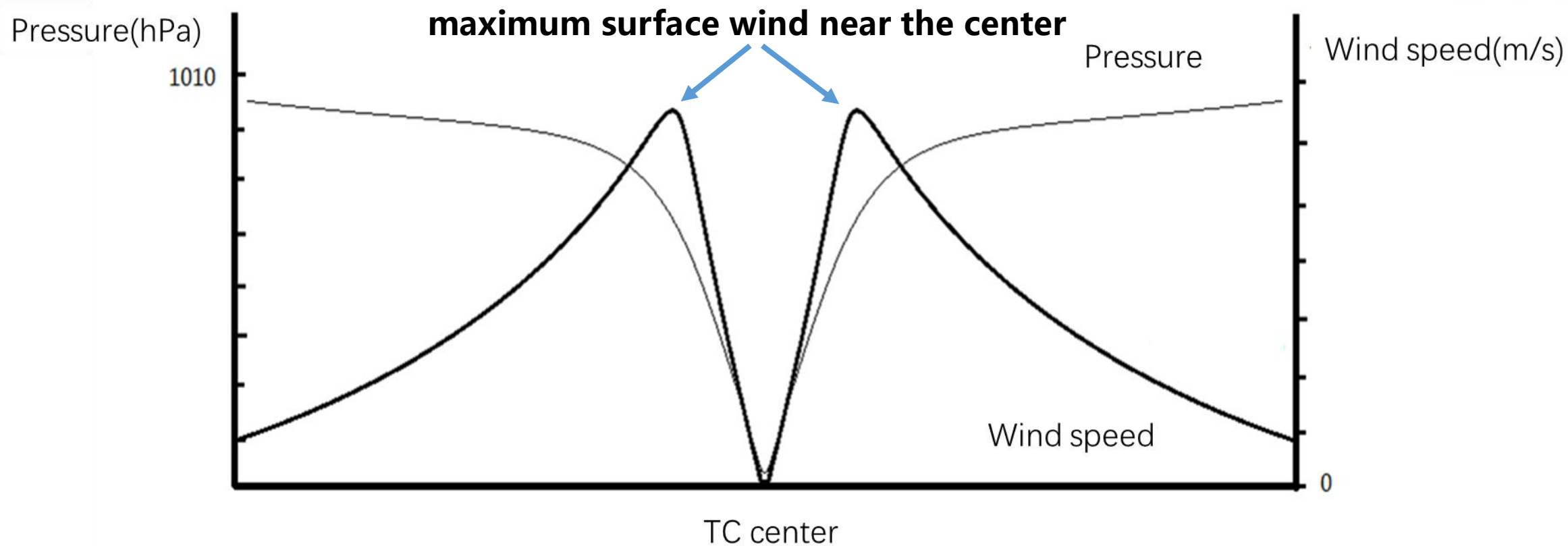


The primary circulation of the tropical cyclone generally has maximum azimuthal mean wind in the planetary boundary layer, which is anti-clockwise in northern hemisphere and clockwise in southern hemisphere. It gets weakened gradually upward as shown in this azimuthal mean wind chart.



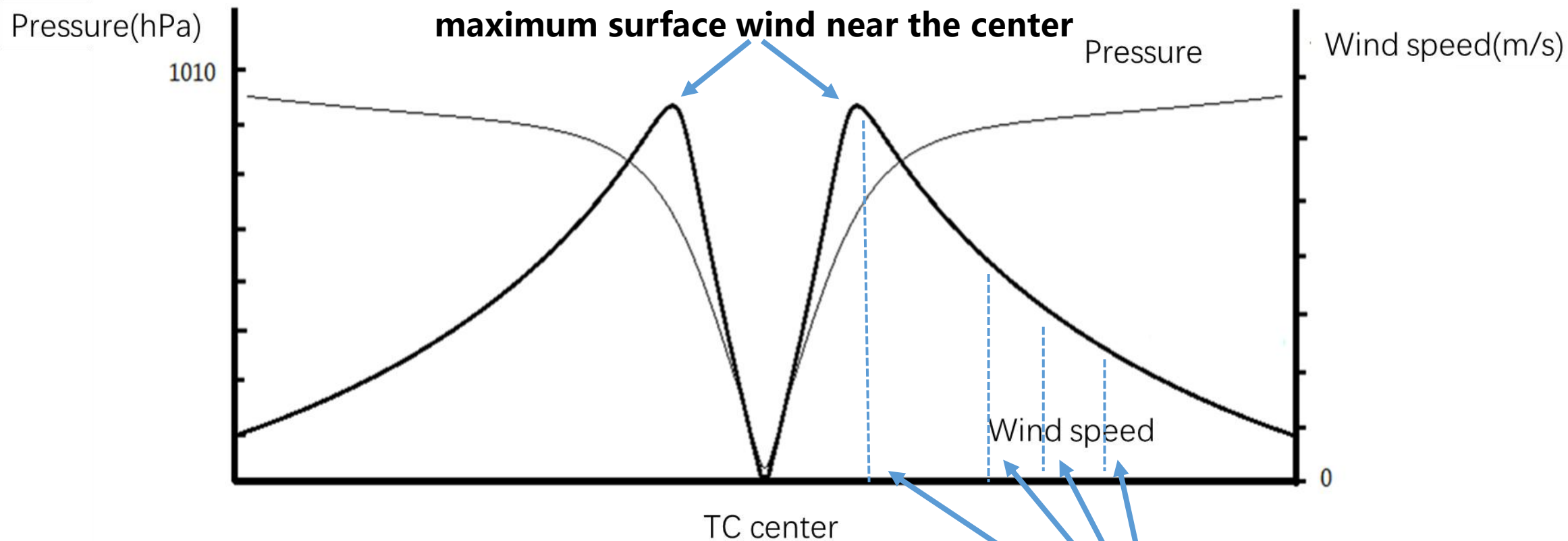


Schematic chart of the radial distribution of surface wind speed and pressure in a tropical cyclone



Pressure distribution: V-shape

The maximum winds appear at the radius with largest pressure gradient.

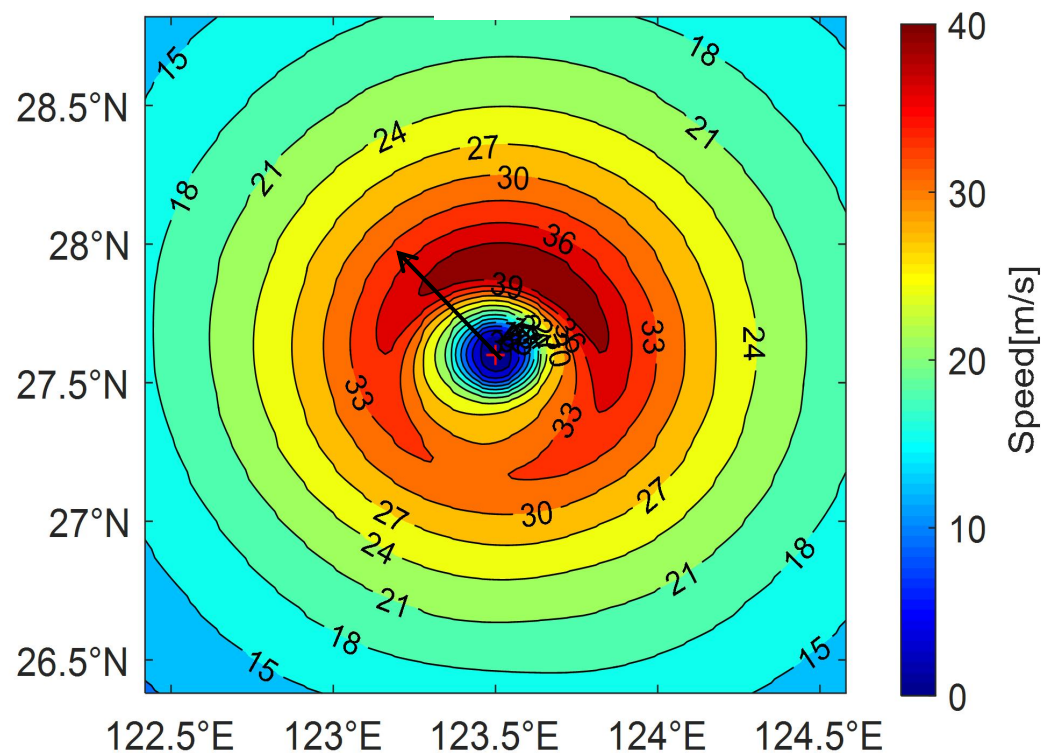


Except for the maximum wind speed, several characteristic wind radii are also adopted in order to describe the surface wind structure in a more quantitative and vivid way.

Wind radii: R_{max} , R_{34} , R_{50} , R_{64}

Notable wavenumber 1 asymmetric structure: the winds are stronger to the front-right of the storm path than to the rear-left.

Such an asymmetric structure is generally a result of the movement of the storm.

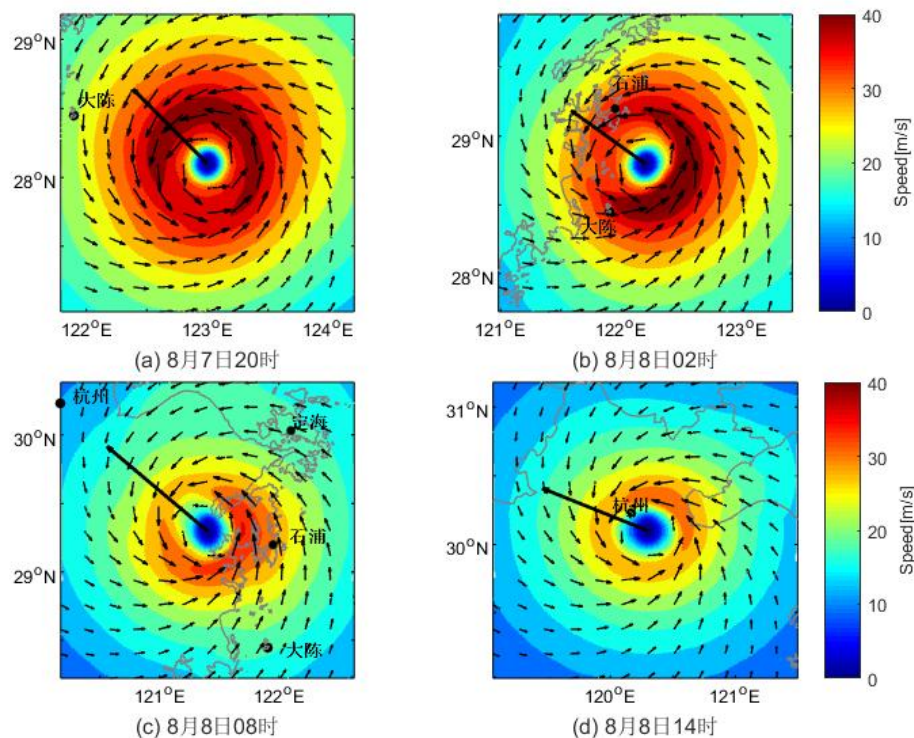


Surface wind of an idealized TC moving toward NW over the ocean (Ye, 2017)



Characteristic wind radii of a typhoon approaching the coast of East China

When a tropical cyclone is affected by land, the winds generally weaken significantly on the side near the land.



Surface wind of a TC during the landfall process: the shift of maximum wind from the front-right quadrant to the rear part of the storm (Ye, 2017)



Characteristic wind radii of a typhoon making landfall on the coast of South China



A parametric wind field model of tropical cyclone: Shanghai Typhoon Institute Engineering Typhoon Model (STI-ETYM)

(Developed to supply guidance for the prompt assessment of risks and impacts that arise from the significant high-speed winds in TCs.)



Parametric wind field model

Gained popularity for their satisfactory modeling accuracy with **limited TC parameters (location, intensity) as inputs**

- **Pressure model**

Holland (1980, 2008)

Willoughby (1995, 2006)

- **Wind field model:** Batts, Shapiro, CE, Yan Meng, Vickery

Gradient model

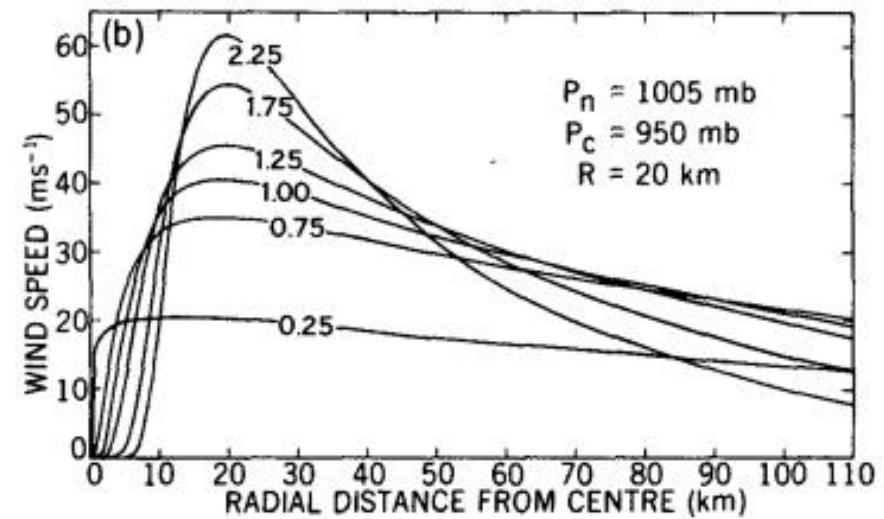
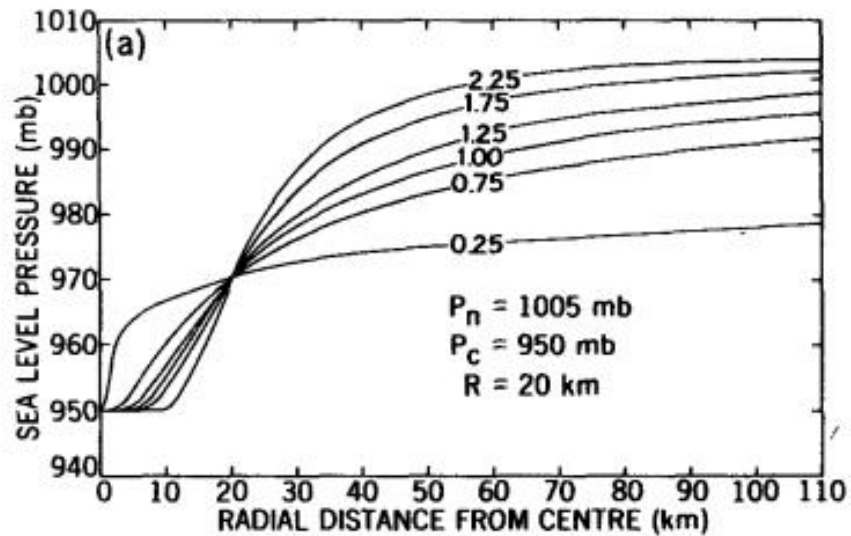
Momentum model vertically averaged in boundary layer

- **Planetary boundary layer (PBL) model:** (U10/U)

Compared with the atmospheric numerical models which account for the dynamic and thermodynamic processes comprehensively, the parametric wind field model is much simpler and can better meet the requirement to simulate several millions of virtual typhoons needed for hazard assessment.

Pressure model

$$p_c(r) = p_0 + \Delta p \exp \left[- \left(\frac{R_{\max}}{r} \right)^B \right]$$



Holland, 1980



Wind field model

Balance	Models	Characteristic	Methods	Applicability
Gradient	Batts (1980)	empirical	/	slowly, symmetric TC
	Shapiro (1984)	symmetric pressure	truncated spectral formulation	fast, symmetric TC
Momentum	Yan Meng (1995)	friction velocity	perturbation analysis	symmetric TC after landing
	CE (1992) Vickery(2000)	asymmetric pressure	finite difference	all, especially asymmetric TC

Vickery et al. 2000; Peng et al. 2005



Wind field model

Based on Chow(1971), Cardone et al.(1992) solved the Navier-Stokes equations by finite difference method, and the model was applied by the US Army Corps of Engineers(CE).

$$\frac{d\vec{V}}{dt} + f \vec{K} \times (\vec{V} - \vec{V}_g) = -\frac{1}{\rho} \nabla p_c + \nabla \cdot (K_H \nabla \cdot \vec{V}) - \frac{C_D}{h} |\vec{V} + \vec{V}_c| (\vec{V} + \vec{V}_c)$$

Momentum balance equation for PBL:

pressure gradient force, Coriolis force, viscosity force, surface drag force

\vec{V} vertical mean wind in PBL

\vec{V}_g environmental gradient wind

P_c central pressure

K_H eddy viscosity coefficient

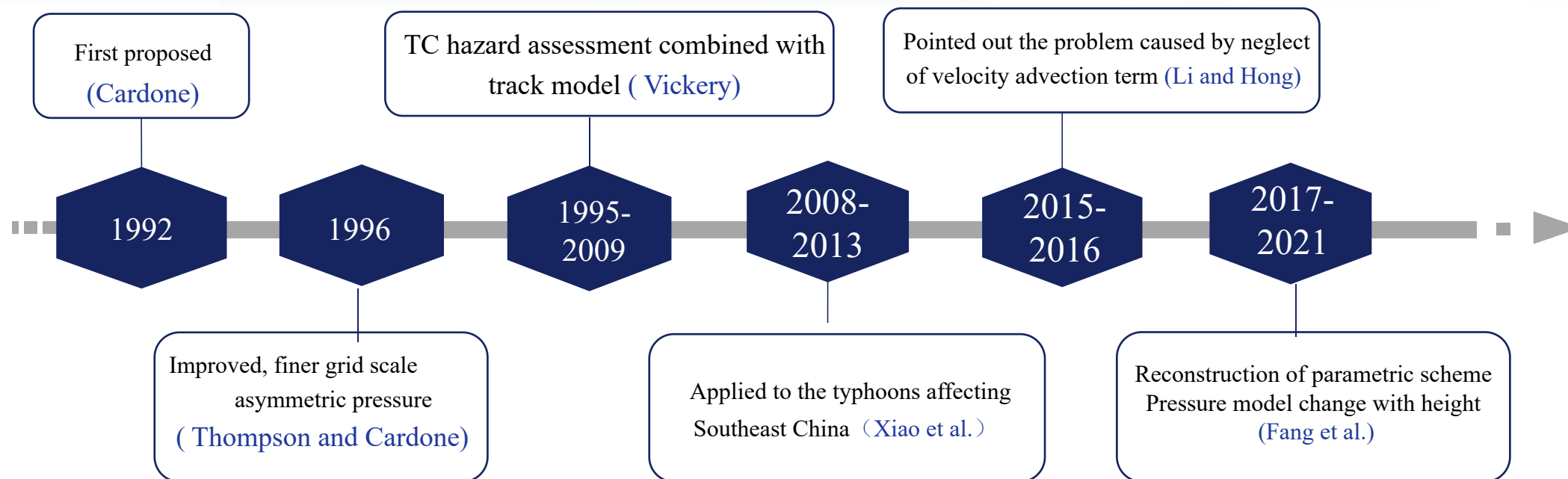
C_D drag coefficient

h PBL height

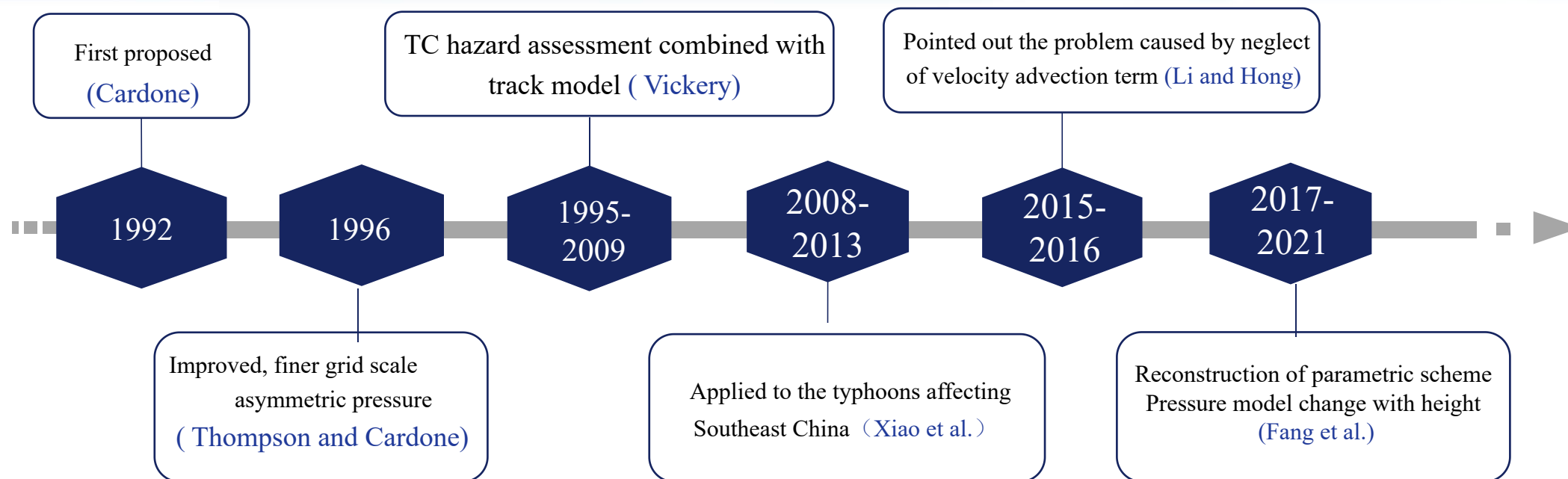
\vec{V}_c moving velocity of TC



Wind field model

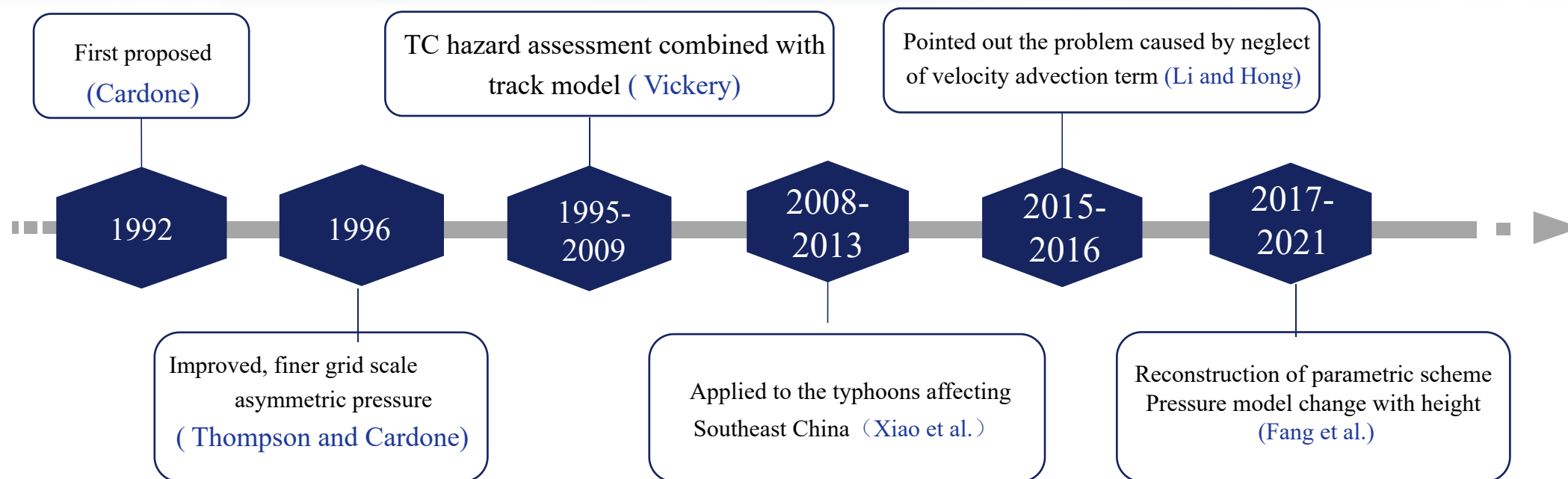


Wind field model



Li and Hong (2015): neglecting the effect of typhoon movement on circulation not only underestimate the maximum wind speeds, but also affect the location of the maximum wind speeds in the simulated wind field, thereby affecting the estimation of the return-period wind speeds at a given location.

Wind field model



Fang et al. (2020): proposed a pressure-field model considering the altitude change, which was then included in a height-dependent parametric wind field model considering roughness change.

PBL model

The PBL model was generally defined as the reduction ratio of the winds at the gradient level to those at 10 m above the underlying surface.

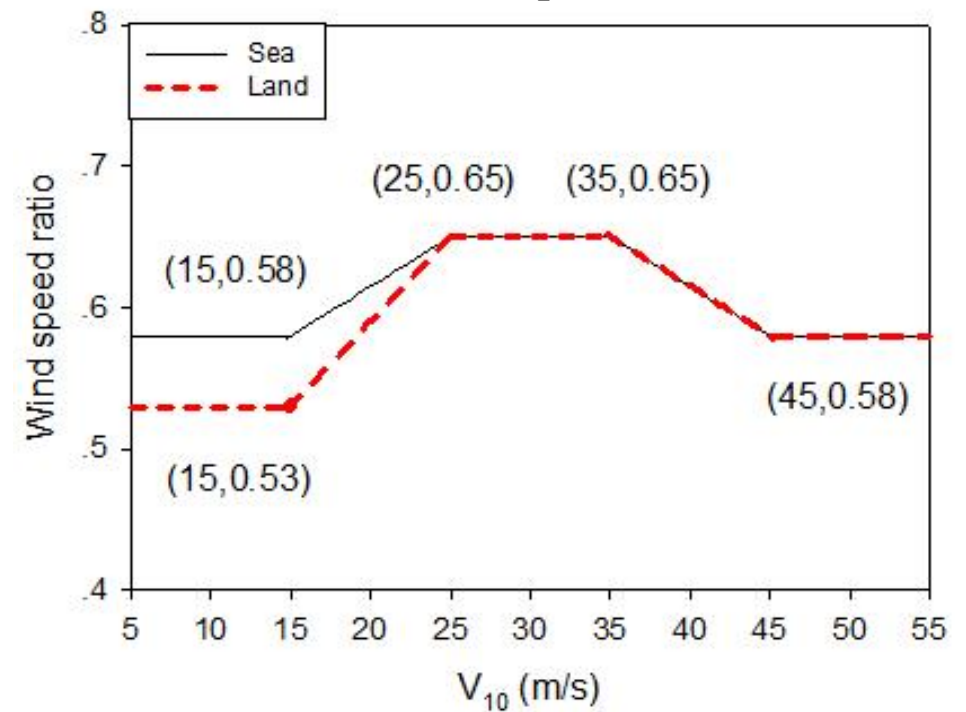
Table 1

Example model values of V_{10}/V_G and sea-land wind speed reductions.

Source	V_{10}/V_G over water (near eyewall)	Sea-land transition (% reduction of mean wind speed at 10 m)
Schwerdt et al. (1979)	0.95 (PMH) 0.90 (SPH)	11%, at coast 22%, 19 km inland
Batts et al. (1980)	0.865	15%, at the coast
Georgiou (1985)	0.825 $r < 2RMW$ 0.75 $r > 5RMW$	0%, at coast 25%, 50 km inland
Vickery et al. (2000a, 2000b)	~0.70–0.72	14–20%, at the coast 23–28%, 50 km inland
Sparks and Huang (2001)	0.65	30%, a few km inland
Powell et al. (2005)	~0.73	15–20%, at the coast
Powell et al. (2003)	~0.71	N/A
Vickery et al. (2009b)	~0.71 (varies from 0.67 to 0.74)	18–20%, at the coast

Vickery et al., 2009

Variation in wind speed reduction ratio with
wind speed



Fang et al., 2020



Key parameters in the parametric surface wind model

Pressure model: $p_c(r) = p_0 + \Delta p \exp \left[- \left(\frac{R_{\max}}{r} \right)^B \right]$ ---- **Holland et al., 2008**

Radius of maximum wind speed

Holland B parameter

Pressure difference between
TC center and environment

Wind field model: $\frac{d\vec{V}}{dt} = -f \vec{K} \times (\vec{V} - \vec{V}_g) - \frac{1}{\rho} \nabla p_c + \nabla \cdot (K_H \nabla \cdot \vec{V}) - \frac{C_D}{h} |\vec{V} + \vec{V}_c| (\vec{V} + \vec{V}_c)$

---- **Chow, 1971**

Drag coefficient

Environmental geostrophic wind

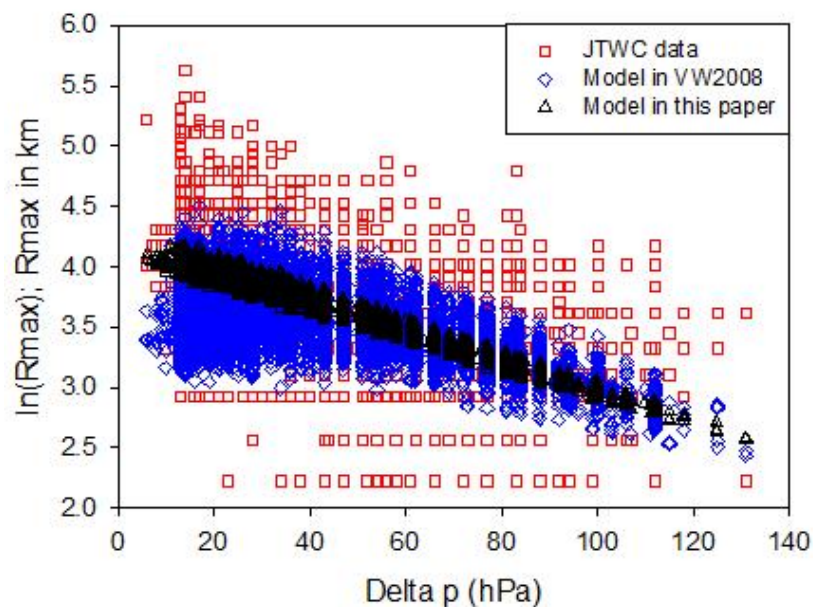
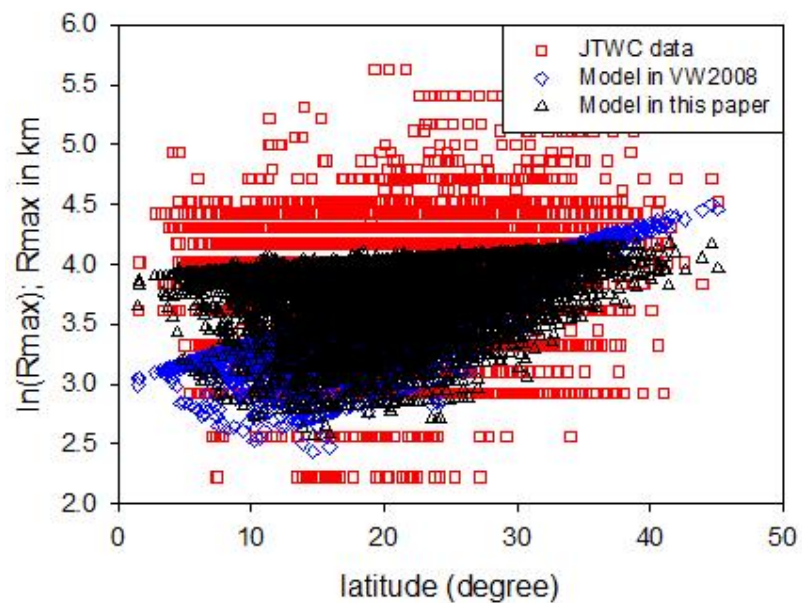
Height of boundary layer

PBL model: Wind speed ratio (U10/U)

Key parameters in the parametric surface wind model

(1) R_{\max}

$$\ln(R_{\max}) = 4.0441 - 1.2090 \times 10^{-2} \Delta p + 7.2694 \times 10^{-3} \Psi$$

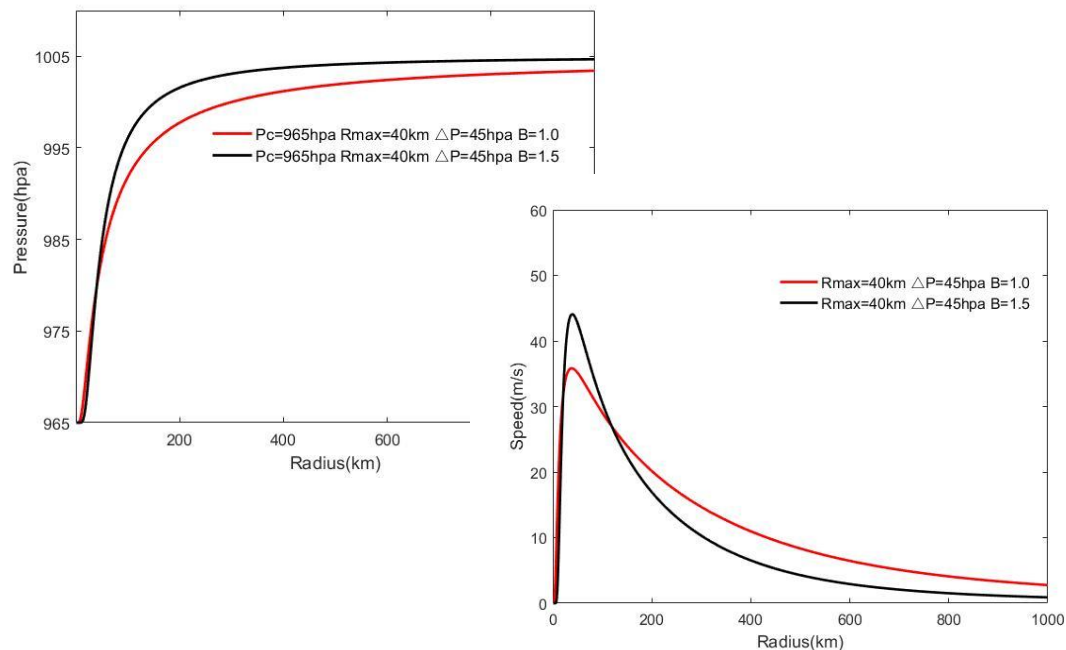


Relationship between R_{\max} and latitude (left) and ΔP (right)

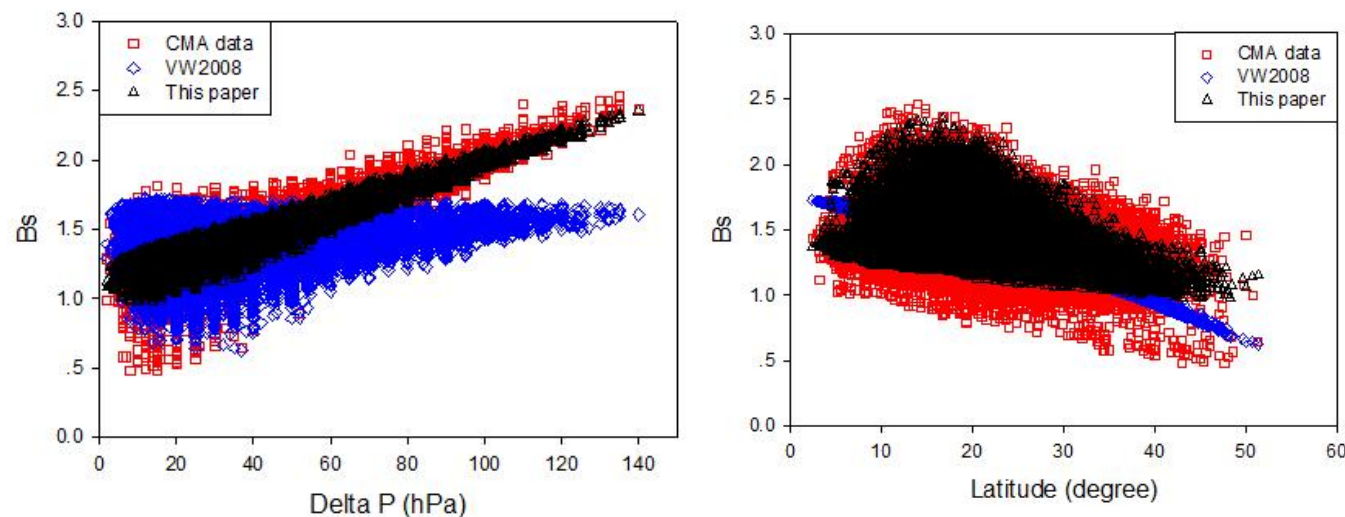
Key parameters in the parametric surface wind model

(2) Holland B parameter

$$Bs = 1.2858 + 8.6396 \times 10^{-3} \Delta p - 8.7745 \times 10^{-3} \Psi$$



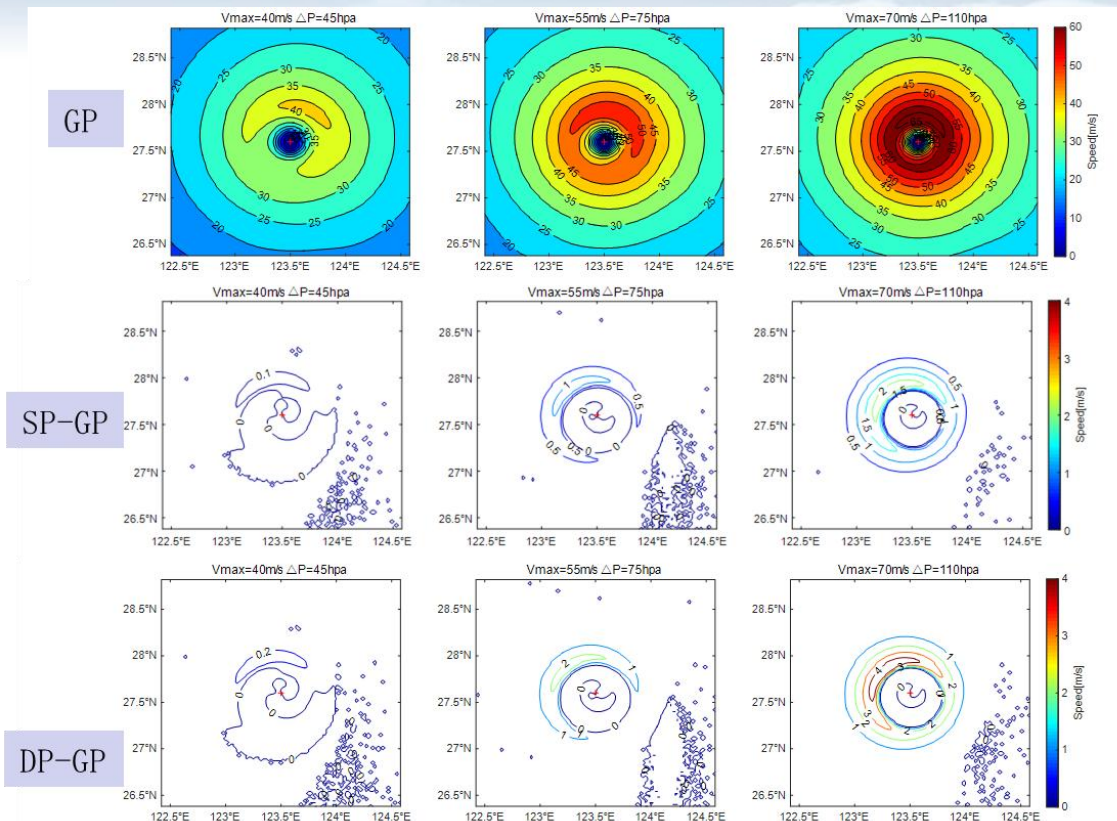
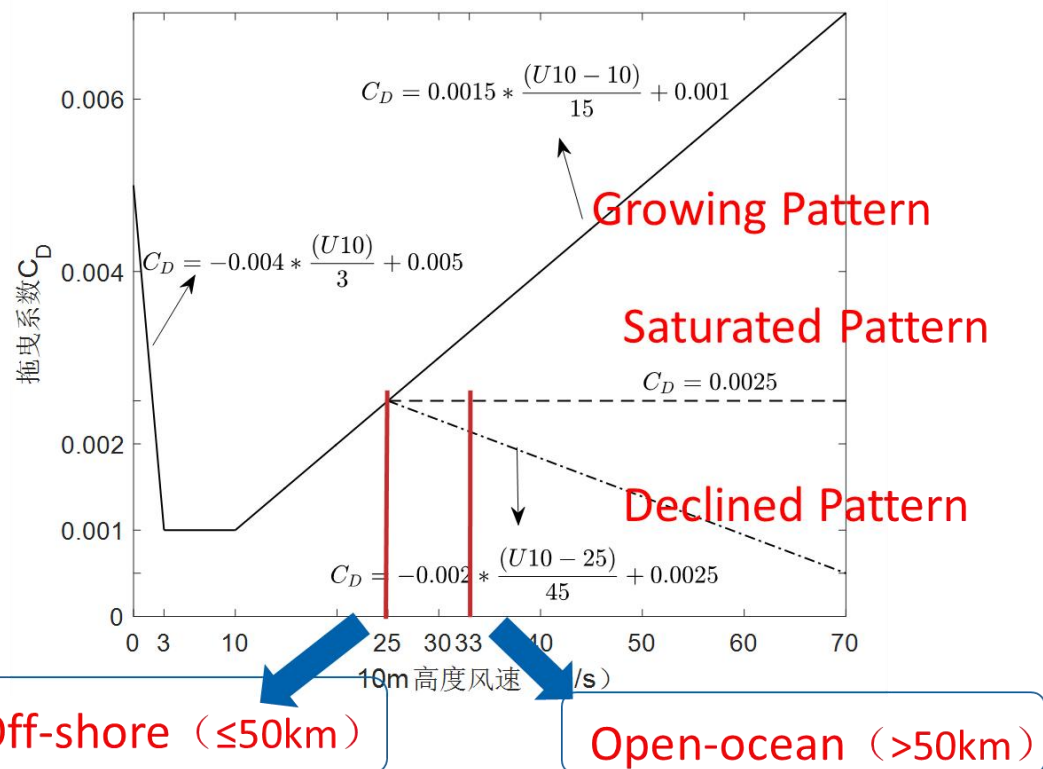
Sensitivity experiments for B
(difference in shape and Vmax)



Relationship between B and latitude (right) and ΔP (left)

Key parameters in the parametric surface wind model

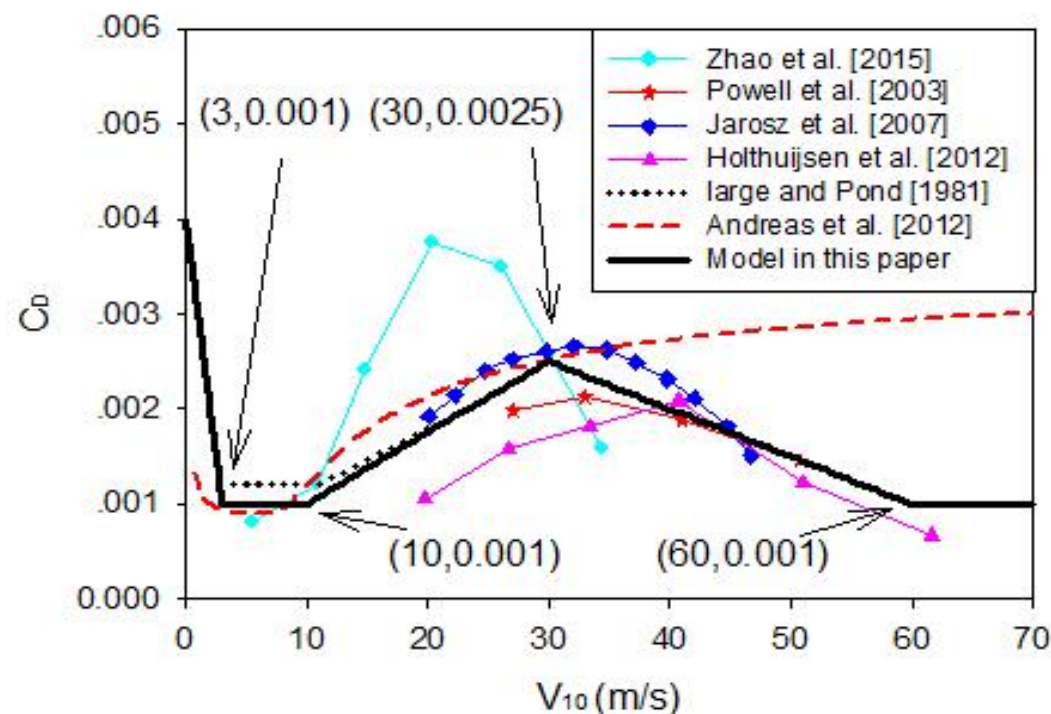
(3) Drag coefficient



Adjustment of the drag coefficient has a significant impact on the wind field in the inner core region of the tropical cyclone (6-7% variation in V_{max})

Key parameters in the parametric surface wind model

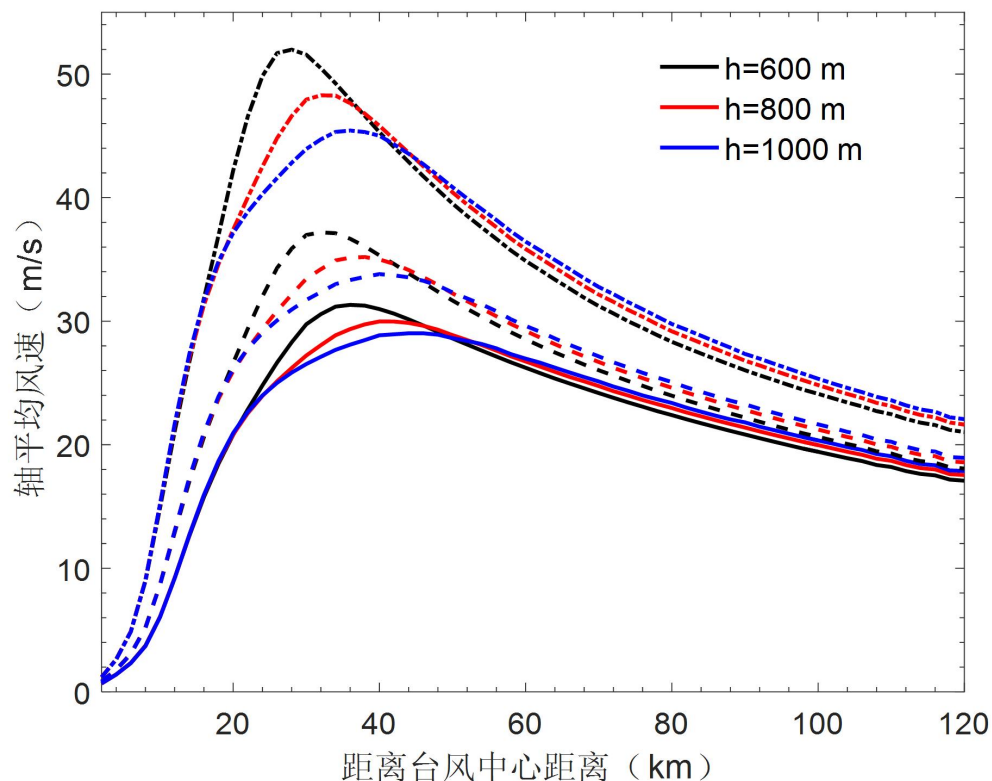
(3) Drag coefficient



The declined pattern of the drag coefficient at high winds: increasing with the wind speeds up to about 30 m/s, but decreasing with the wind speeds when the wind is stronger than 30 m/s.

Key parameters in the parametric surface wind model

(4) Height of boundary layer



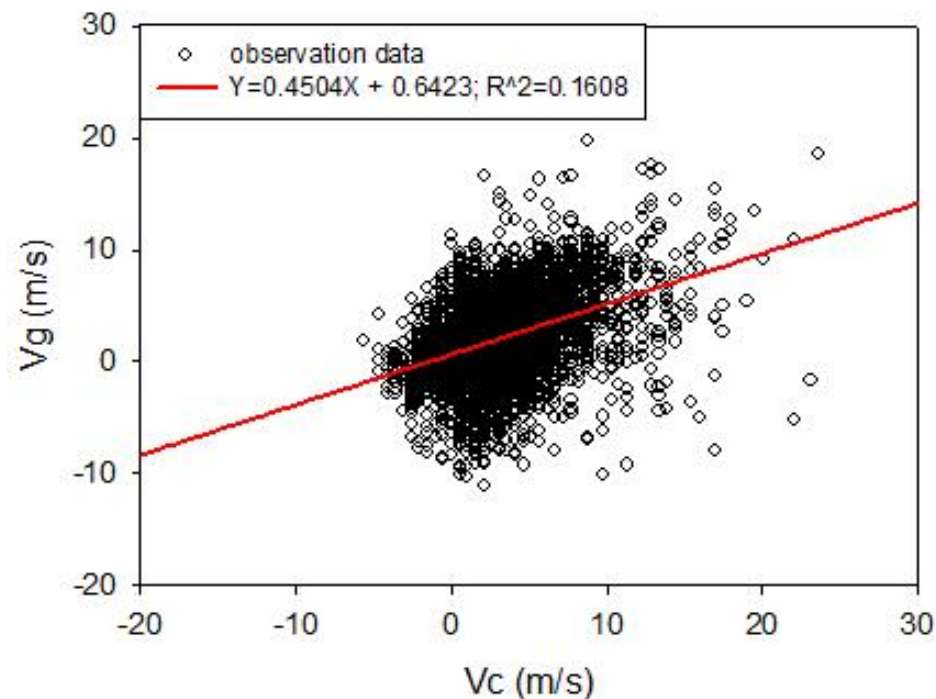
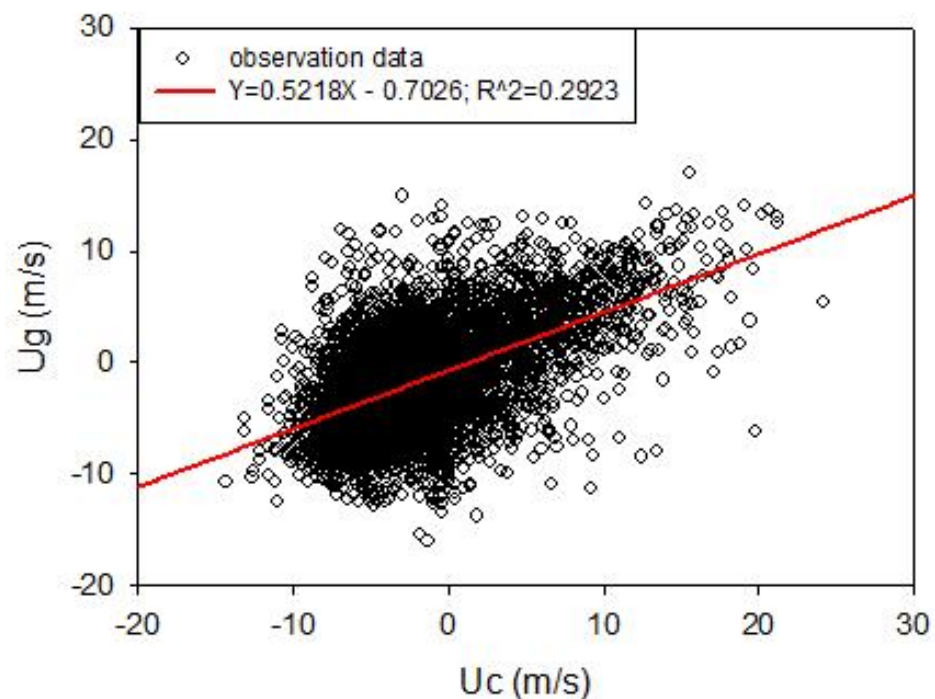
Group	1	2	3
Vmax (m/s)	30	40	55
Rmax (km)	39.89	35.62	30.77

The height of the planetary boundary layer in TC varies between 300 and 1000 m, and it increases with the distance to TC center.

Sensitivity experiments showed that the greater the depth of the PBL, the smaller the simulated maximum wind, the larger R_{max} .

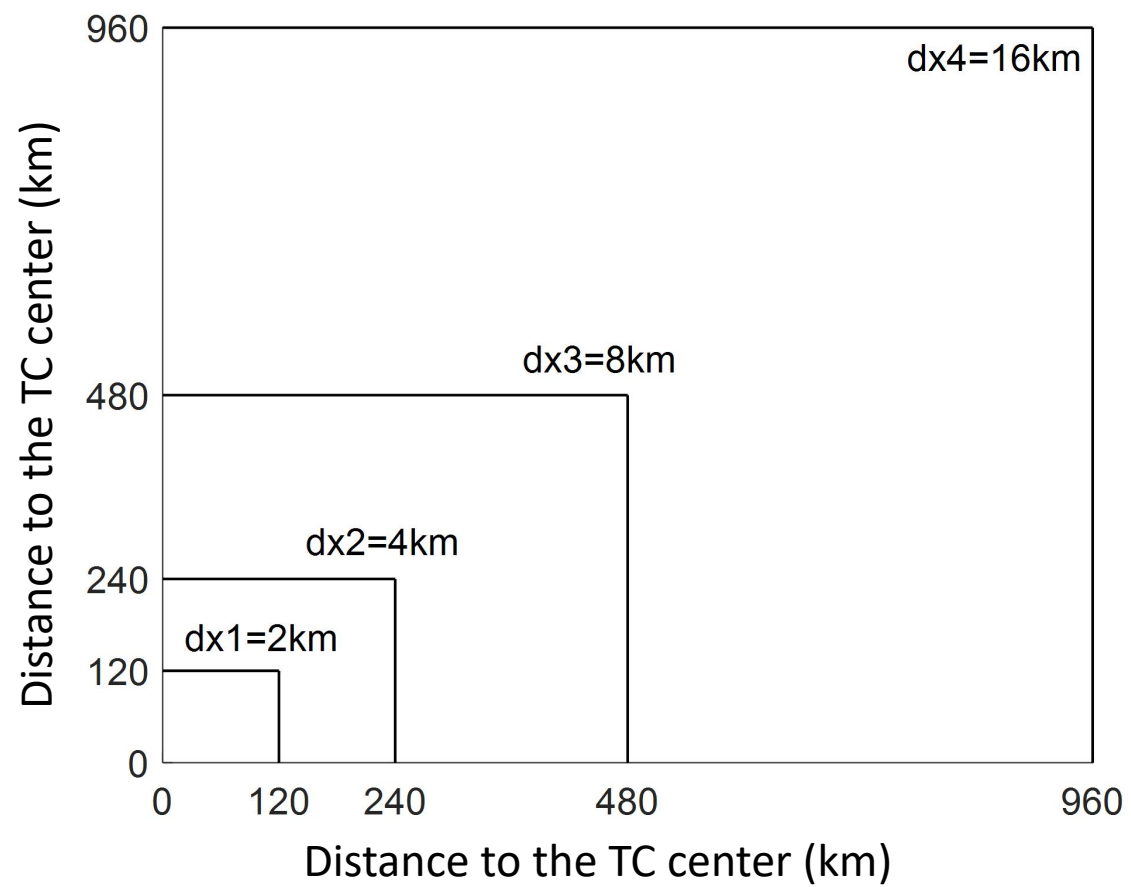
Key parameters in the parametric surface wind model

(5) Environmental geostrophic wind





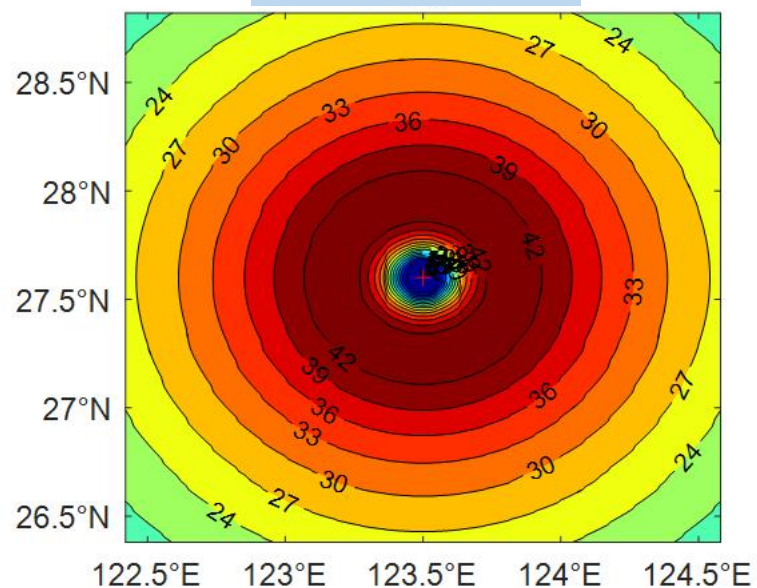
Nested domains with the inner most 240 km * 240 km
at a resolution of 2 km



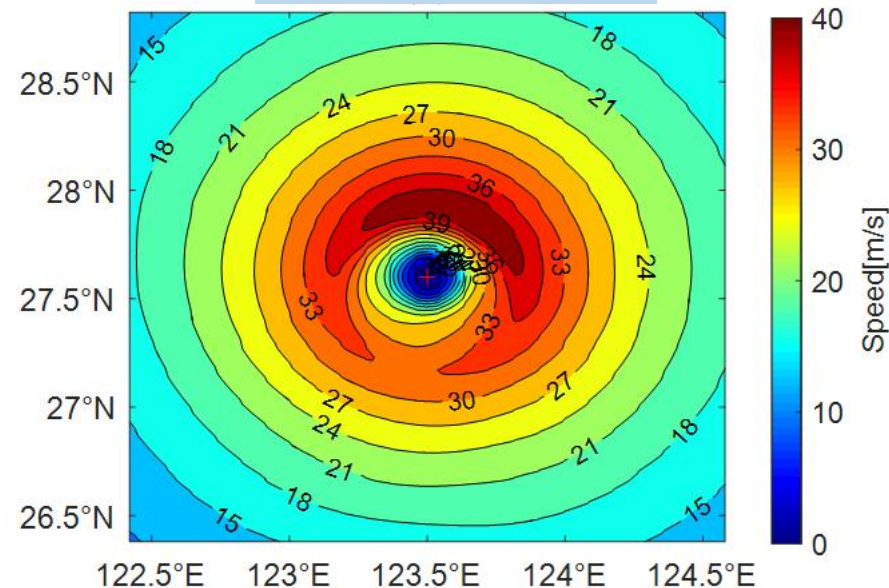
Simulation experiments

Idealized TC

Initial wind field



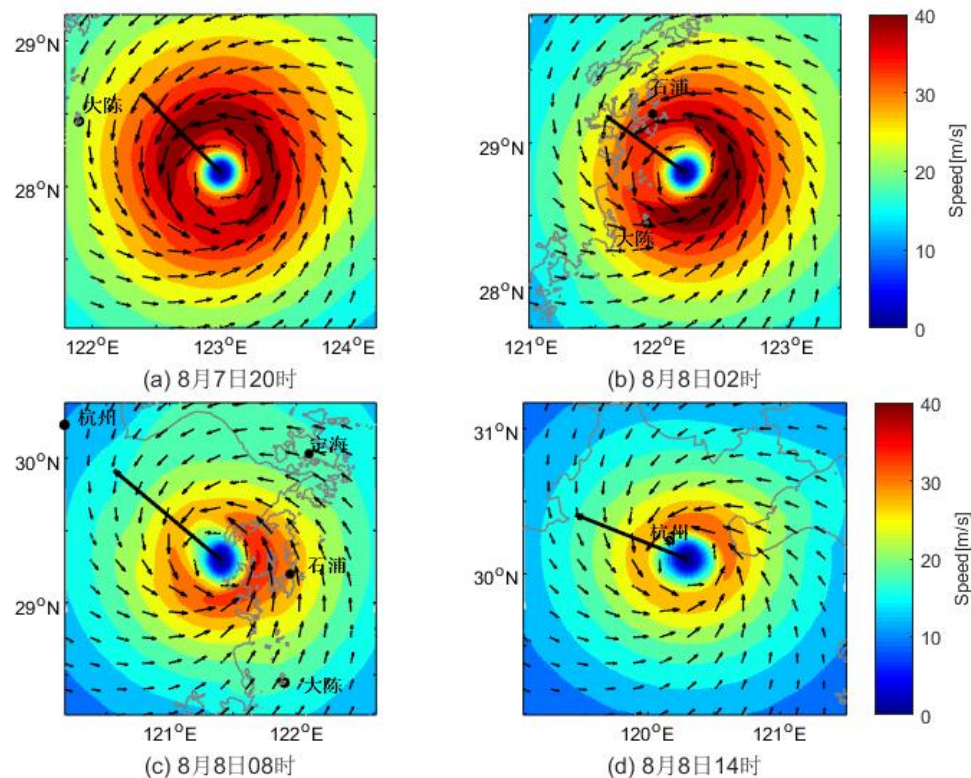
Simulated wind field



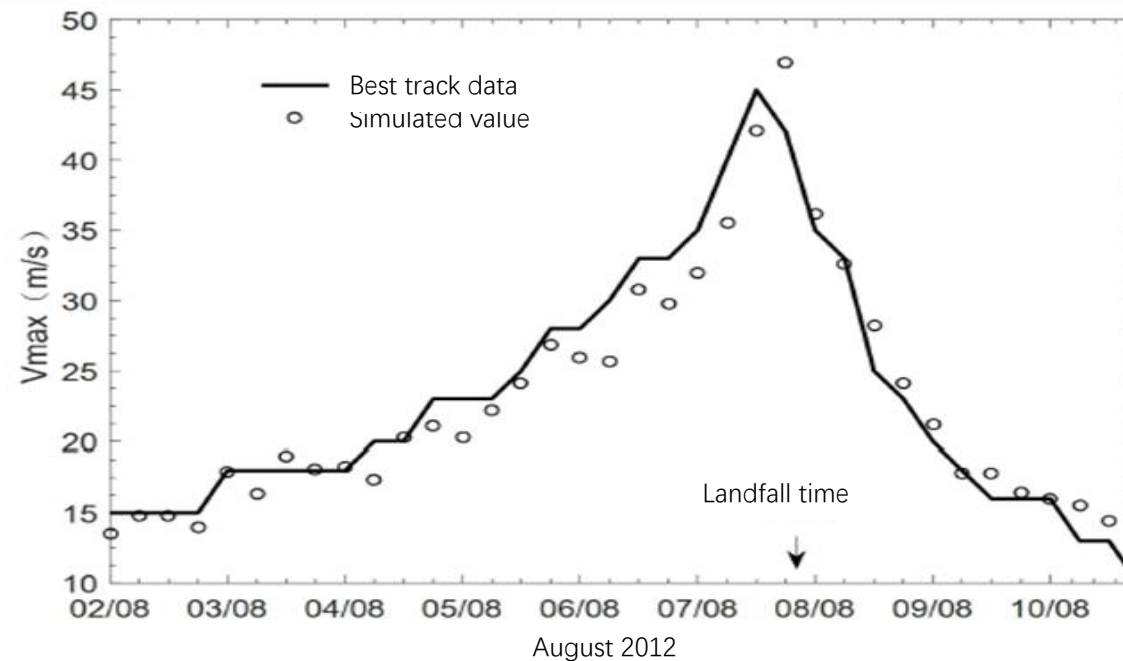
	Vmax (m/s)	Rmax (km)
Observed	40	35.62
Simulated	41.95	31.31

Simulation experiments

Typhoon HAIKUI(2012)



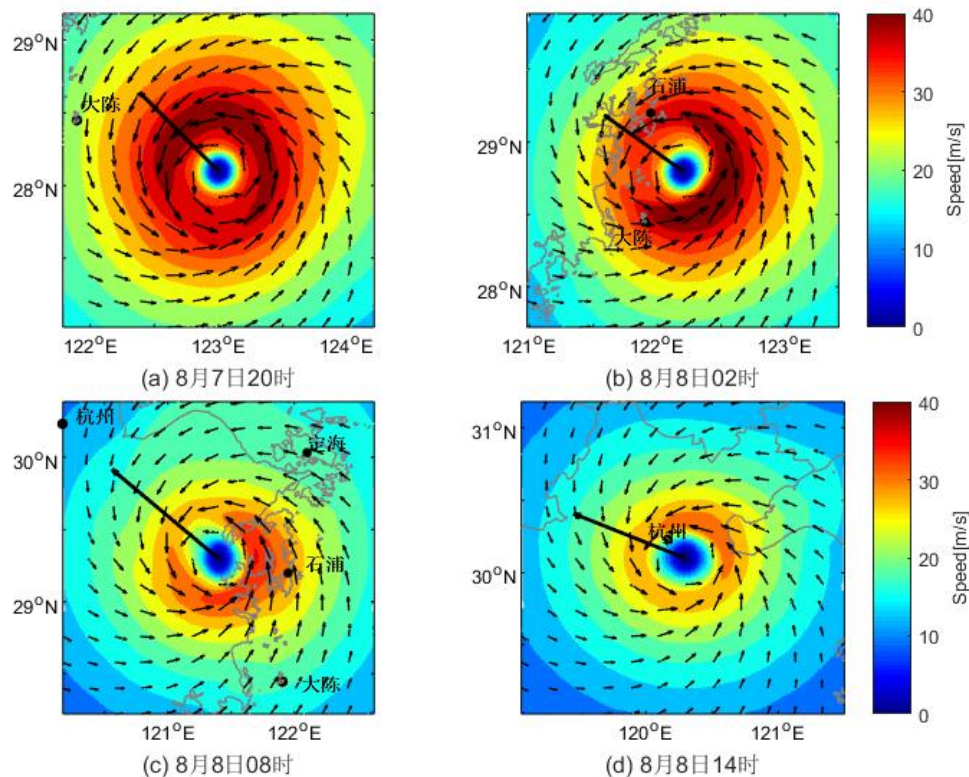
Evolution of simulated wind field



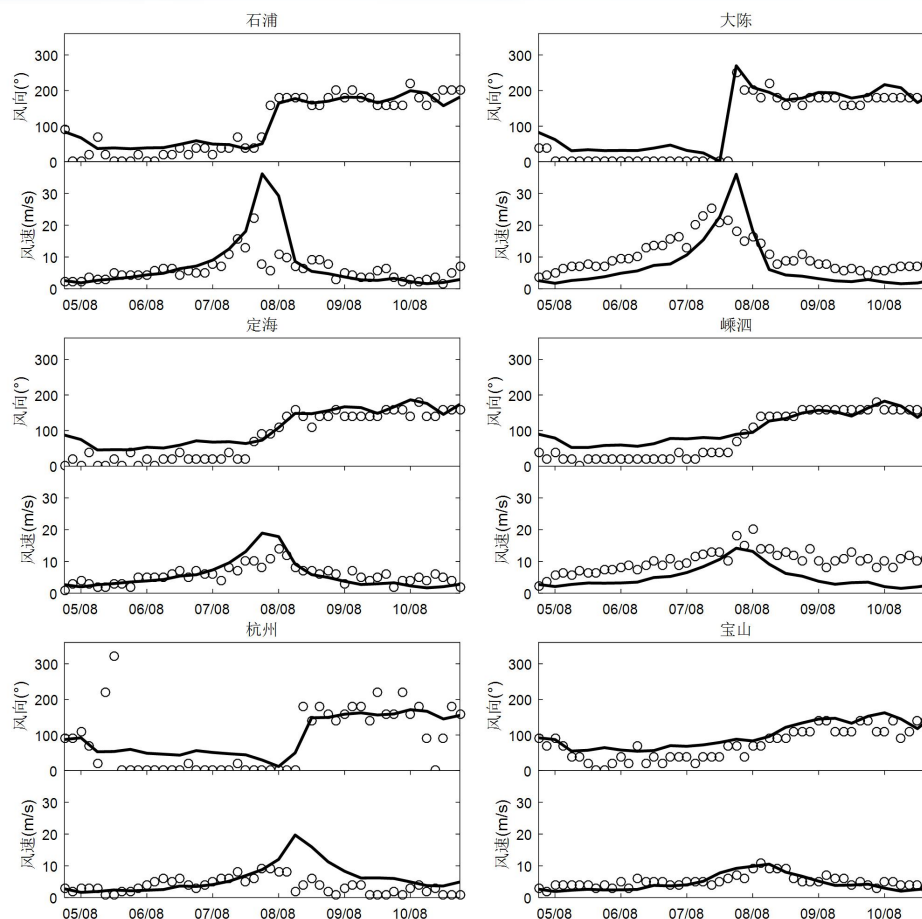
The observed and simulated maximum wind speed of HAIKUI (2012)

Simulation experiments

Typhoon HAIKUI(2012)

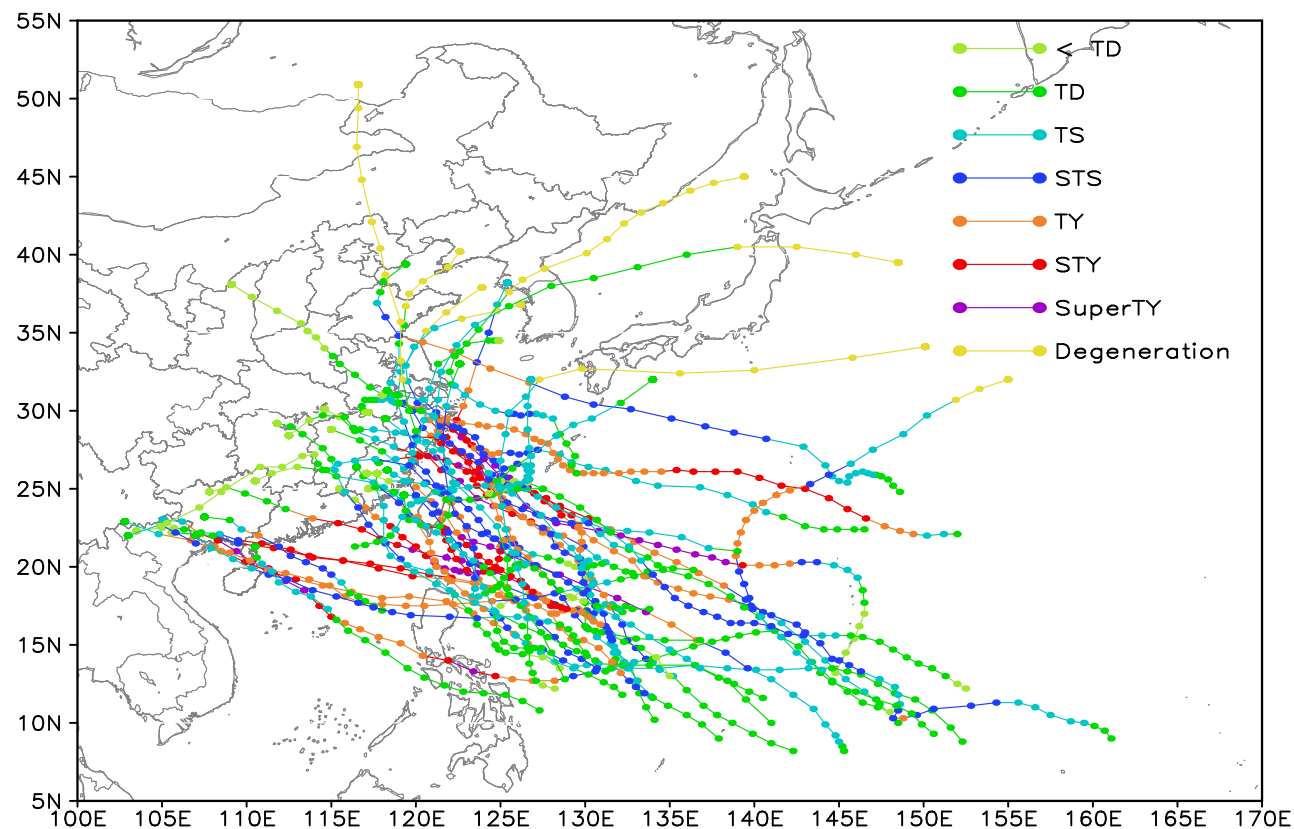


Evolution of simulated wind field



Simulated (solid line) vs Observed (dots) velocity

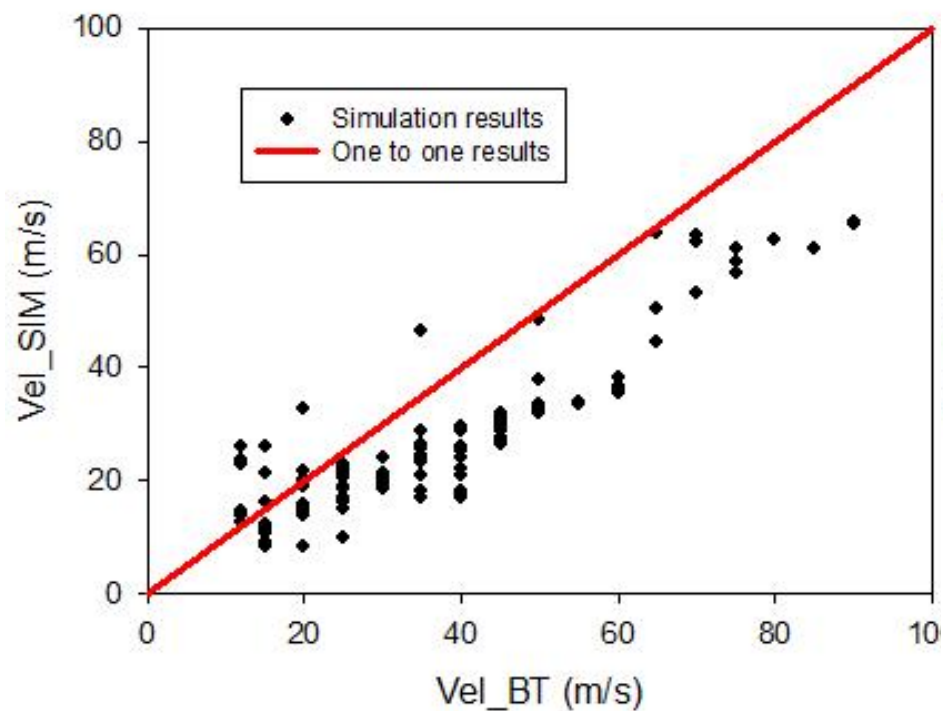
Simulated TC wind dataset for the NWP region (1949-2018)



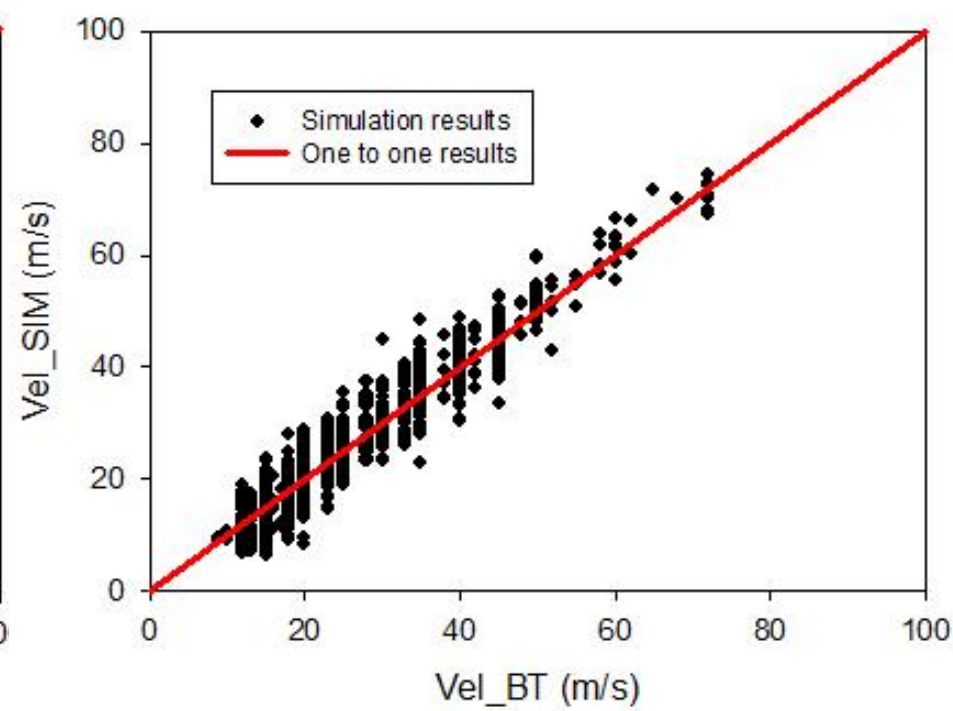
Tracks and intensities for the 46 simulated typhoons (randomly selected).

Simulated TC wind dataset for the NWP region (1949-2018)

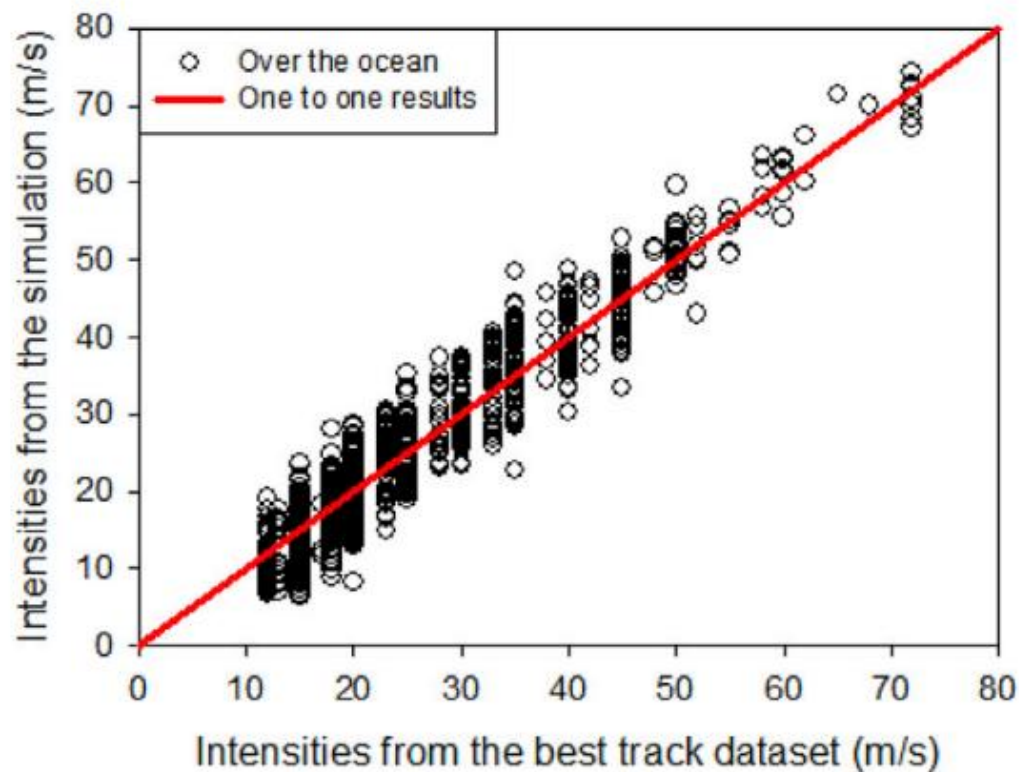
Comparison between the simulated maximum wind speed and the best track data



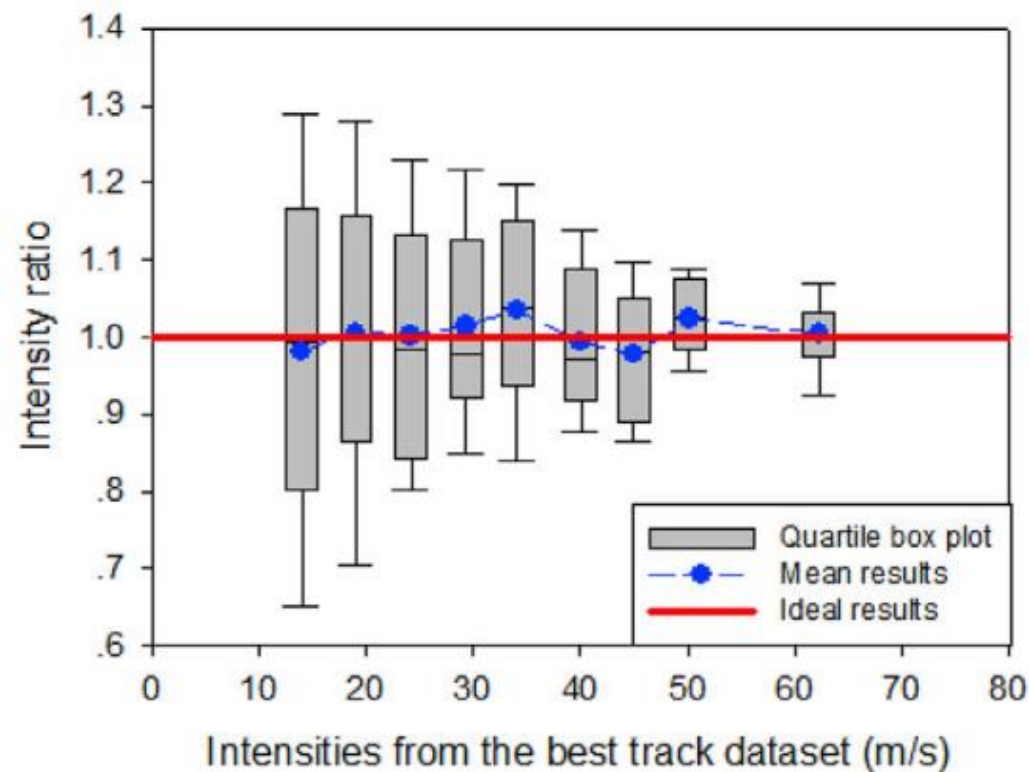
Before 1980



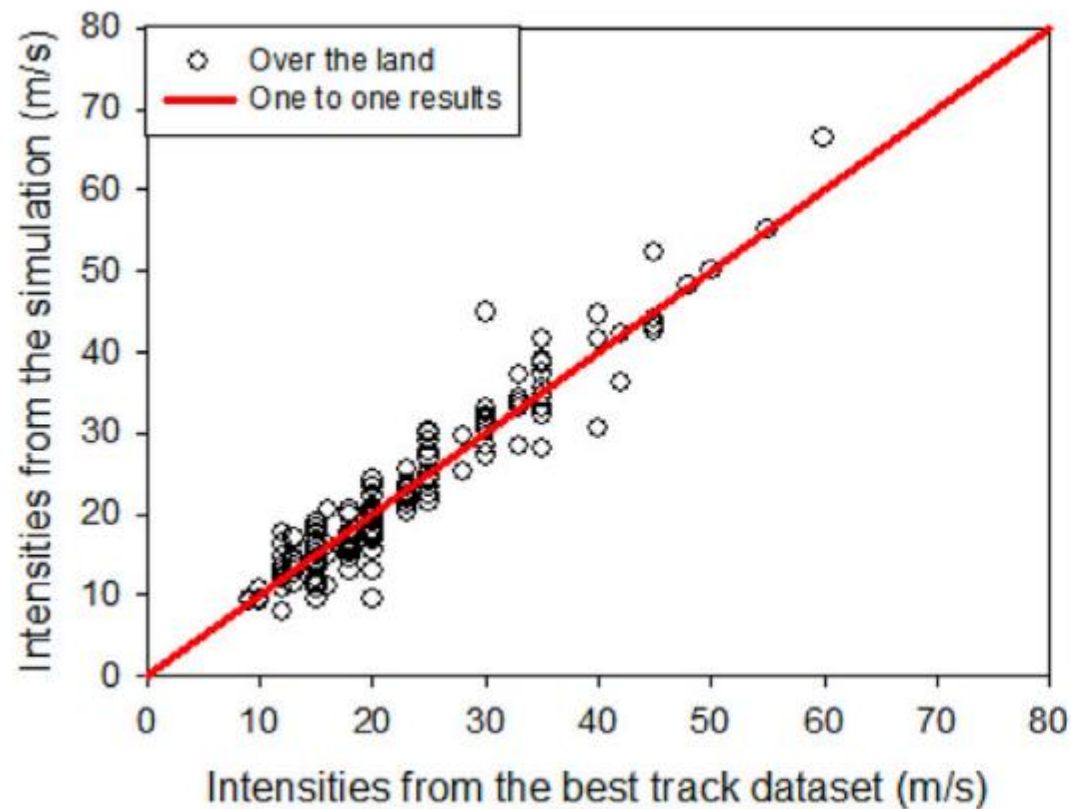
After 1980



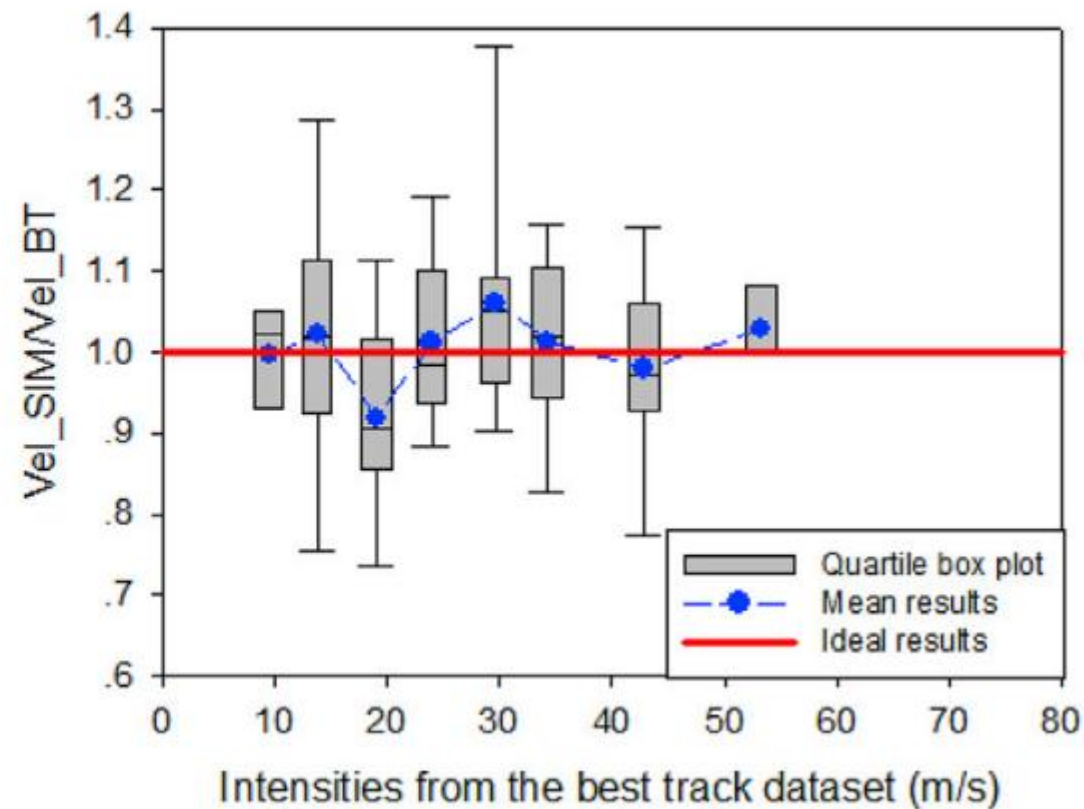
Comparison of simulated intensities over ocean with those from the best track dataset issued by the CMA for typhoons generated after 1980.



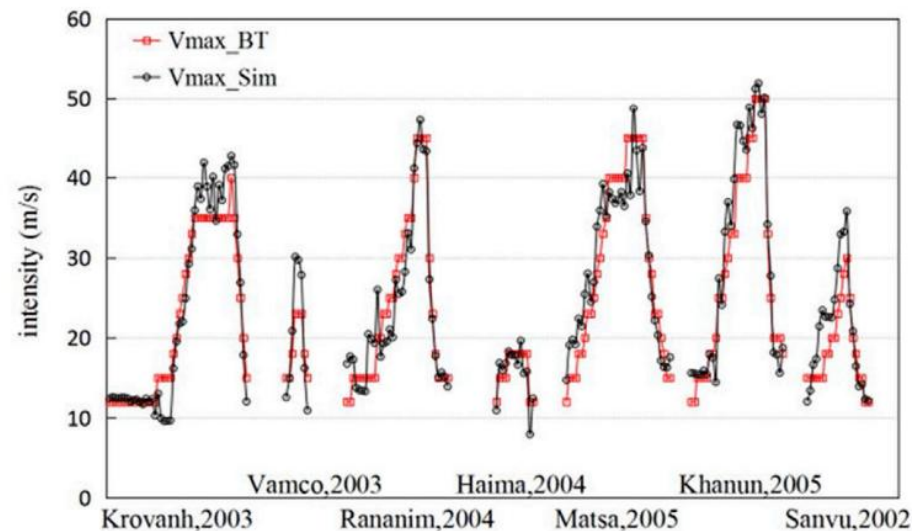
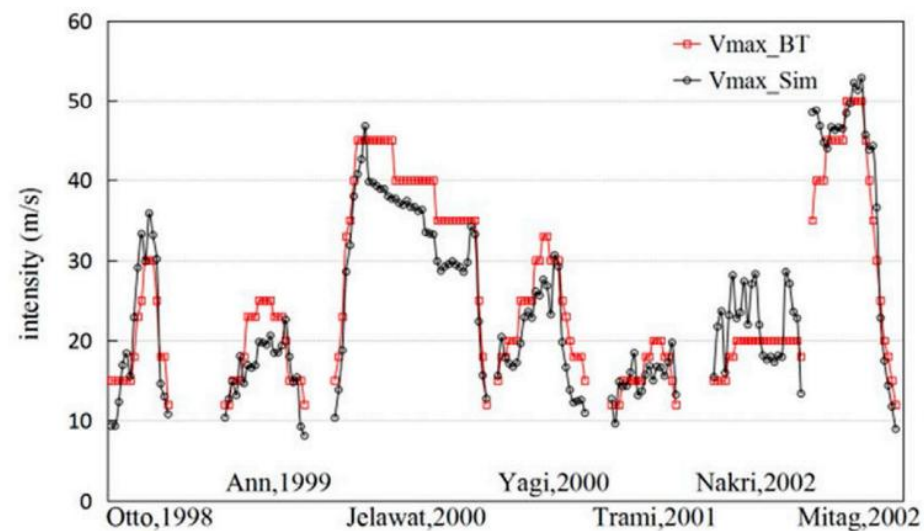
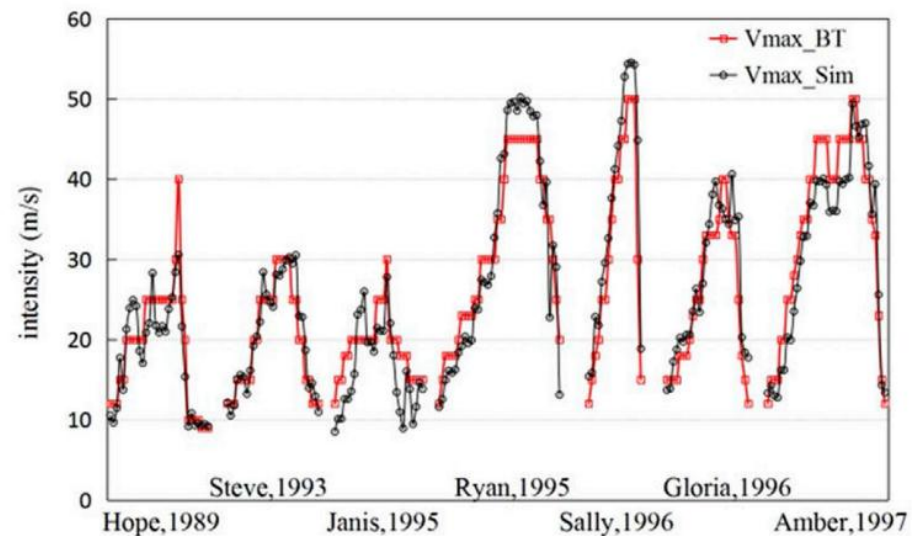
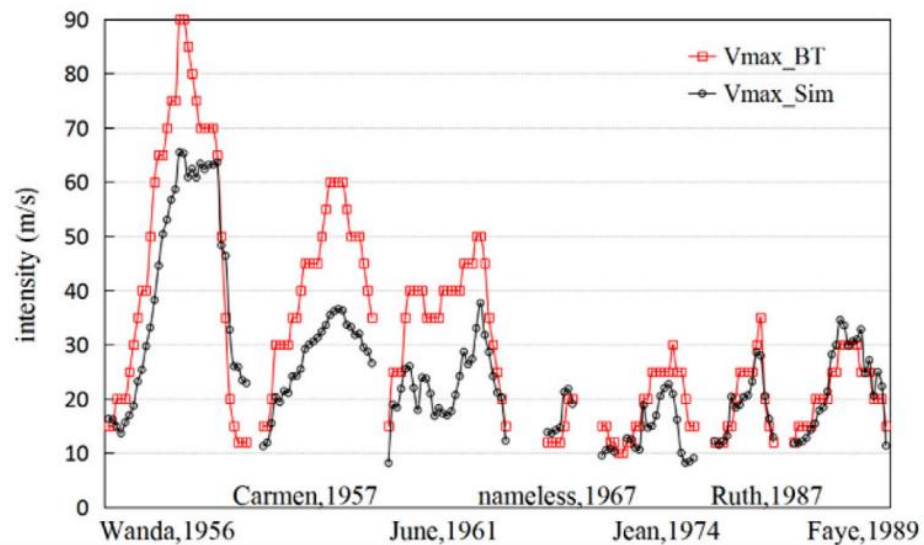
Corresponding intensity ratio of the simulated results to the best track dataset.



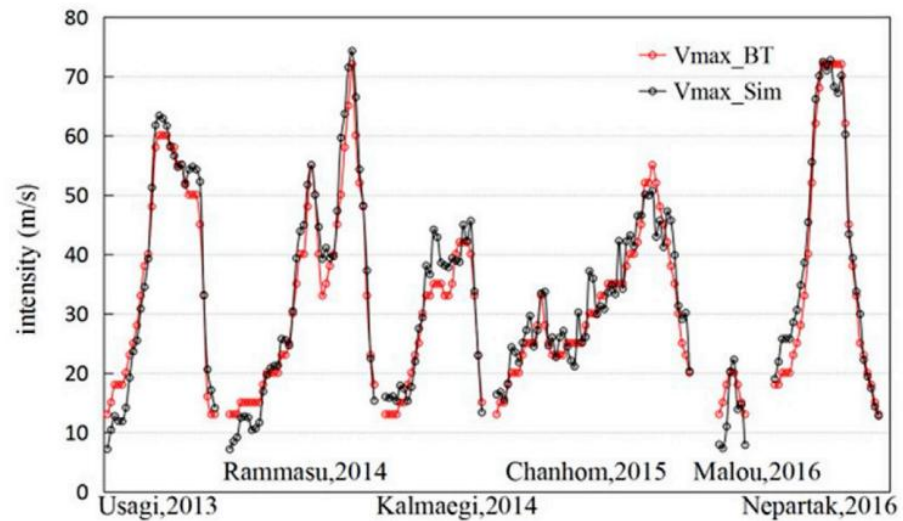
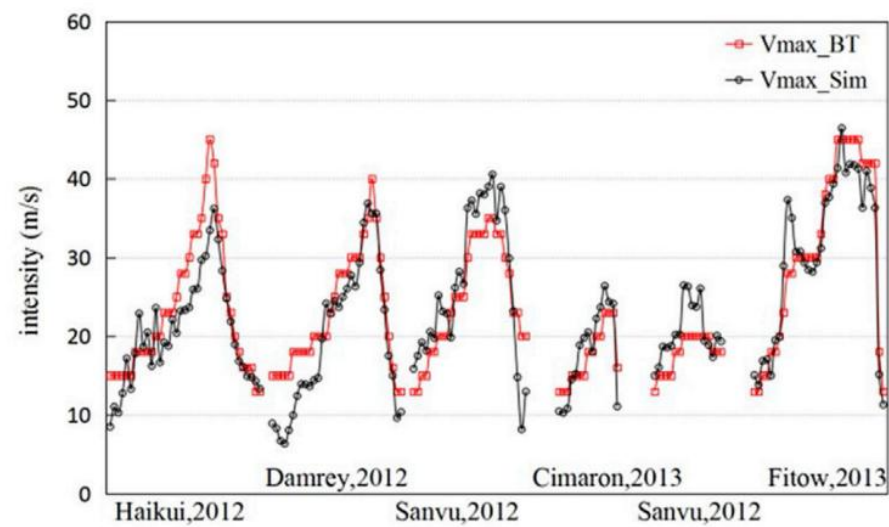
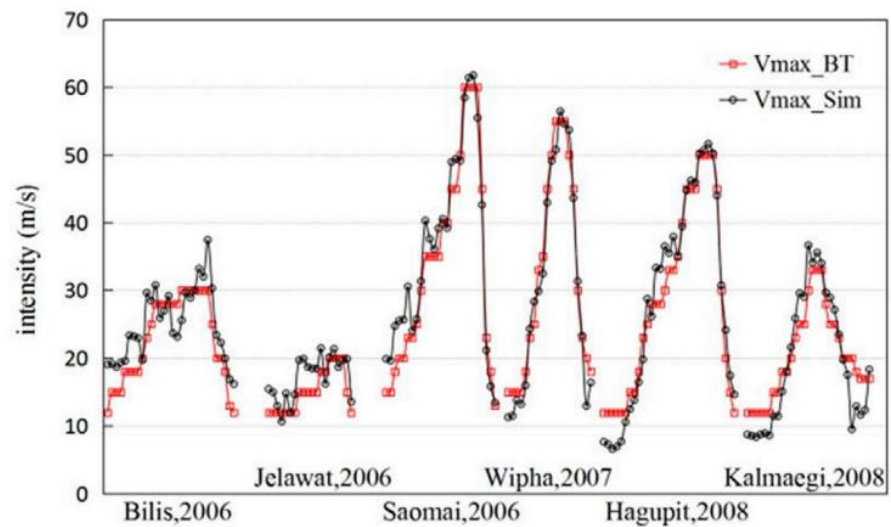
Comparison of simulated intensities over land with those from the best track dataset issued by the CMA for typhoons generated after 1980.



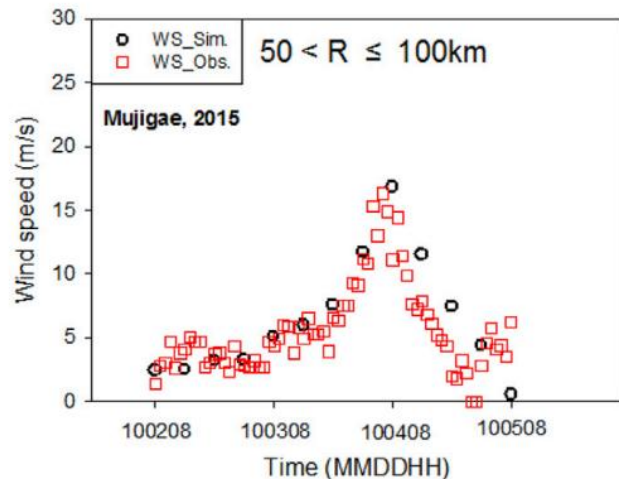
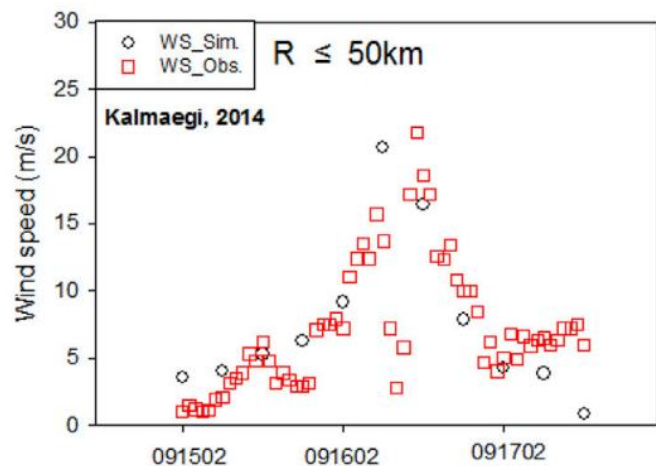
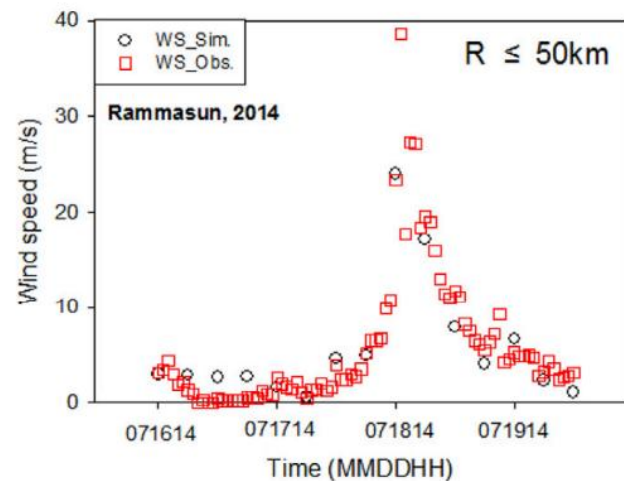
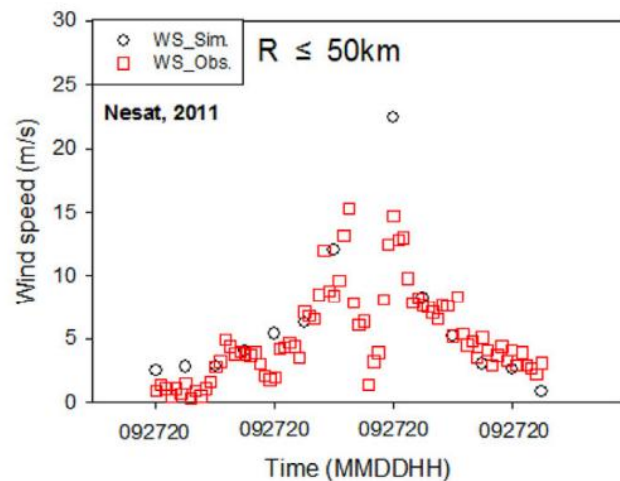
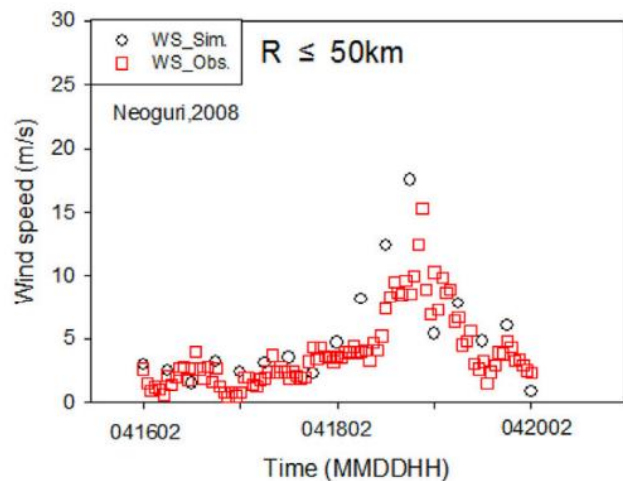
Corresponding intensity ratio of the simulated results to the best track dataset.



Comparisons of the simulated intensities with those from the best track dataset issued by CMA for the 46 simulated typhoons in time sequence.



Comparisons of the simulated intensities with those from the best track dataset issued by CMA for the 46 simulated typhoons in time sequence.

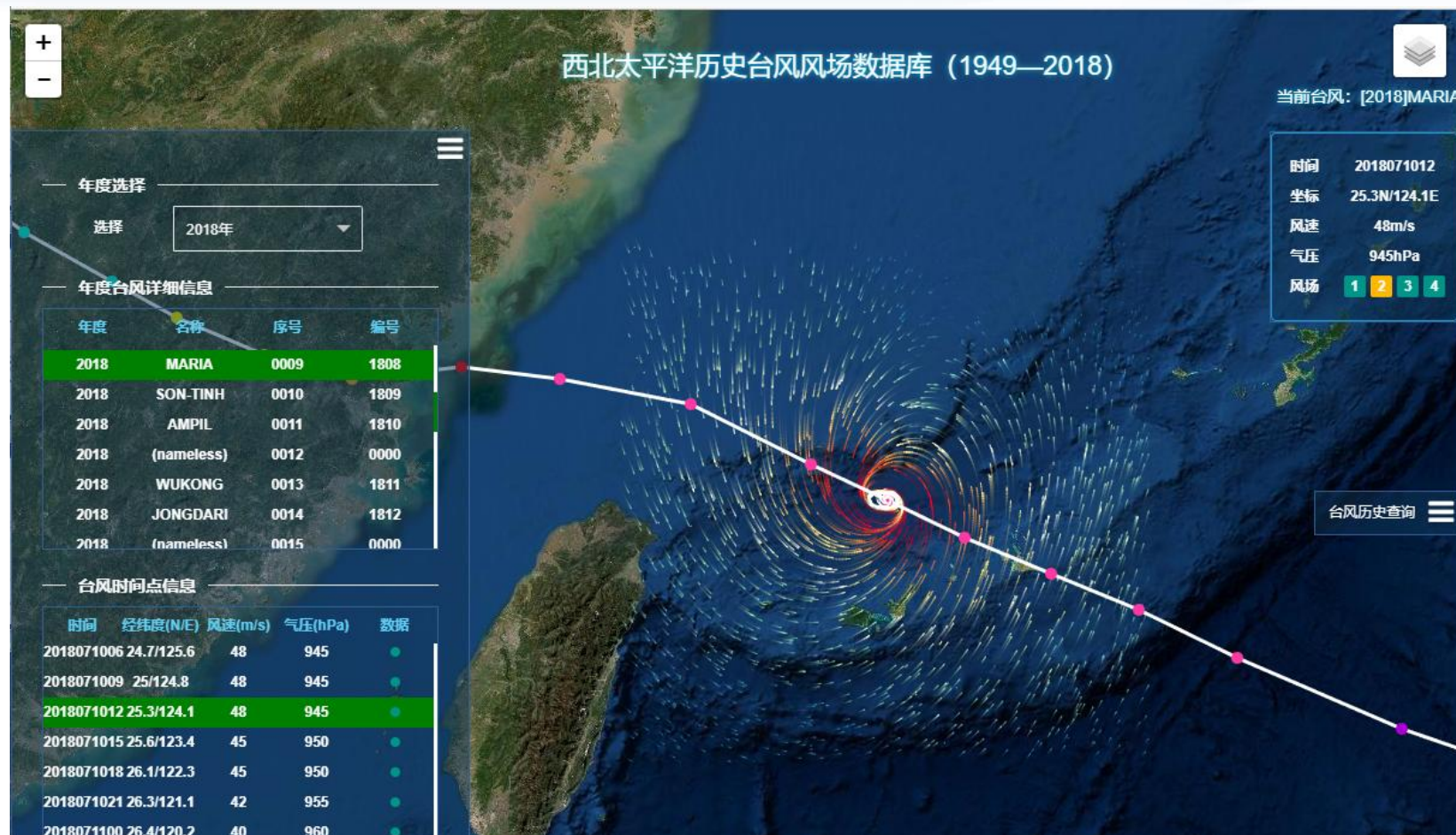


Wengtian weather station:
located in northeast Hainan Island

Comparisons of simulated wind speeds (WS) with those observed at the Wengtian weather station for 5 typhoons. R is the distance from the station to the typhoon center.



Simulated TC wind dataset for the NWP region (1949-2018)





- Fang, P. Z., B. K. Zhao, Z. H. Zeng, et al., 2018: Effects of wind direction on variations in friction velocity with wind speed under conditions of strong onshore wind. *J. Geophys. Res. Atmos.*, **123**, 7340-7353.
- Fang, P. Z., B. K. Zhao, S. Zhang, et al., 2015: An observation of the behavior of nearshore drag coefficient with moderate to strong wind speed. *J. Trop. Meteor.*, **31**, 713-720.
- Fang, P. Z., G. J. Ye, and H. Yu, 2020: A parametric wind field model and its application in simulating historical typhoons in the western North Pacific Ocean. *J. Wind. Eng. Ind. Aerodyn.*, **199**, 104131.
- Ye, G. J., H. Yu, P. Z. Fang, X. Q. Lu, and H. F. Cheng, 2018: Effects of the parameterization scheme of drag coefficient on the simulation of typhoon wind field in engineering application (in Chinese). *J. Trop. Meteor.*, **34**, 188-197.

The background of the slide is a composite image. The top half features a dark blue world map with a grid overlay. A bright, swirling hurricane-like storm is depicted over the Pacific Ocean, with a red dot and a small red square at its center. The bottom half of the slide shows a satellite view of a large, swirling oceanic eddy or cyclone in shades of blue and white.

**Thank you for your attention !
Questions?**

THE SENIOR MANAGEMENT AND OPERATION COURSE ON TROPICAL CYCLONE MONITORING AND FORECASTING
(20 November to 1 December 2023, Guangzhou, China)

Tropical Cyclone Gale Monitoring and Forecasting Technology (Part II)

Hui YU
Shanghai Typhoon Institute/CMA



Outline

- Surface wind structure of tropical cyclones and a parametric wind field model for tropical cyclones
- **Tropical cyclone intensity and size estimation techniques based on satellite observations**
- **Tropical cyclone gale forecast techniques**

Contents of the Tropical Cyclone Annual Book



Tropical Cyclone Annual Book (1949-)

Track and intensity	<ul style="list-style-type: none"> • Longitude, latitude, MSW, and MSLP back to 1949 • Extratropical cyclone stage • Landfalling TC data including landfall location, date and time, and TC intensity at the time of landfall in China
Wind radius	<ul style="list-style-type: none"> • 10.8 m/s, 17.2 m/s, and 24.5 m/s wind radii
TC-induced wind and precipitation in China	<ul style="list-style-type: none"> • Total and daily precipitation, maximum 1-h precipitation • TC-induced extreme sustained wind and extreme gust • The date and duration of the TC' s influence on China
Characteristics of TC activity in this year	<ul style="list-style-type: none"> • Annual features of TC activity including TC frequency, intensity, genesis locations and paths.
TC damages in China	<ul style="list-style-type: none"> • Direct economic losses • Casualty • Affected and evacuation population • Affected area



CMA TROPICAL CYCLONE DATA CENTER for the western North Pacific Basin

English 中文

Location: Introduction

Introduction

National-level operational data product

Scientific Research Data Products

Key Project: Research and demonstration application of key physical processes of typhoon variable resolution prediction model

Other Product Metadata

Publications

Laws & Regulations

Useful Resources

Contact Us

Download Statistics

Last Updated: July 10, 2023

The CMA Tropical Cyclone Database

Tropical cyclones (TCs) are among the most destructive weather systems to occur over China, and the entire coastal area between the tropics and the midlatitudes has been affected. Almost all provinces of China, except Xinjiang and Qinghai, have felt the effects of either the damaging winds or torrential rainfall associated with tropical cyclones.

In China, the disastrous consequences of tropical cyclones have long been recorded in the annals of local history, ancient notes, and books, and these documents are an important source of information regarding the impact of tropical cyclones on human society.

With the development of modern meteorological techniques, an increasing amount of observational data became available for creating a specialized tropical cyclone database. Between 1969 and 1972, the China Meteorological Administration (CMA) sponsored a reanalysis project for tropical cyclone related data (1949–1971), and established the basis for the current CMA tropical cyclone database. Today, the post-season reanalysis and annual updating of the database has become a routine task for the Shanghai Typhoon Institute (STI), with the endorsement of the CMA and support from various institutions of the CMA. Based on the annually updated database, the *Tropical Cyclone Yearbook* and its CD version are published each year.

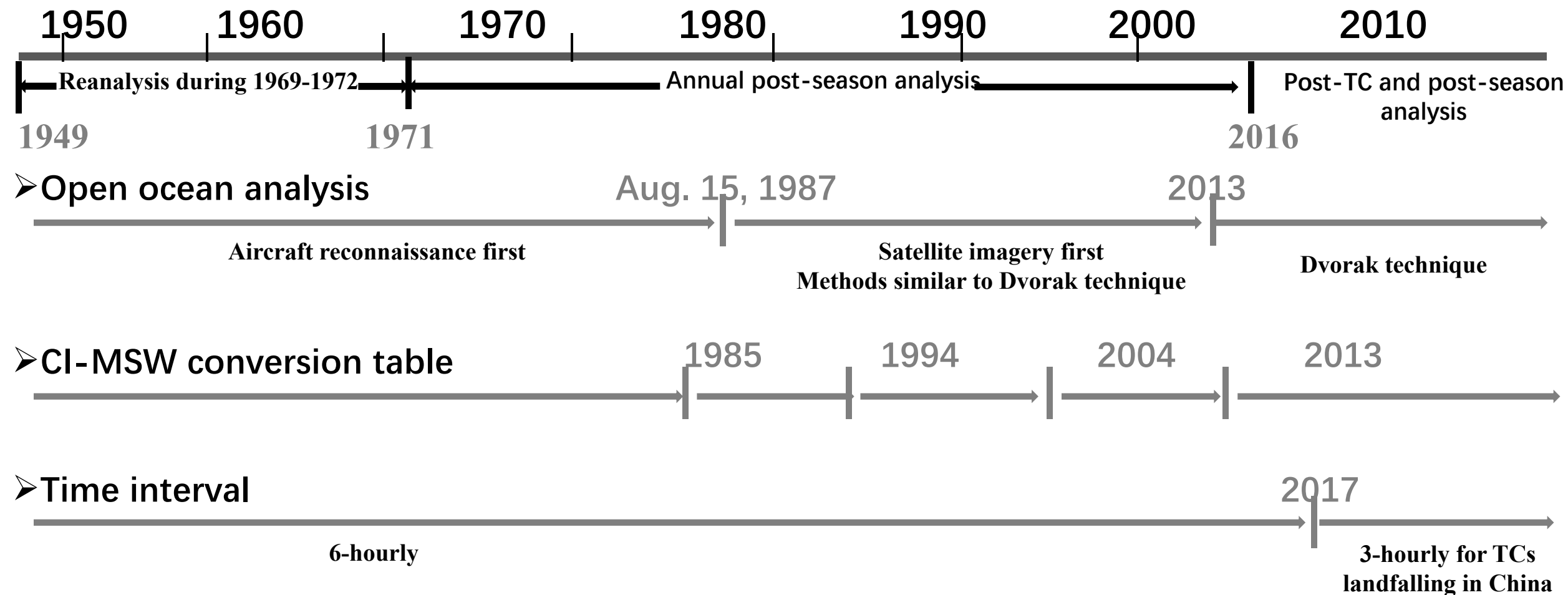
A Brief History of Tropical Cyclone Data in China

- Details of tropical cyclones and their impacts on the population can be found in local records and historical texts. Quantitative observation of precipitation began during the Ming Dynasty.
- Modern meteorological instruments started to become available in the 1880s, and tropical cyclone data have been

<https://tcdata.typhoon.org.cn/en/index.html>



Timeline about the evolution of analysis procedure and other important events related to the CMA best track dataset

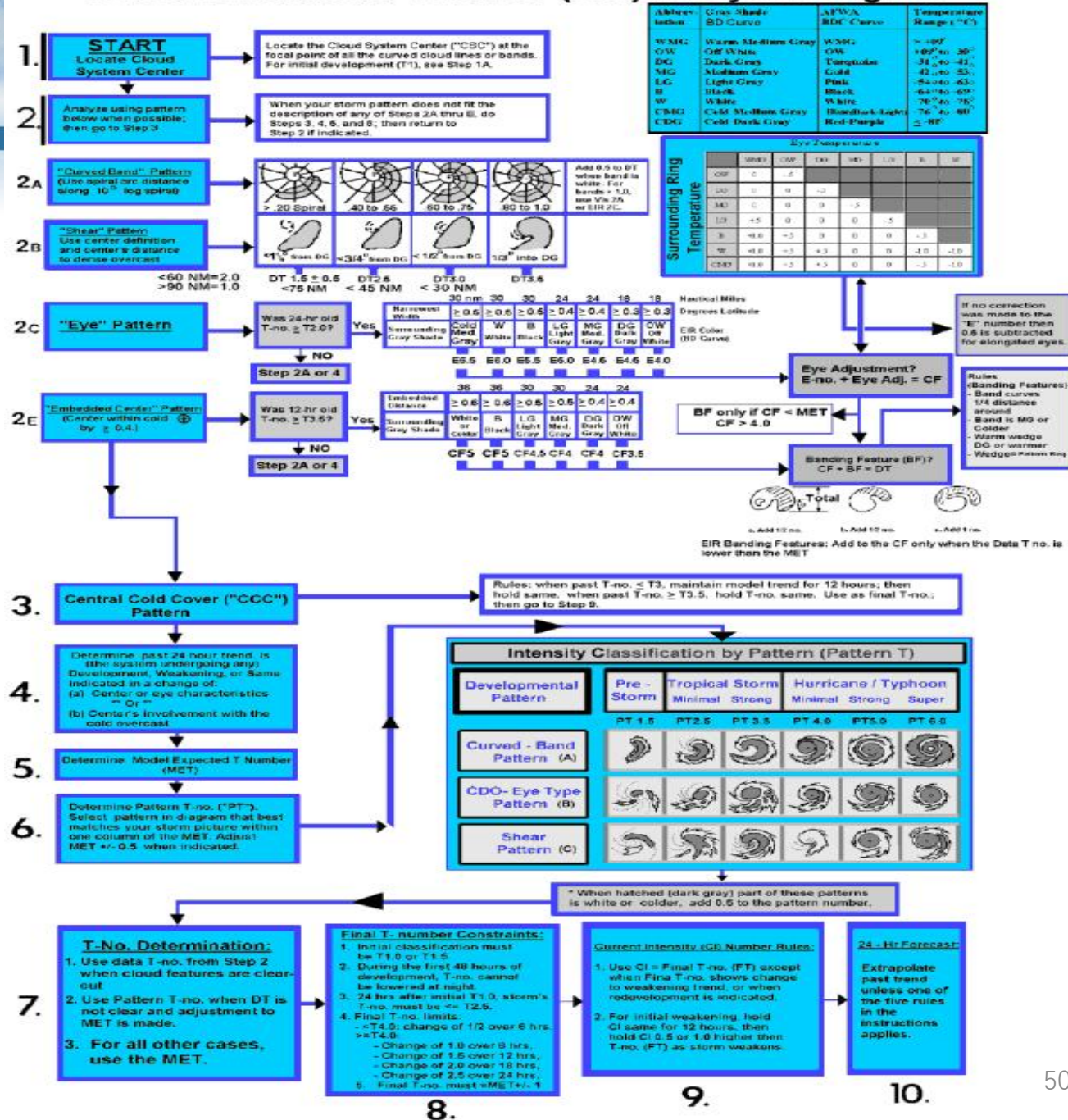






















Vernon Dvorak(1972, 1984)

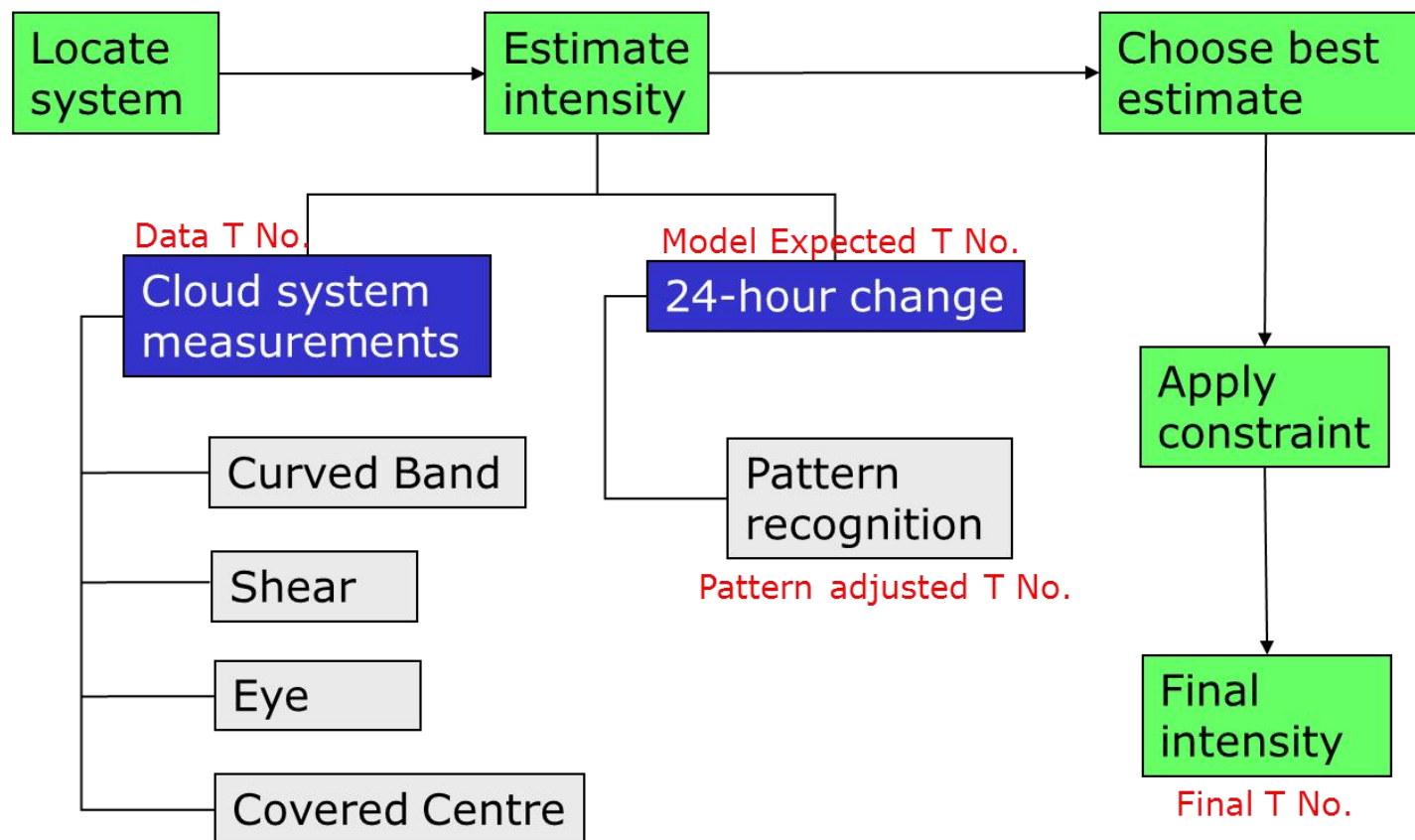
Over the open ocean:
Dvorak technique has been widely used globally since it was proposed in 1972 and modified in 1984, irreplaceable up to now.

Dvorak Enhanced Infrared (EIR) Analysis Diagram

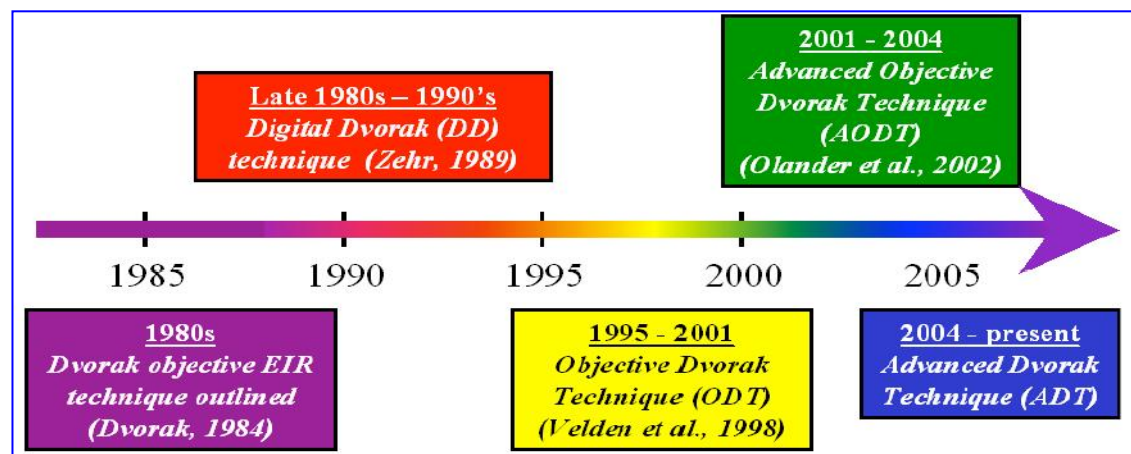


Major steps of Dvorak analysis (C.T. Chan, 2013)

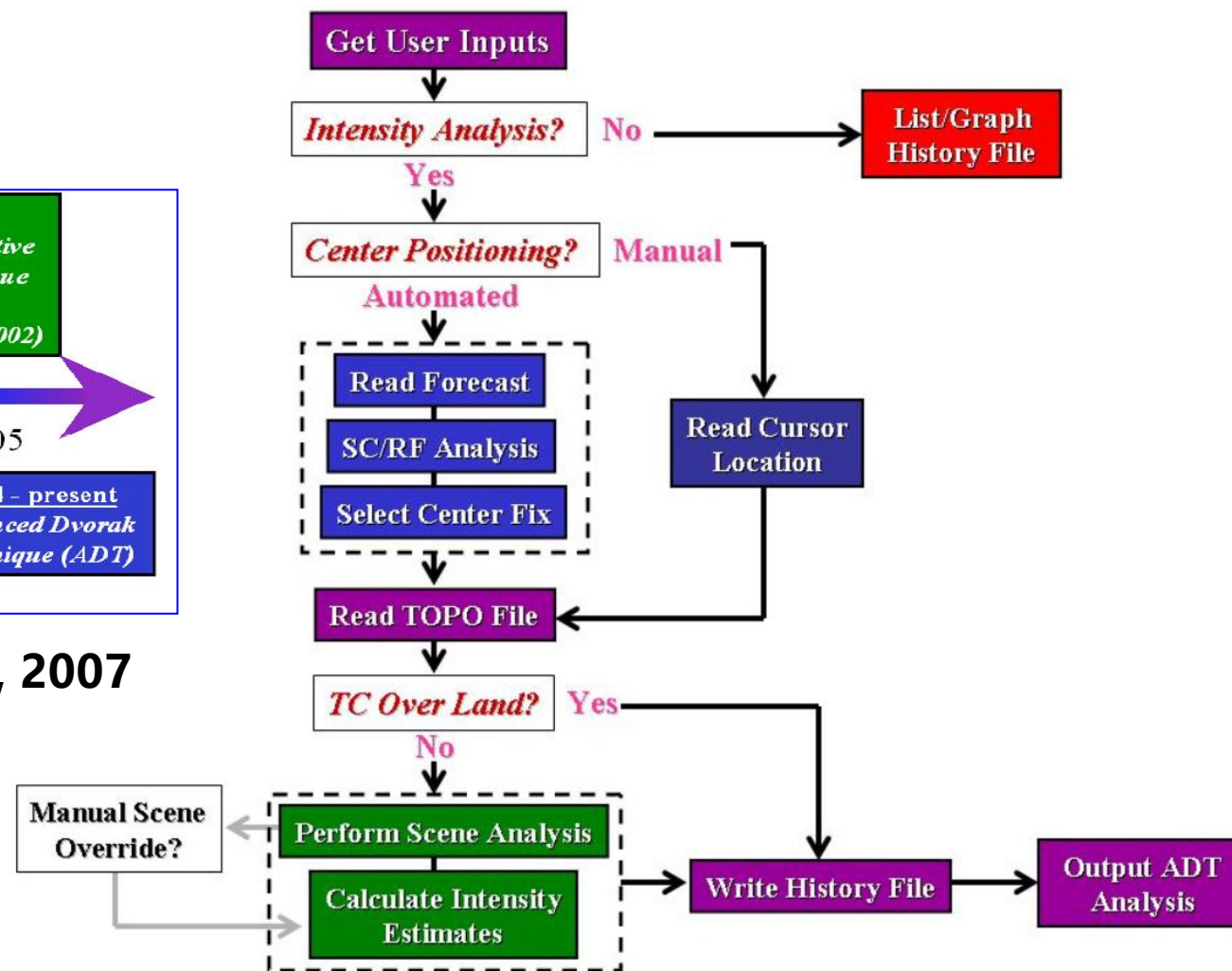
Pattern T-number estimate from cloud feature on Enhanced IR pictures (PT number)						
Cloud pattern	TD	TS	STS	TY	STY	SuperTY
types	PT 1.5	PT 2.5	PT 3.5	PT 4.0	PT 5.0	PT 6.0
Curve Band (A)						
CDO-Eye (B)						
Shear (C)						

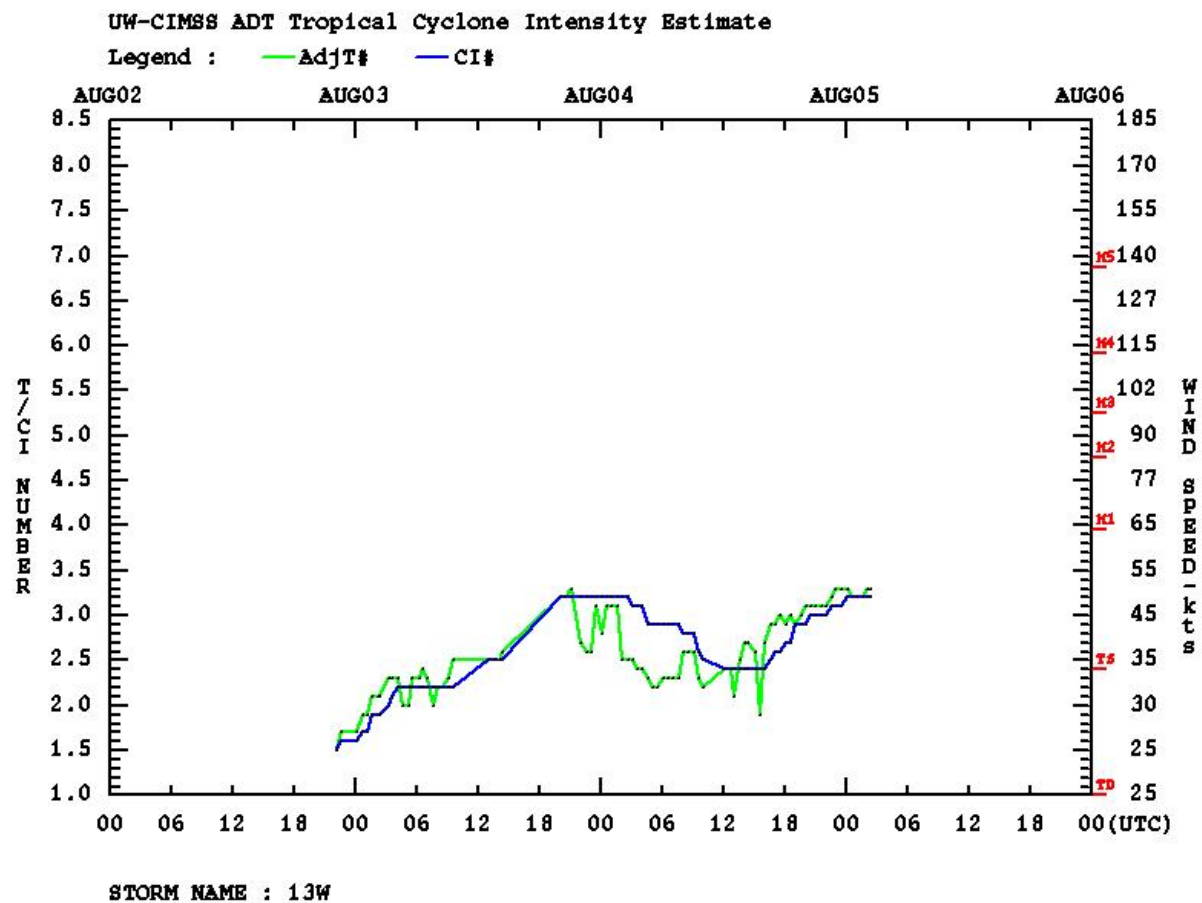
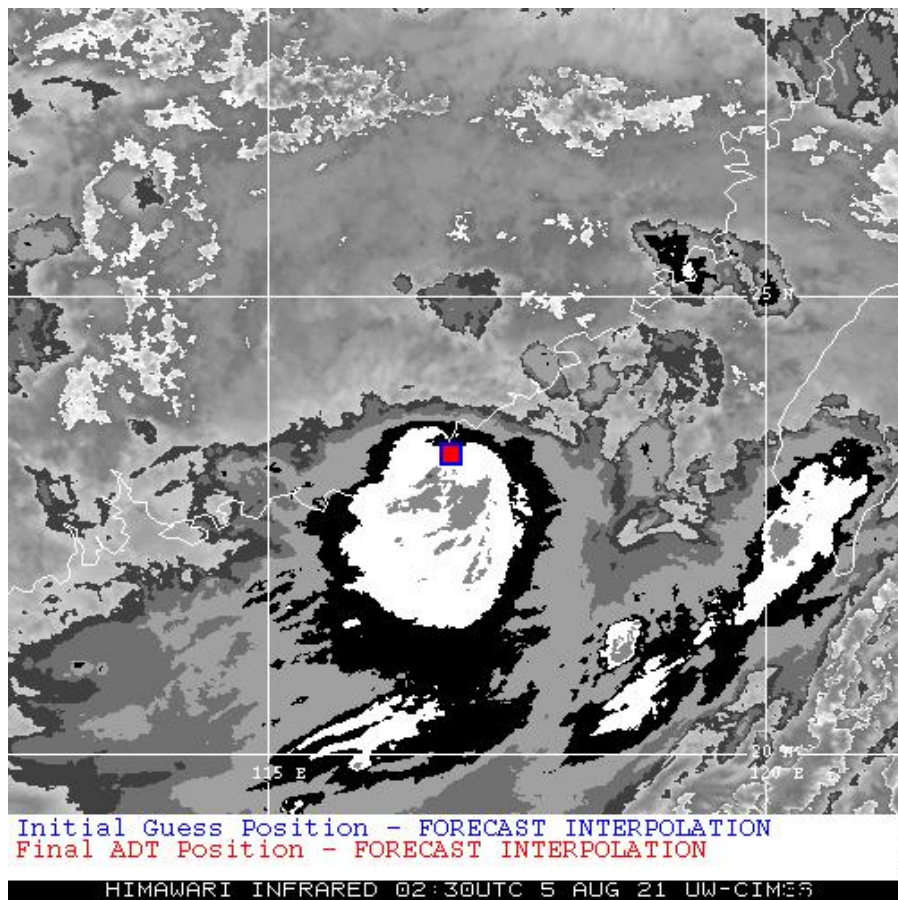


A major defect of Dvorak technique:
Depend heavily on the forecaster's experience

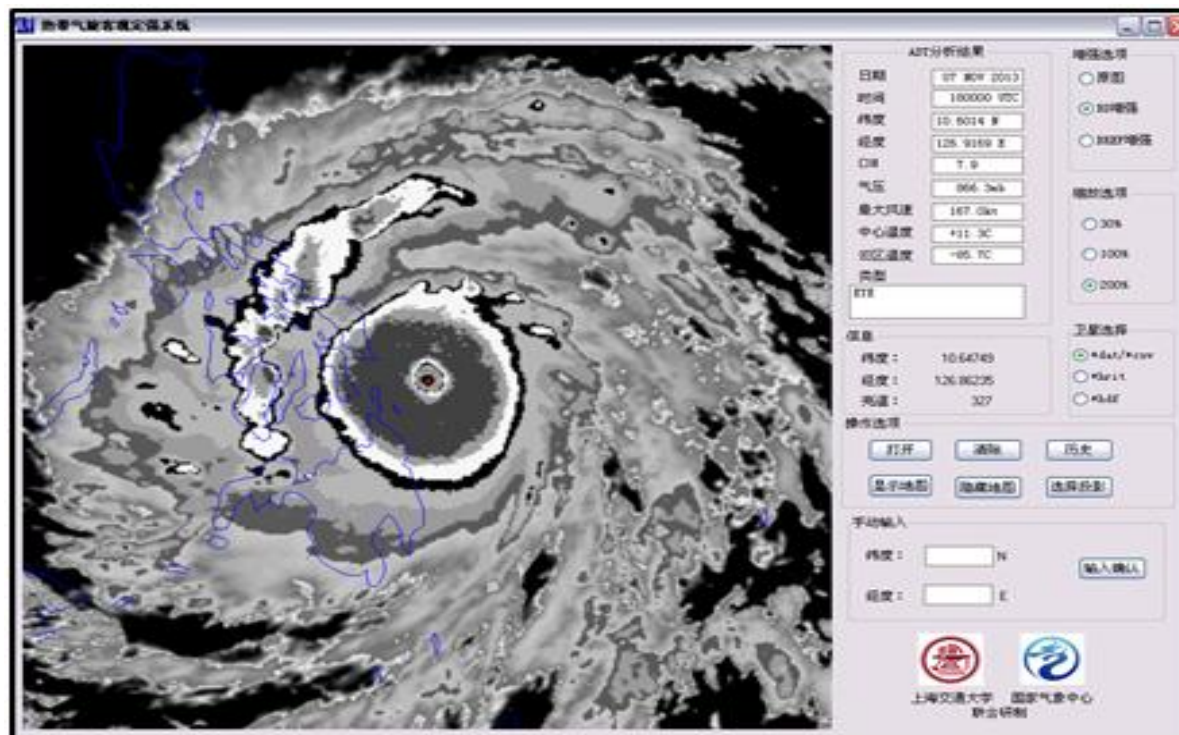


Olander and Velden, 2007





<http://tropic.ssec.wisc.edu/real-time/adt/adt.html>



the ADT analyses tool installed in CMA

The RMSE between ADT and OpCen(operational tropical cyclone analysis and forecasting centers) Dvorak estimates of TC intensity in different basins in 2018 (Olander and Velden, 2019)

Basin		Atlantic	East-central Pacific	Western North Pacific	North and South Indian Ocean	South Pacific
V _{max} (kt)	ADT	11.12	9.18	11.24	10.35	12.18
	Dvorak	10.40	9.71	11.19	10.27	12.08
MSLP(hPa)	ADT	9.71	6.78	8.43	6.99	8.97
	Dvorak	10.17	7.13	10.80	6.67	10.20

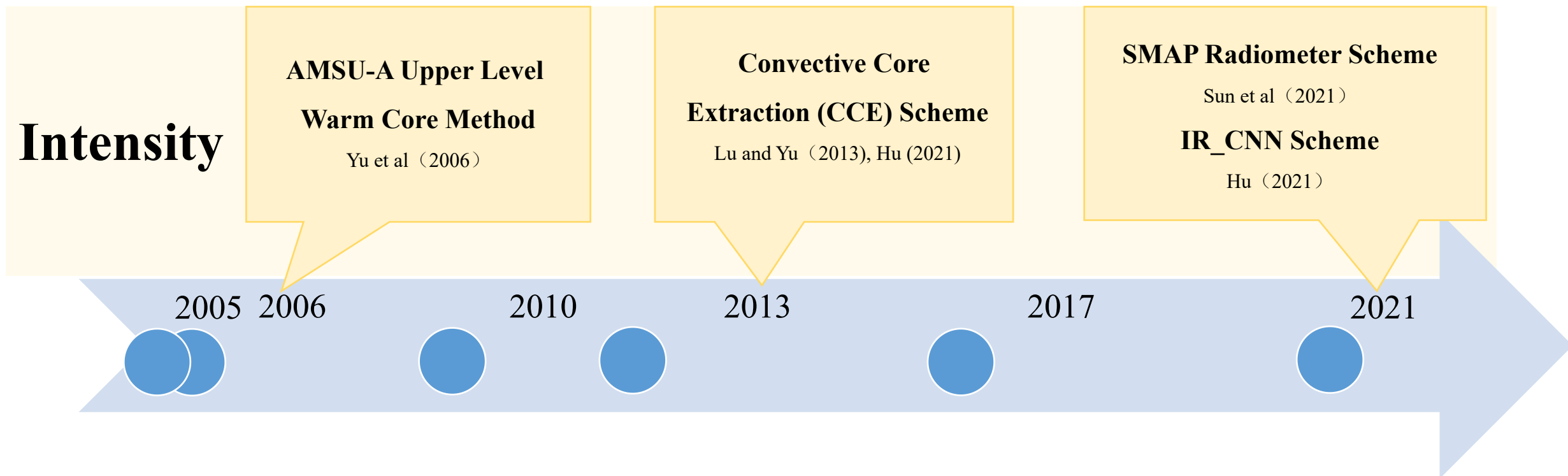


Data type	Method	RMSE (kt)	References	
data of geostationary satellite	Visible & Infrared data (DVORAK Technique)	determinantion of cloud types	9.71-12.08	Dvorak et al.1975,1984 Velden et al.1998 Olander et al.2002,2019
	IR data (Objective methods)	linear regression	10.18-14.48	Ritchie et al.2012,2014 Fetanat et al.2013 Lu et al.2013,2014,2021 Hu et al.2021 Zhuo andTan.2021
		K Nearest Neighbor (KNN)		
		Deviation Angle Variance Technique (DAV-T)		
		Convolutional Neural Network(CNN)		
.....				
data of other satellites	Passive microwave data	Stepwise Regression	12.0-19.8	Bankert et al.2002 Yu et al.2006 Hoshino et al.2007 Jiang et al.2019
		multi-variable statistical method		
		KNN		
			
	Infrared data (multi-channel)	Multiple Linear Regression(MLR)	4.08-14.70	Zhuge et al.2015 Wimmers et al.2019 Chen et al.2019 Zhang et al.2020
Passive microwave data(image data 、 wind data...)	Stepwise Regression			
	CNN			
.....				

Hu and Yu (2021)



TC intensity estimation techniques developed in STI





Convective Core Extraction (CCE) technique for intensity estimation

Lu and Yu, 2013
Hu, 2021



Data sources

- IR image datasets

MTSAT <http://weather.is.hochi-u.ac.jp/sat/GAME/>

resolution: 0.05 x 0.05 lat/lon degree

- Best track datasets

CMA <http://tcdata.typhoon.org.cn/en/index.html>

6 hourly lat, lon, vmax, pmin

JTWC <http://www.metoc.navy.mil/jtwc/jtwc.html>

6 hourly wind radii

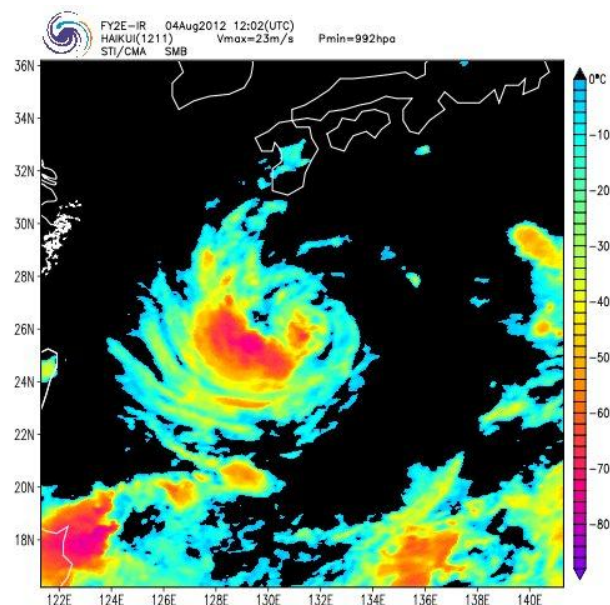
Convective Cell Extraction (CCE) technique for intensity estimation – methodology

Convective cells are searched by Convective-Stratiform Technique (CST, Adler et al. 1988).

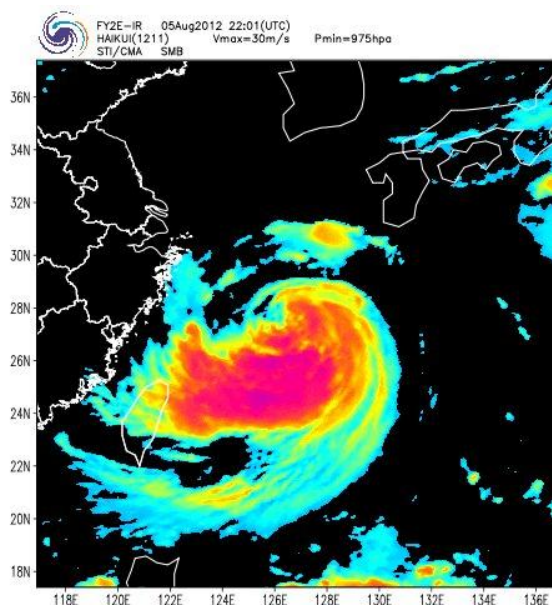
Minimum TBB pixel are regarded as the core of a convective cell if its gradient meets a given criterion.

$$S = \frac{5.8}{4} \times \left(\frac{T_{BB}(i-1,j) + T_{BB}(i+1,j) - 2T_{BB}(i,j)}{3.1} + \frac{T_{BB}(i,j+1) + T_{BB}(i,j-1) - 2T_{BB}(i,j)}{8.0} \right), \quad (1)$$

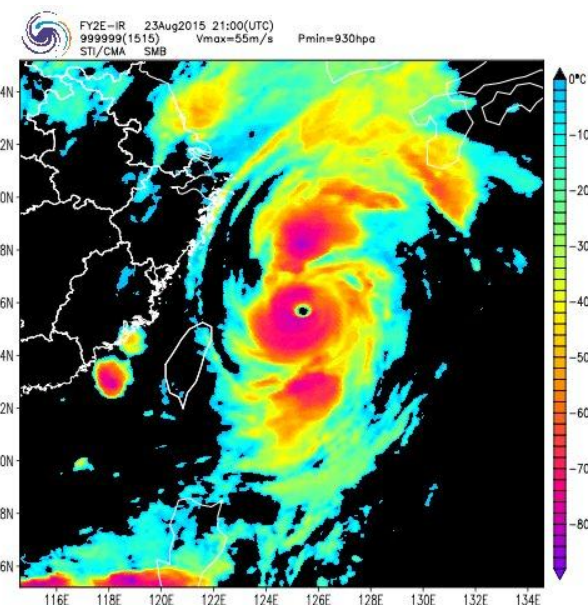
$$C = e^{0.0826 \times (T_{BB}(i,j) - 217)}. \quad (2)$$



Vmax=23 m/s



Vmax=30 m/s



Vmax=55 m/s



Convective Cell Extraction (CCE) technique for intensity estimation – methodology

Attributes of the convective cells

TABLE 1. Descriptions of convective-core attributes obtained from the IR images

Attribute	Description
DIS_{min}	Minimum distance between convective cores and TC center
DIS_{max}	Maximum distance between convective cores and TC center
TBB_{min}	Minimum convective core TBB value
TBB_{max}	Maximum convective core TBB value
Num	Number of convective cores
TBB_{mean}	Mean convective core TBB value
DIS_{mean}	Mean distance between convective cores and TC center
TBB_{dif}	Difference between TBB_{max} and TBB_{min}
I_{TBB}	$\sqrt{\frac{(TBB_{max})^2 + (TBB_{mean})^2}{2}}$
I_{DIS}	$\sqrt{\frac{(DIS_{max})^2 + (DIS_{mean})^2}{2}}$

Number



Intensity



Distance

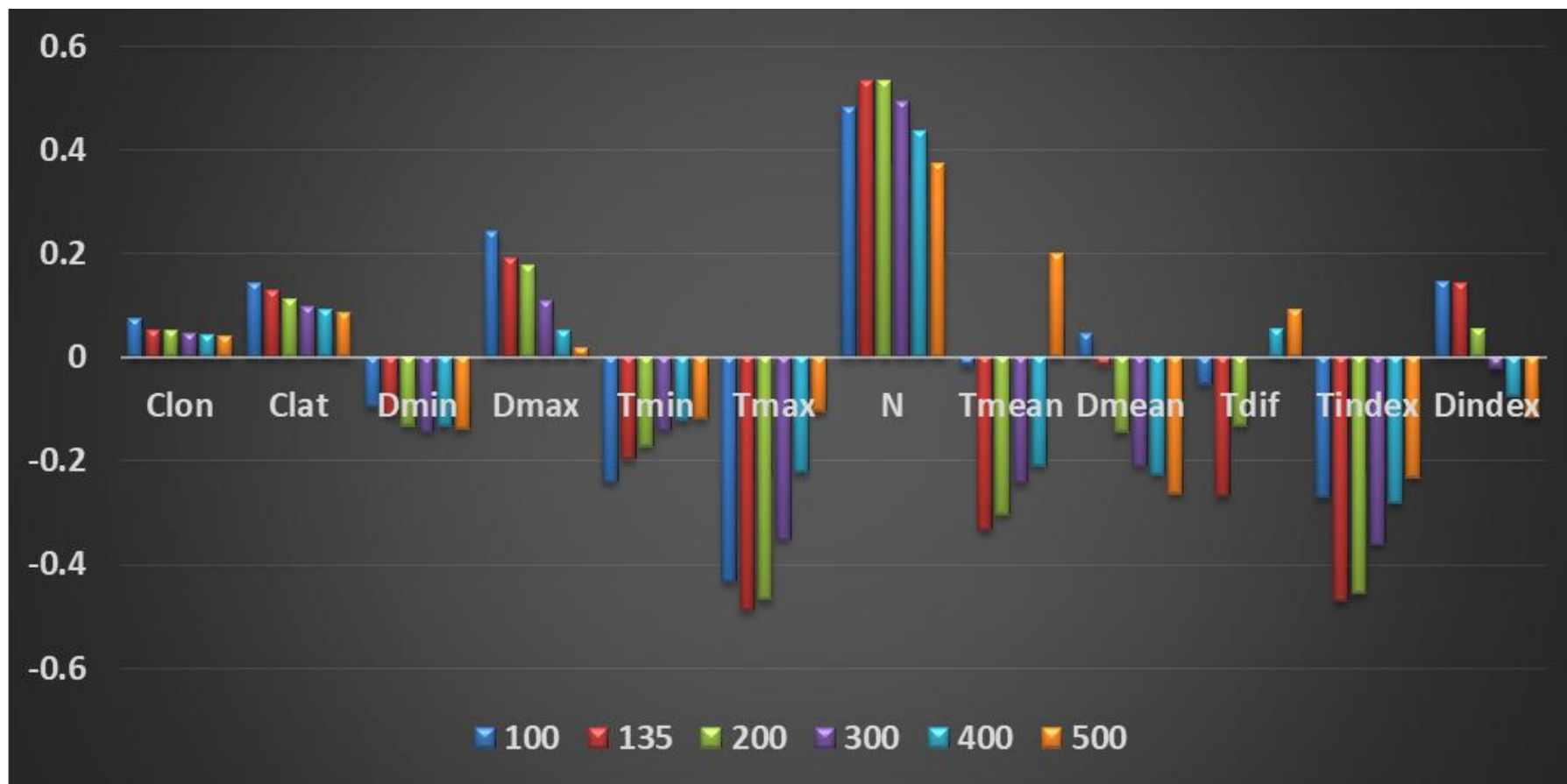


TC
intensity



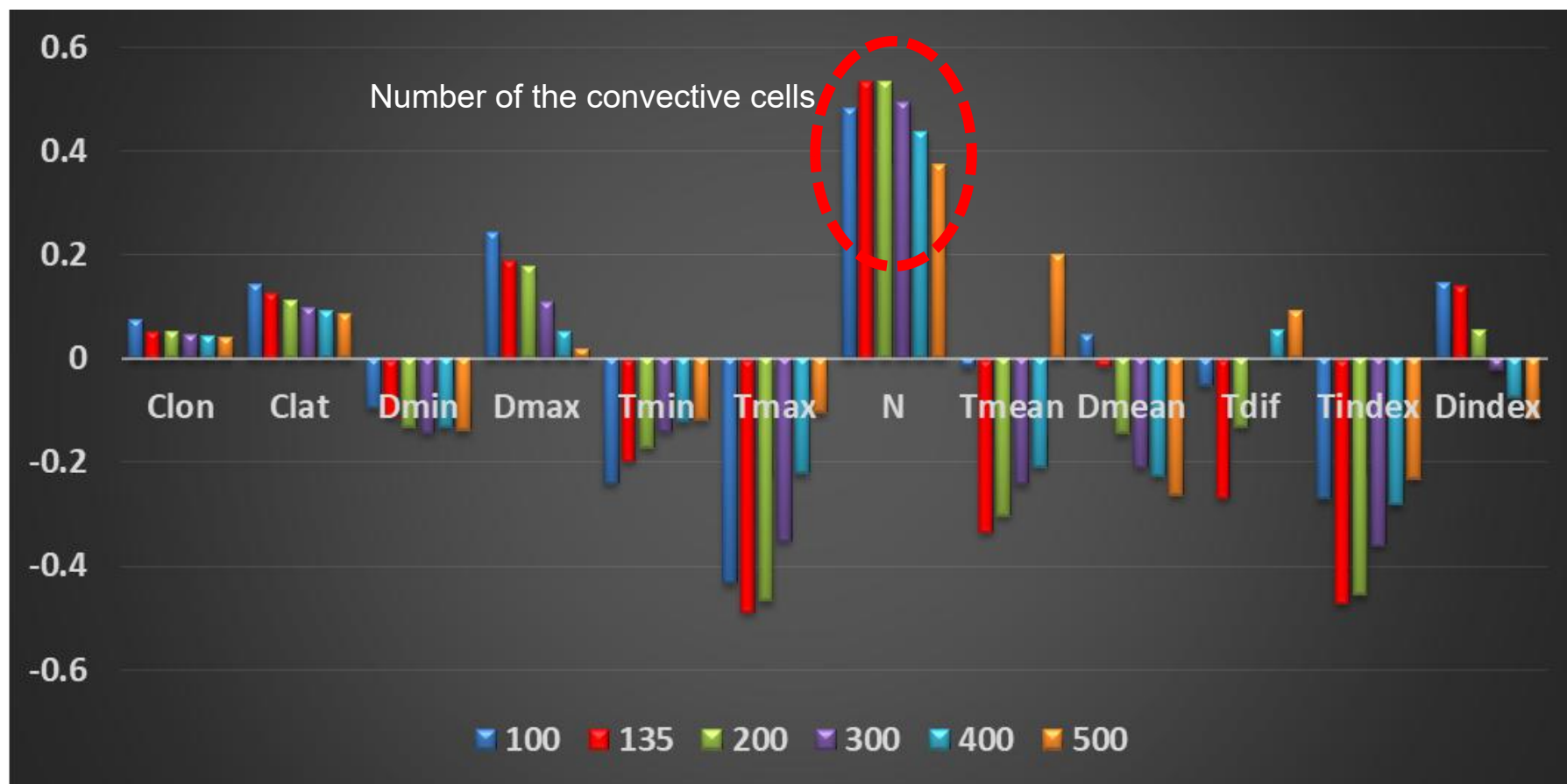
Convective Cell Extraction (CCE) technique for intensity estimation – sensitivity tests

What is the best radius for searching the convective cells?



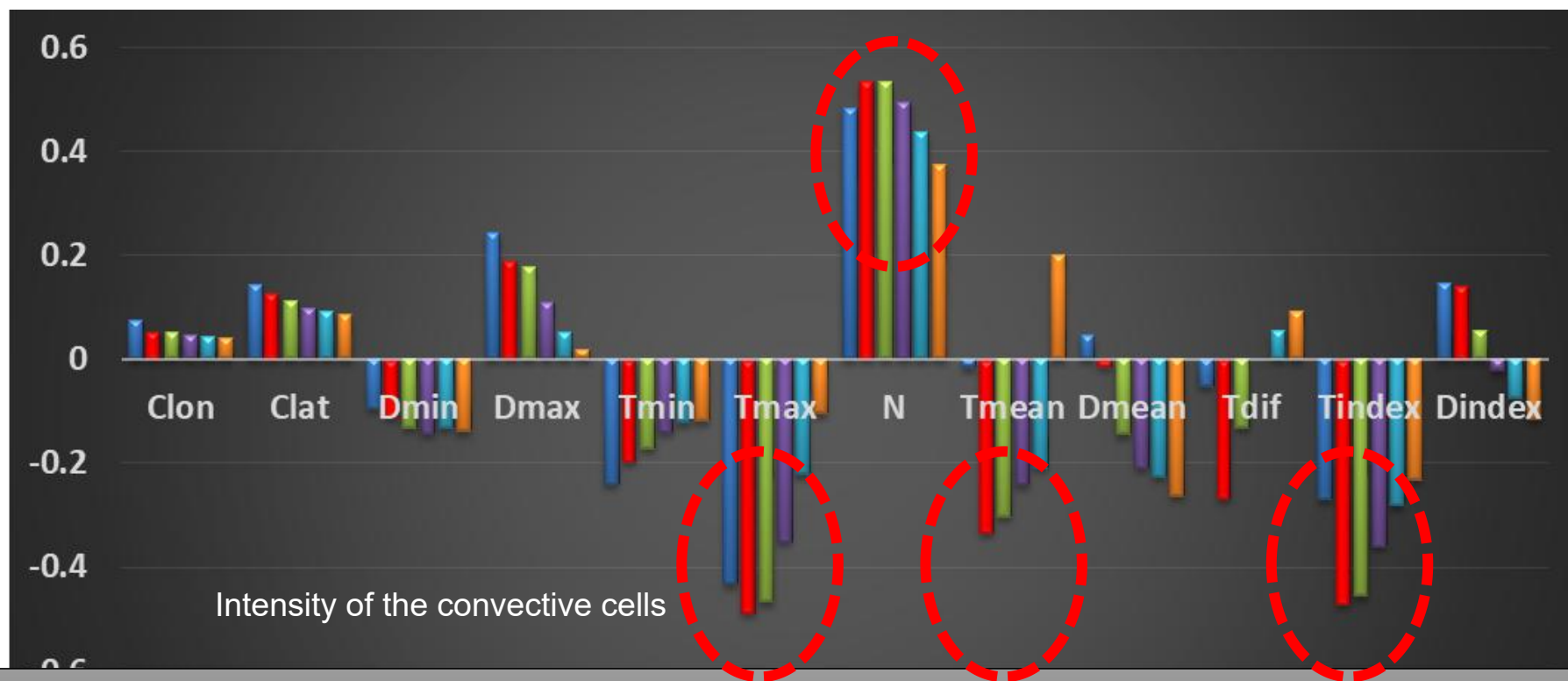
Convective Cell Extraction (CCE) technique for intensity estimation – sensitivity tests

What is the best radius for searching the convective cells?



Convective Cell Extraction (CCE) technique for intensity estimation – sensitivity tests

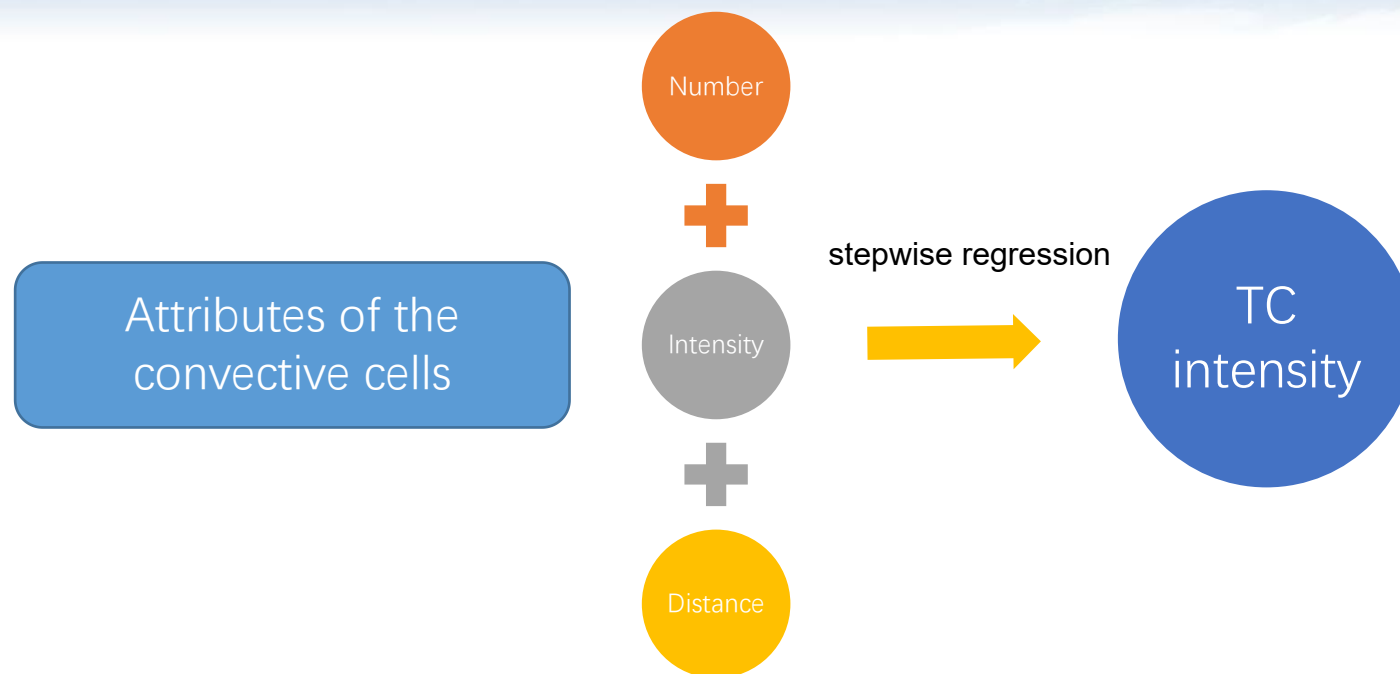
What is the best radius for searching the convective cells?



135km ~ maximum value of the radius of maximum wind



Convective Cell Extraction (CCE) technique for intensity estimation – sensitivity tests



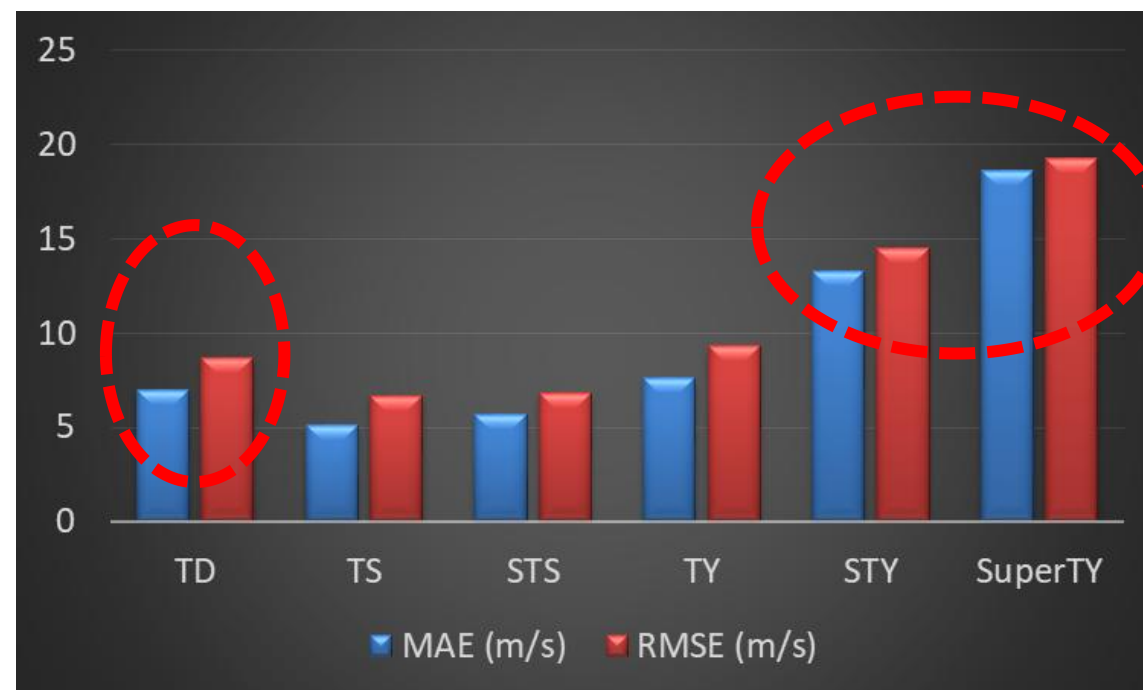
	Dependent samples (1494)	Independent samples (406)
MAE(m/s)	7.3	7.4
RMSE(m/s)	9.2	9.6



Convective Cell Extraction (CCE) technique for intensity estimation – sensitivity tests

	Dependent samples (1494)	Independent samples (406)
MAE(m/s)	5.5 (7.3)	5.9 (7.4)
RMSE(m/s)	6.9 (9.2)	7.7 (9.6)

Bias correction for weak and strong TCs.





Convective Cell Extraction (CCE) technique for intensity estimation – sensitivity tests

	Dependent samples (1494)	Independent samples (406)
MAE(m/s)	5.5 (7.3)	5.9 (7.4)
RMSE(m/s)	6.9 (9.2)	7.7 (9.6)

Persistency in intensity:

The correlation coefficient is 0.973 between current Vmax and the Vmax 6 hours before (sample size: 2676).

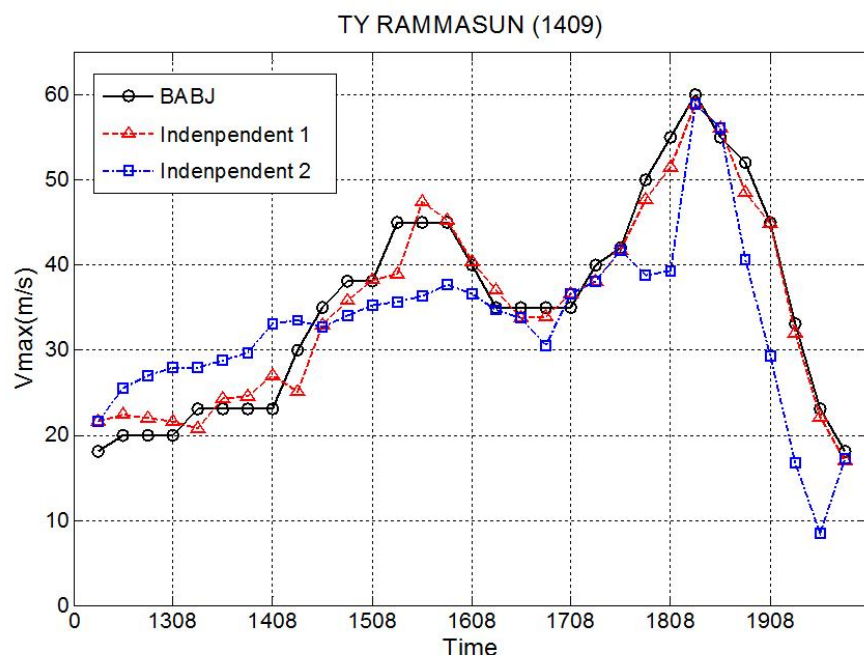
	Dependent samples (2676)	Independent samples (1221)
MAE(m/s)	1.77	1.75 (5.4)
RMSE(m/s)	2.42	2.42 (7.3)

Based on the best track

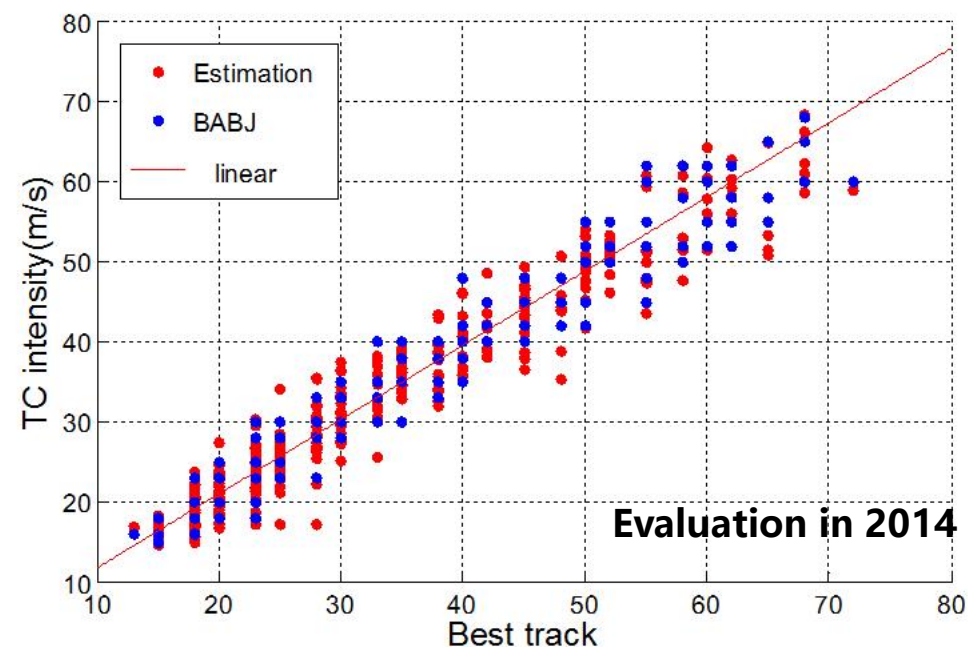
Based on the real time warning

Convective Cell Extraction (CCE) technique for intensity estimation – application

CCE technique was put into use as a guidance for the best track analyses in CMA since 2014.



	CCE (2014-2016)	Dvorak (Knaff, 2010)
MAE(m/s)	4.6	4.1
RMSE(m/s)	6.5	5.7





Application and improvement of CCE technique in Atlantic

method		Channel	RMSE (kt)	
CCE	Stepwise Regression	IR(11 μ m)	13.16	
	Deep Neural Network		12.64	3.4%
	Convolutional Neural Network		10.59	19.5%

Structure optimization of convolutional neural networks

1

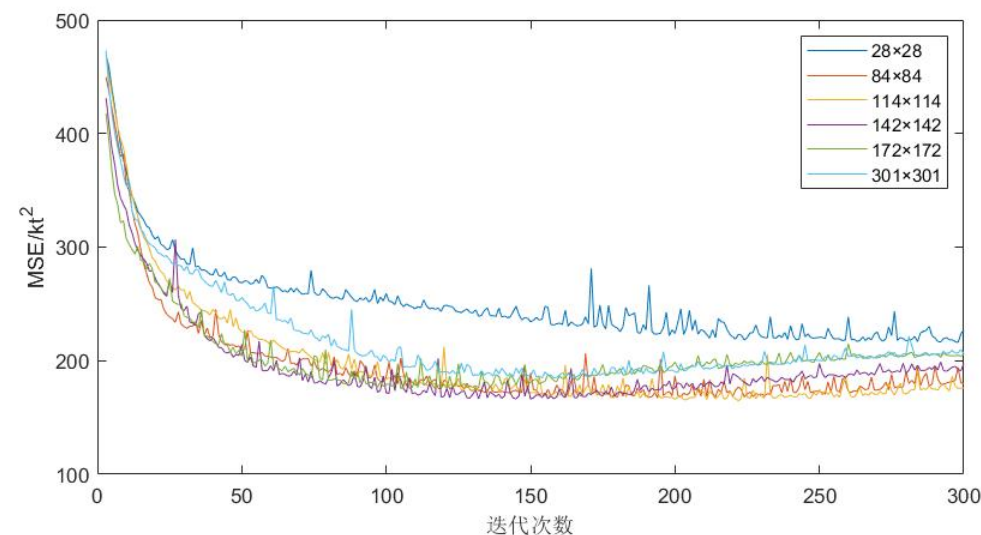
Optimization of
input range

2

Optimization of
convolution and
pooling layer

3

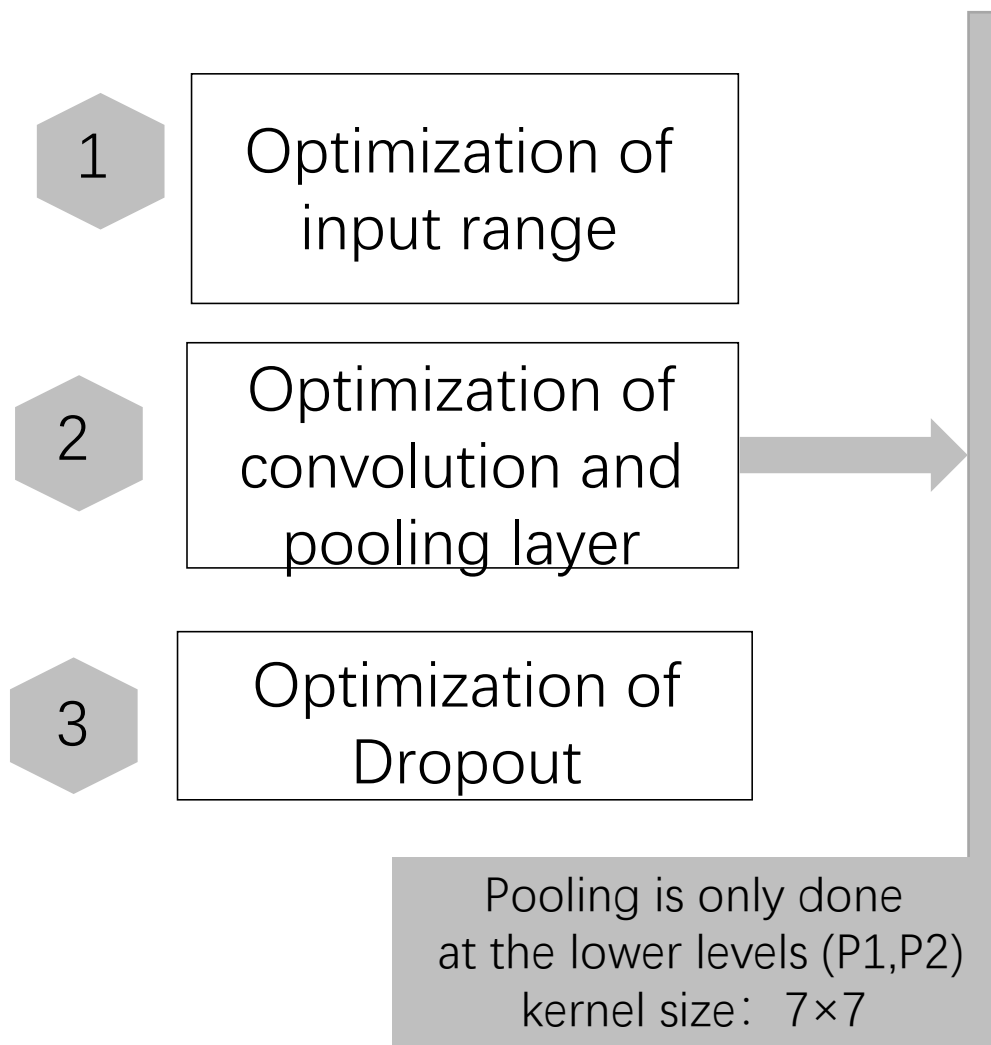
Optimization of
Dropout



Training results of experiments with
different input ranges

optimum input range: 114×114

Structure optimization of convolutional neural networks



The RMSE of different models in test samples

model structure	RMSE (kt)
C1P1C2P2C3P3C4P4F1F2F3	13.21
C1P1C2P2C3P3C4F1F2F3	12.80
C1P1C2P2C3C4F1F2F3	12.57
C1C2C3C4F1F2F3	13.80

Training results with different size of convolution kernels

Convolution kernel size	Error of training set (MAE / kt)	Error of validation set (MAE / kt)
1×1	10.31	11.33
3×3	7.11	10.18
5×5	8.28	10.18
7×7	7.97	9.66
7×7 (Dropout)	8.37	9.60



Structure optimization of convolutional neural networks

1

Optimization of
input range

2

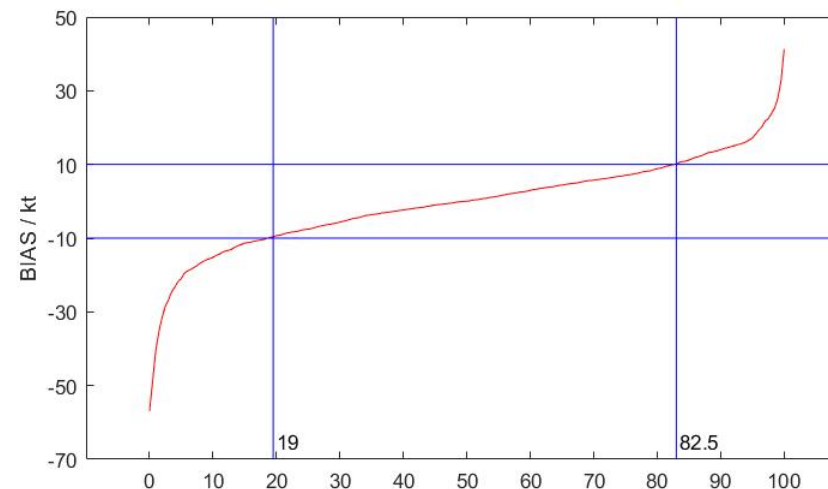
Optimization of
convolution and
pooling layer

3

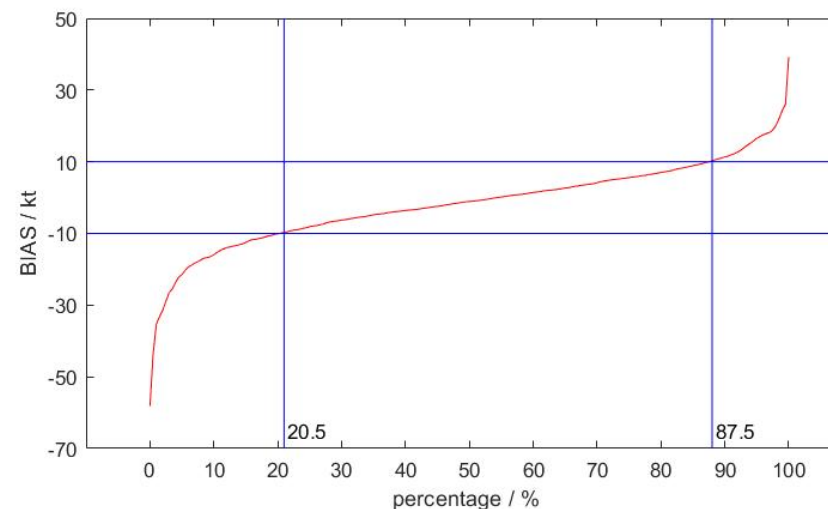
Optimization of
Dropout



(a)



(b)

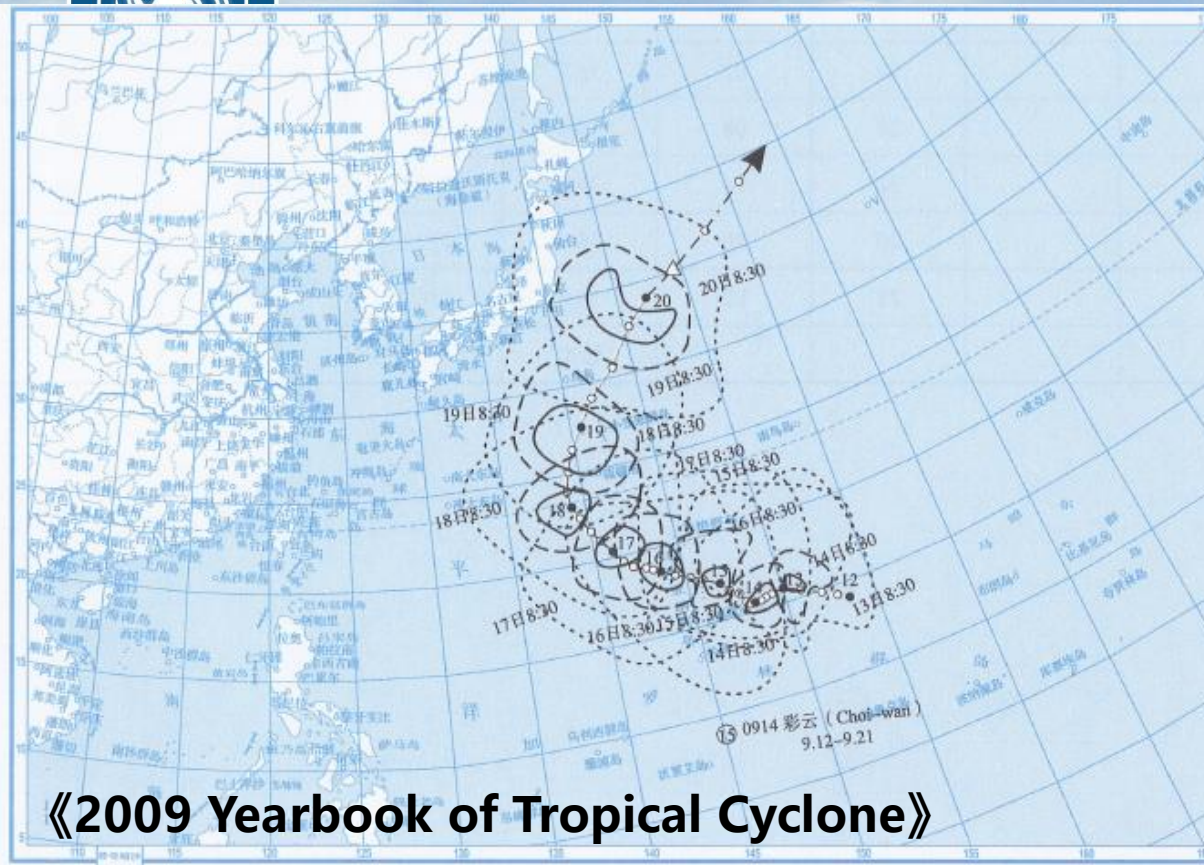


Error distribution of TC intensity estimation on test set
(a) without Dropout (b) with Dropout



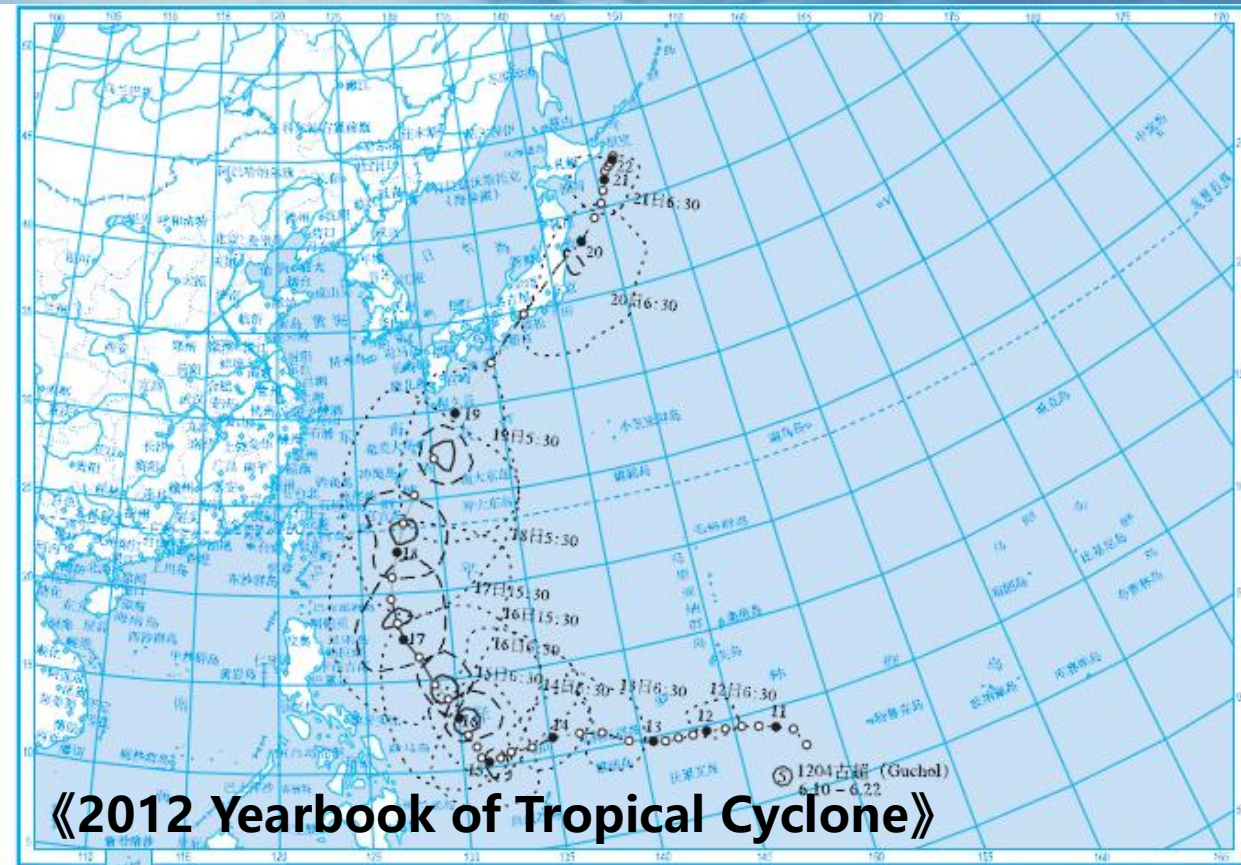
Application and improvement of CCE technique in Atlantic

Method		Channel	RMSE (kt)	
DAV		IR(10.7 μ m)	14.7	
DAV		IR(10.7 μ m)	12.9 (V \geq 34 kt)	
Histogram matching approach		IR(10.7 μ m)	14.8-15.47	
KNN		IR(11 μ m)	12.7	
ADT		IR(PMW)	11.67	
CCE	Stepwise Regression	IR(11 μ m)	13.16	3.4%
	Deep Neural Network		12.64	
	Convolutional Neural Network (CNN)		10.59	19.5%



《2009 Yearbook of Tropical Cyclone》

图 2.15.2 超强台风“彩云 (Choi-wan)”大风区域演变图



《2012 Yearbook of Tropical Cyclone》

图 2.5.2 1204 号超强台风“古超 (Guchol)”大风区域演变图 (6 月 10—21 日)

QuikScat

Lu (2005-2009)

SSMI和SSMIS

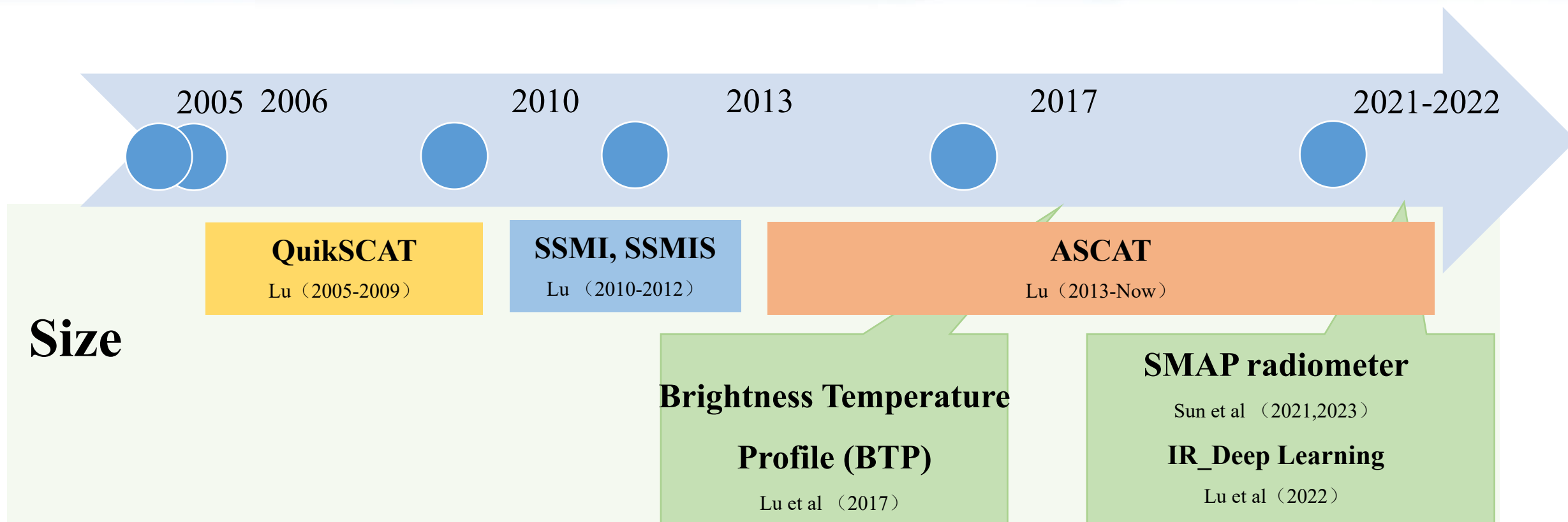
Lu (2010-2012)

ASCAT

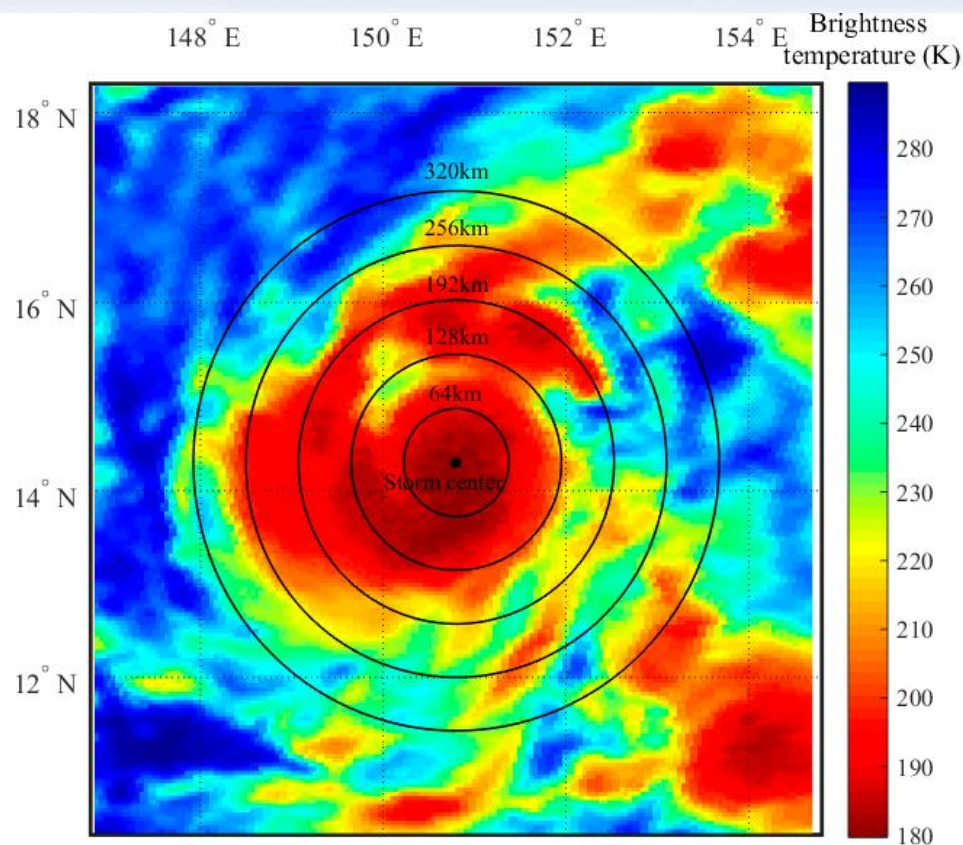
Lu (2013-now)



TC Size estimation techniques developed in STI

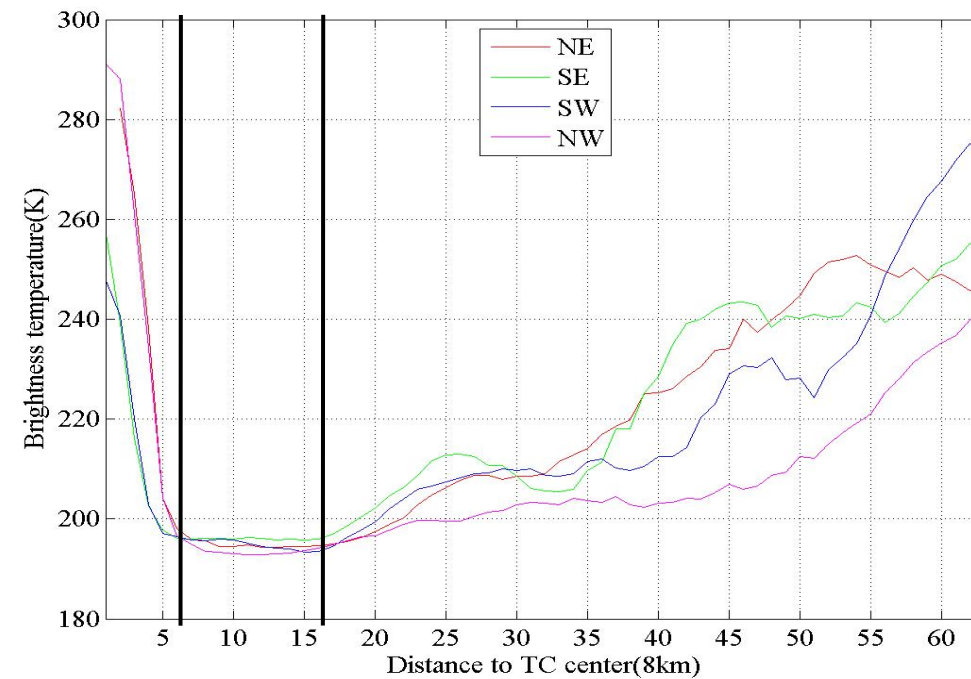
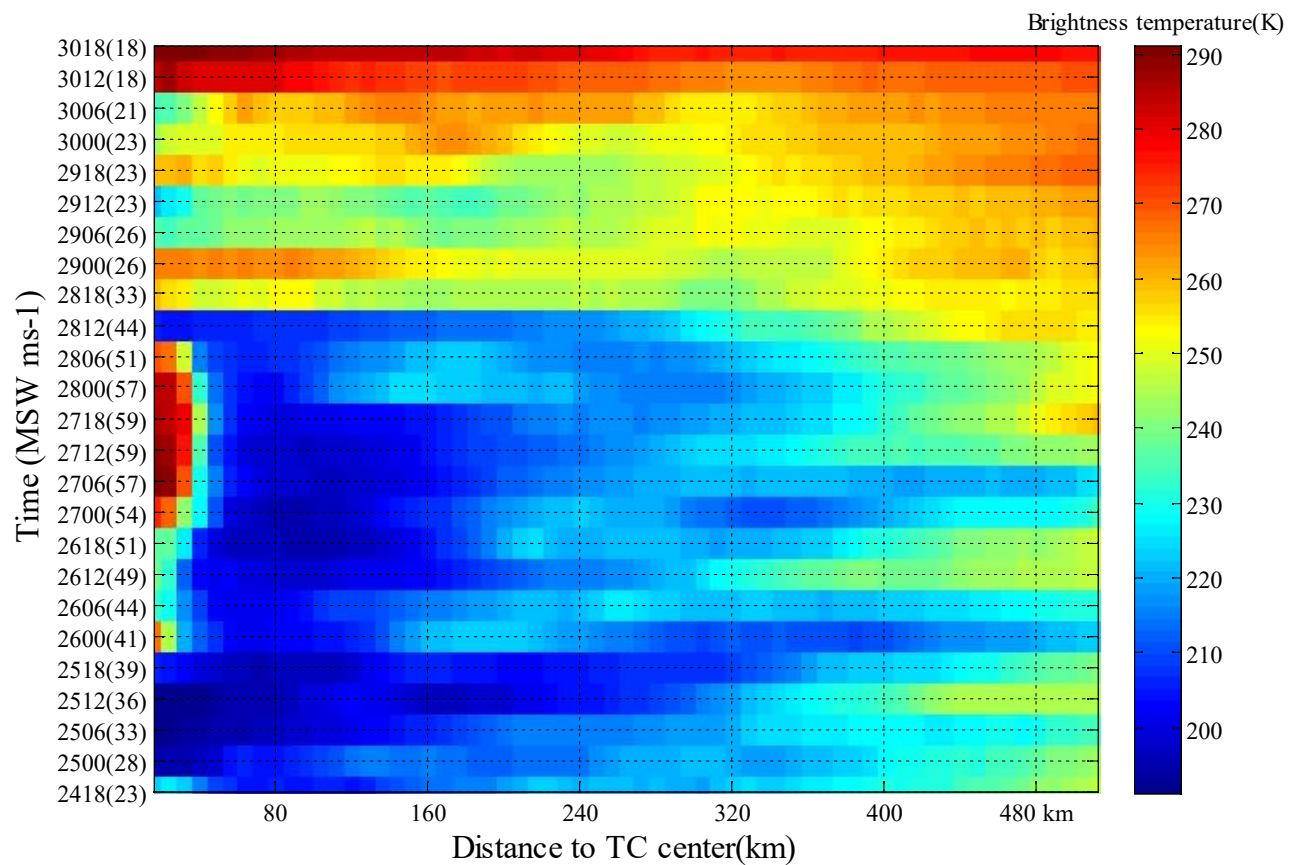


Brightness Temperature Profile (BTP) technique for size estimation – methodology



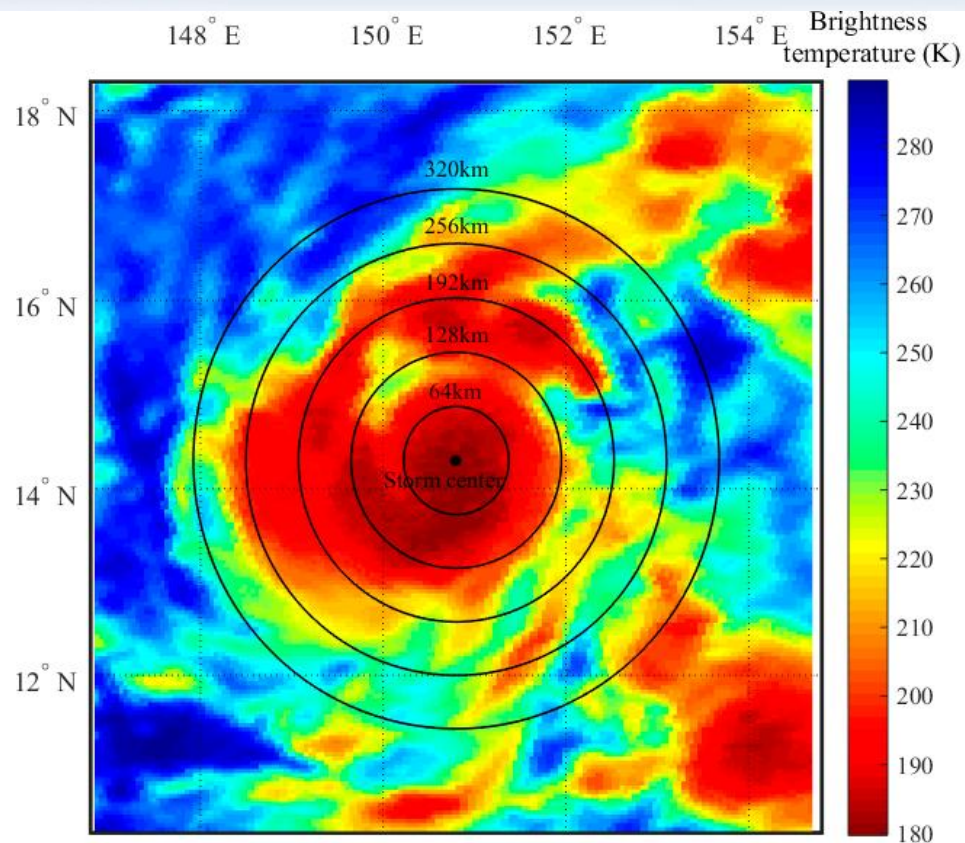
Mean brightness temperature is calculated in 20 annuli every 16km from the TC center.

Schematic diagram for the definition of concentric annuli (every 16 km). The black filled circle is the TC center. The large black circles are the annuli at the radii of 64, 128, 192, 256, and 320 km. Other annuli are not shown here for a visibility purpose.



2008 Jangmi (MTS-1)

Brightness Temperature Profile (BTP) technique for size estimation – methodology



Attributes of cloud-top brightness temperature (BT) in the defined annuli

Mean BT



Mean BT Difference



TC intensity

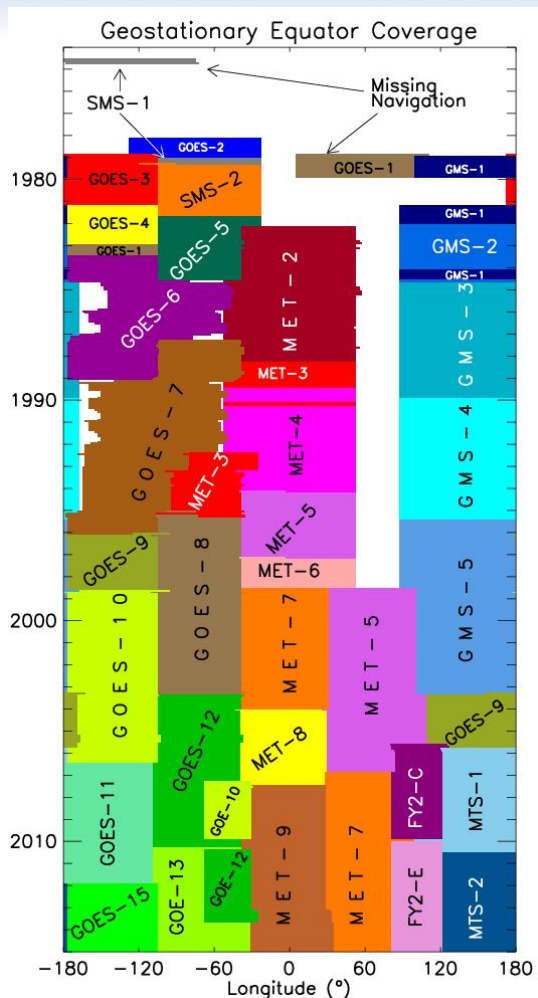


TC size

Schematic diagram for the definition of concentric annuli (every 16 km). The black filled circle is the TC center. The large black circles are the annuli at the radii of 64, 128, 192, 256, and 320 km. Other annuli are not shown here for a visibility purpose.



Brightness Temperature Profile (BTP) technique for size estimation – methodology



HURSAT dataset

Knapp and Kossin, 2007

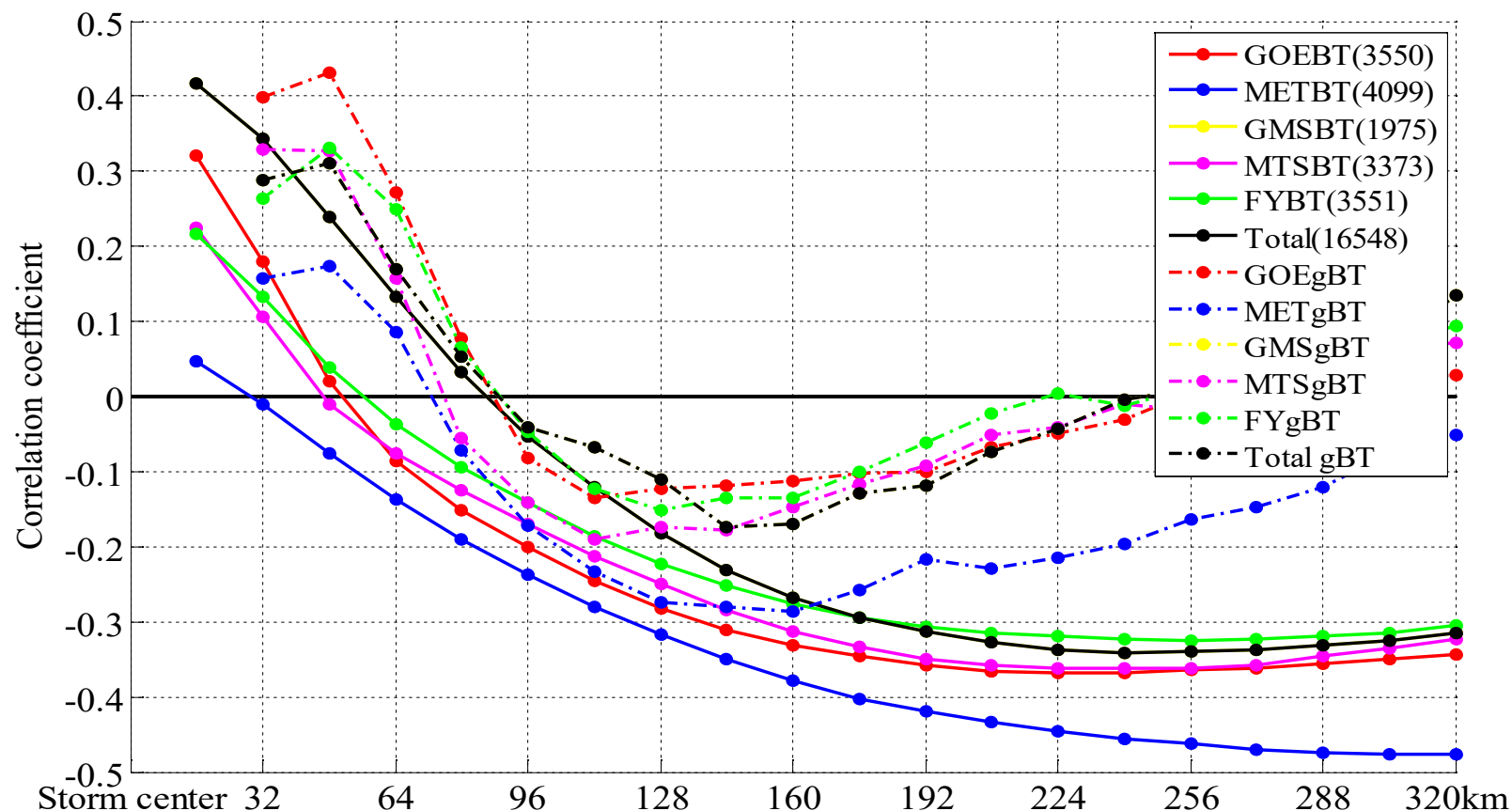
Table 1. Satellite data used to establish and test the model for the estimation of the size of TCs.

Satellite	Time Period	No. of TCs	Sample Size	Dependent Sample Size (Time)	Independent Sample Size (Time)
GOES	2001–2009	85	3550	3480 (2001–2006)	70 (2007–2009)
MET	2001–2009	132	4099	3079 (2001–2006)	1020 (2007–2009)
FY2	2005–2009	97	3551	2783 (2005–2008)	768 (2009)
MTS	2005–2009	85	3373	2552 (2005–2008)	821 (2009)
GMS	2001–2003	49	1975	1792 (2001–2002)	183 (2003)
Total	2001–2009	197	16,548	11,288 (2001–2006)	5260 (2007–2009)



Brightness Temperature Profile (BTP) technique for size estimation – methodology

Positive in the inner core region.

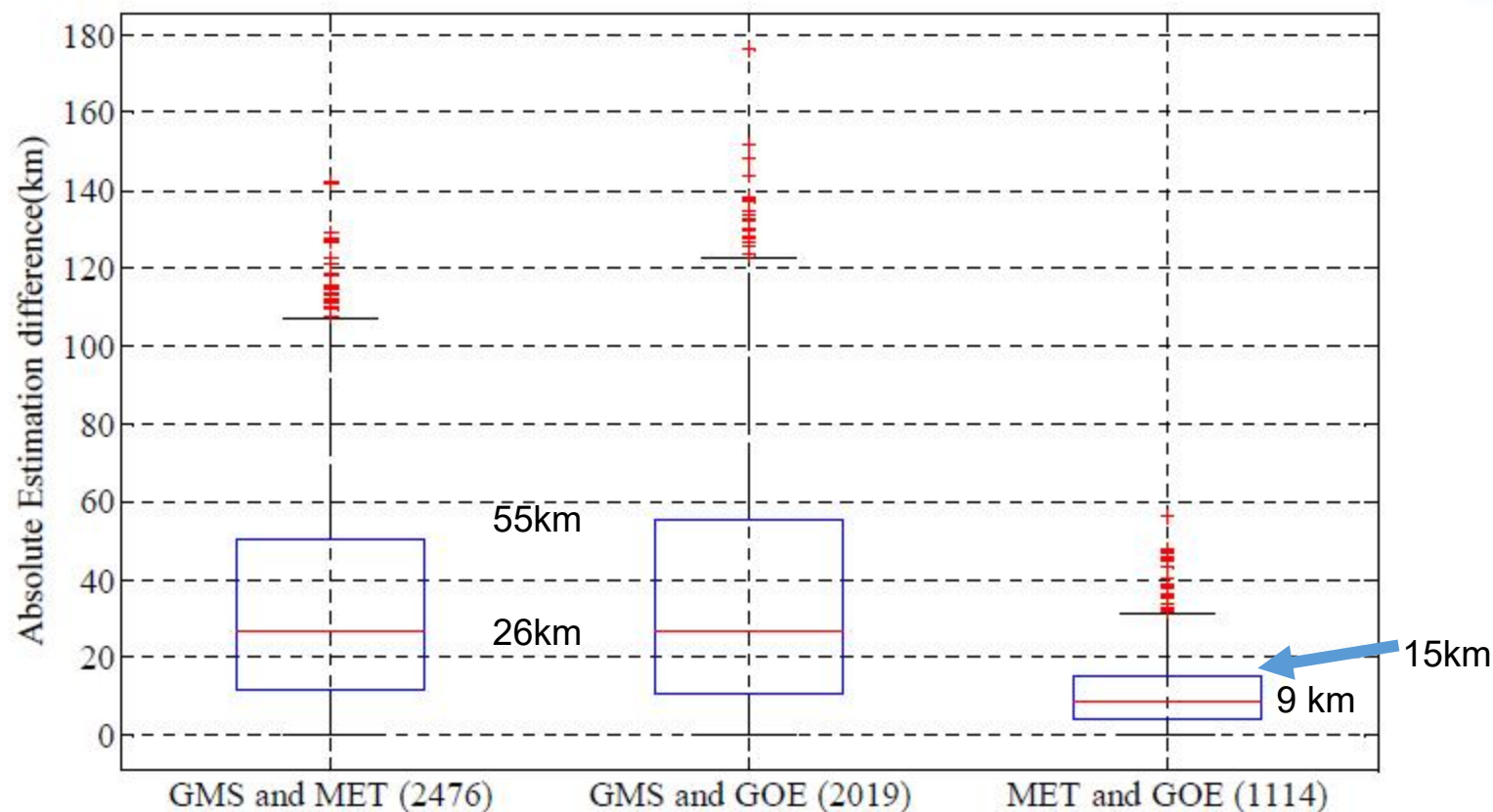


Negative further away.

Correlation coefficients between R34 and BTP attributes from different satellites. Solid: mean BT. Dashed: difference in neighboring mean BT.



Brightness Temperature Profile (BTP) technique for size estimation – sensitivity tests



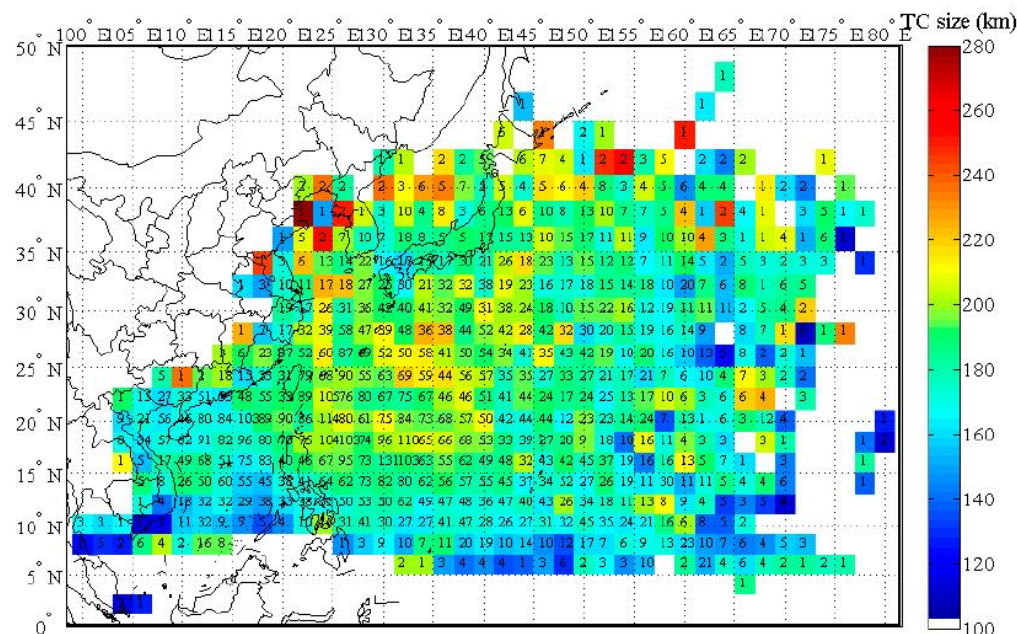
Box-plot of the difference in size as estimated from different satellites.

The difference in TC size estimation using observations from different satellites is operationally acceptable.

Brightness Temperature Profile (BTP) technique for size estimation – application

R34 of 721 TCs from 1980 to 2009 were obtained for 13726 samples.

	R34 (km)
Mean	184
25%	148
75%	215



Geographical distribution of R34 during 1980-2009.



CMA TROPICAL CYCLONE DATA CENTER

for the western North Pacific Basin

English 中文

Location: Scientific Research Data Products > TC Size Analysis

Introduction

National-level operational data product

Scientific Research Data Products

- TC Size Analysis
- Field Experiment
- TC Potential Risk

Key Project: Research and demonstration application of key physical processes of typhoon variable resolution prediction model

Other Product Metadata

Publications

General description of the retrieved Tropical Cyclone Size Dataset (v1.0)

The retrieved Tropical Cyclone Size Dataset covers tropical cyclones that developed over the western North Pacific and captured by satellites. The basin is to the north of the equator and to the west of 180°E, and includes the South China Sea (SCS).

The present version (2.0) of the dataset includes 6-hourly track, intensity analyses and retrieval size between 1980 and 2016 for TCs with intensities of and above tropical storms (MSW>17.2m/s).

Updates and downloads:

Recently updated: Nov., 2020

Since Nov., 2020, the total number of downloads: 3031

Citation

Please indicate that the Tropical Cyclone size data was obtained from tcdata.typhoon.org.cn, and refer to the following paper in any written work using the dataset:

- Xiaoqin Lu, Hui Yu, Xiaoming Yang and Xiaofeng Li, 2017: Estimating Tropical Cyclone Size in the Northwestern Pacific from Geostationary Satellite Infrared Images. Remote Sens. 9: 728. doi:10.3390/rs907072

Improvements with machine learning algorithms (Lu et al. 2022)

Previous studies	Dataset used for estimation	Dataset used for validation	RMW	R64	R50	R34
Demuth et al., 2006	AMSU	Aircraft reconnaissance and best track	/	13	25	31
Mueller et al., 2006	IR	Aircraft reconnaissance data	27	/	/	/
Kossin et al., 2007	IR	Aircraft reconnaissance data	21	27	37	45
Knaff et al., 2011	Scatterometer, AMSU, and IR et al.	H*wind	/	24	33	68
Knaff et al., 2016	IR	Best track	/	22	37	69
Lu et al., 2017	IR	Best track	/	/	/	27~65
This study	IR	Best track	13	18	30	43

(general regression neural network & support vector machine)

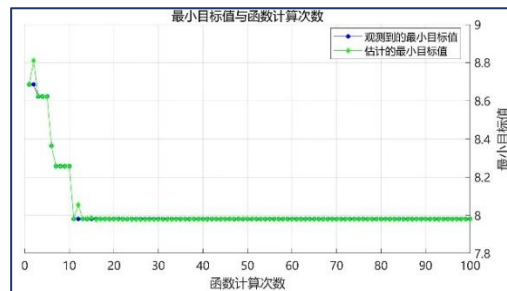


Table 1. Parameters for the different machine learning methods used in the experiments.

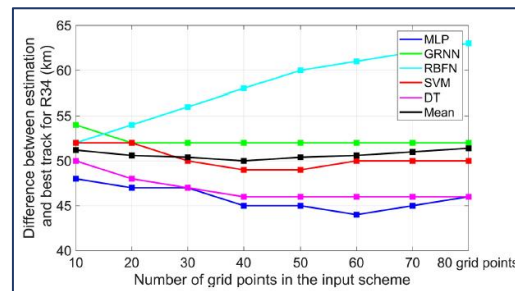
Algorithm	Parameter setting	Input
Multi-Layer Perceptron (MLP)	Epochs = 10000; Learning rate = 0.005; Learn function = 'tansig'; Transform function = 'purelin'; Max fail = 10; Goal = 0.01; Perform function = 'mse'; Hidden layer size = $\log_2 N$ (N is the input size).	The longitude (Lon) and latitude (Lat) of TC center, TC intensity (MSW), and (BT) radial profile (BTP) within the radius R
General Regression Neural Network (GRNN)	Spread = 25.	Ditto
Radial Basis Function Network (RBFN)	Maximum number of neurons = 1000; Number of neurons to add between displays = 10; Spread = 25; Goal = 0.01.	Ditto
Support Vector Machine (SVM)	Kernel function = 'gaussian'; Kernel scale = 'auto';	Ditto
Decision Tree (DT)	Number of trees = 50; Method = 'regression'.	Ditto

Algorithm	Parameter setting	Input
Multi-Layer Perceptron (MLP)	Epochs = 10000; Learning rate = 0.005; Learn function = 'tansig'; Transform function = 'purelin'; Max fail = 10; Goal = 0.01; Perform function = 'mse'; Hidden layer size = log ₂ N (N is the input size).	The longitude (Lon) and latitude (Lat) of TC center, TC intensity (MSW), and (BT) radial profile (BTP) within the radius R
General Regression Neural Network (GRNN)	Spread = 25.	Ditto
Radial Basis Function Network (RBFN)	Maximum number of neurons = 1000; Number of neurons to add between displays = 10; Spread = 25; Goal = 0.01.	Ditto
Support Vector Machine (SVM)	Kernel function = 'gaussian'; Kernel scale = 'auto';	Ditto
Decision Tree (DT)	Number of trees = 50; Method = 'regression'.	Ditto

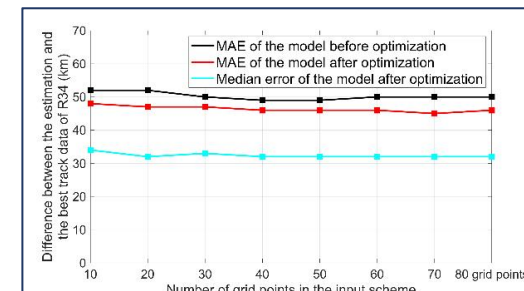
Parameter settings



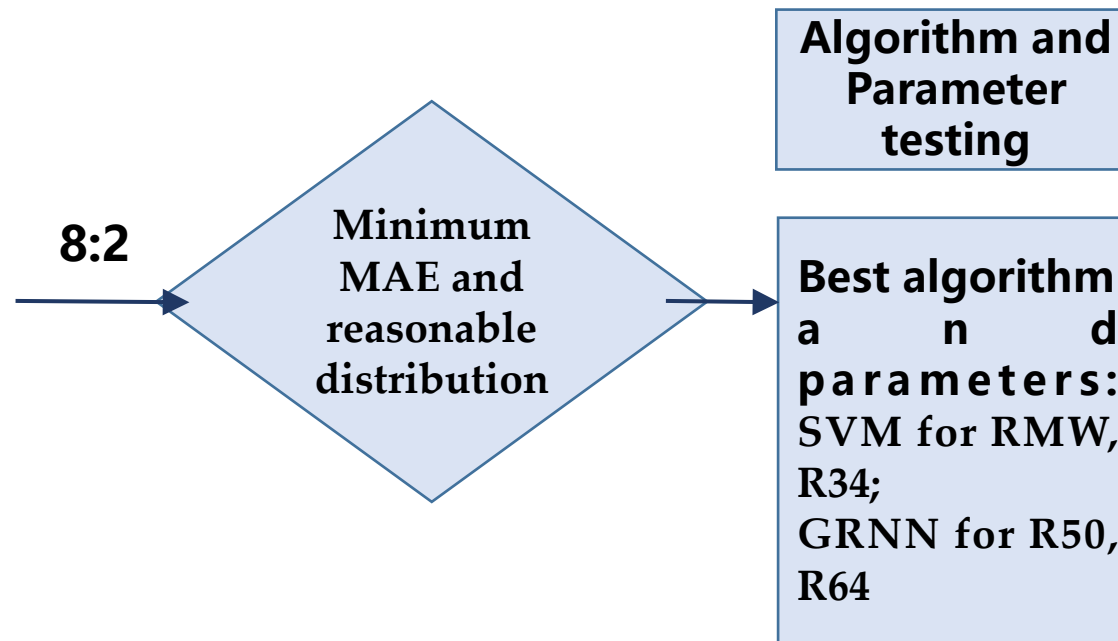
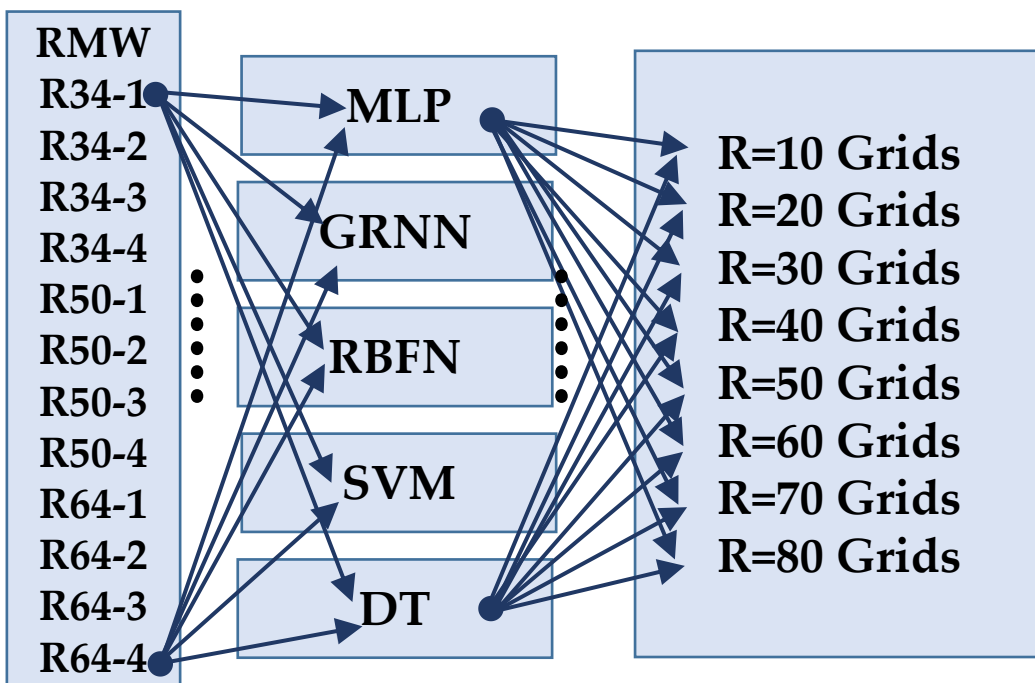
Training (R34)

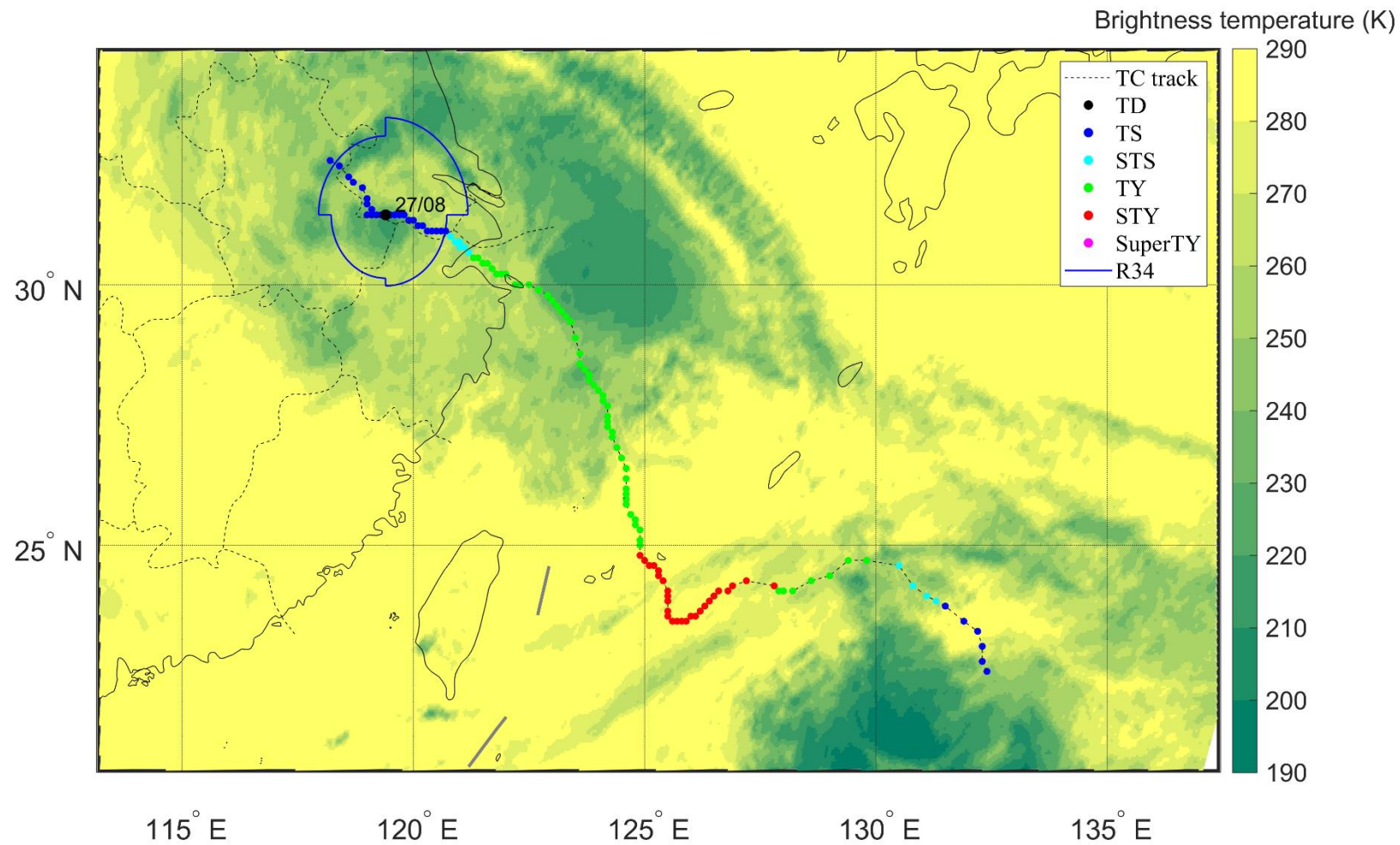


Evaluation (R34)

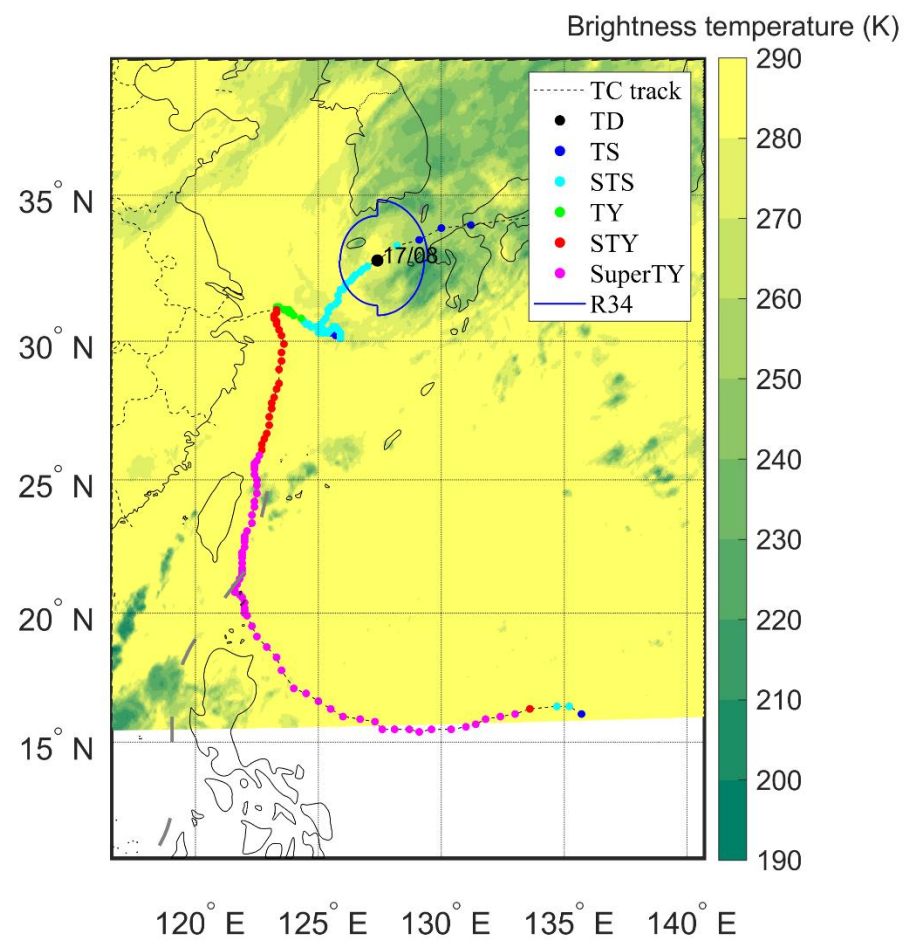


Optimization (R34)





Evolution of R34 for In-fa (2021)



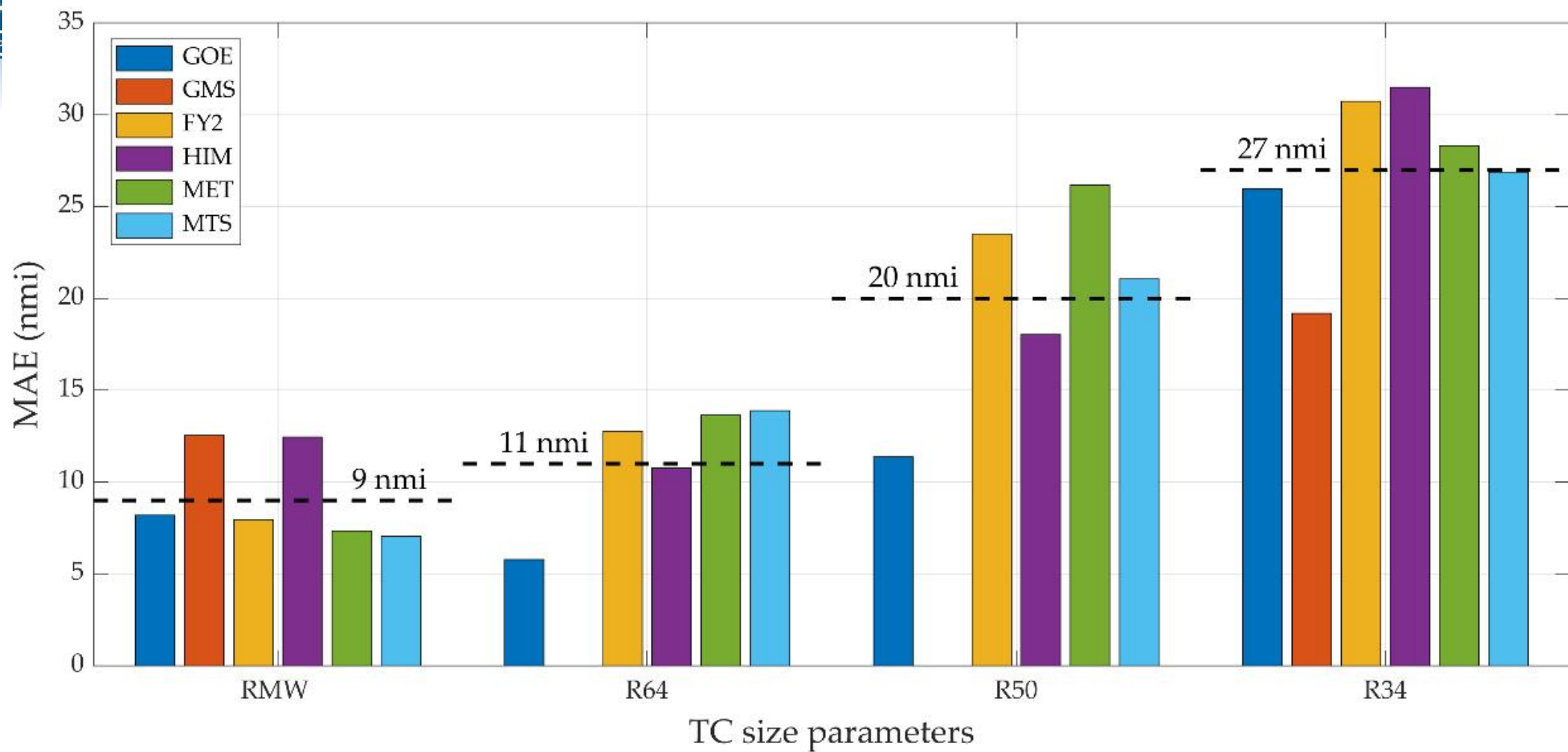
Evolution of R34 for Chanthu (2021)



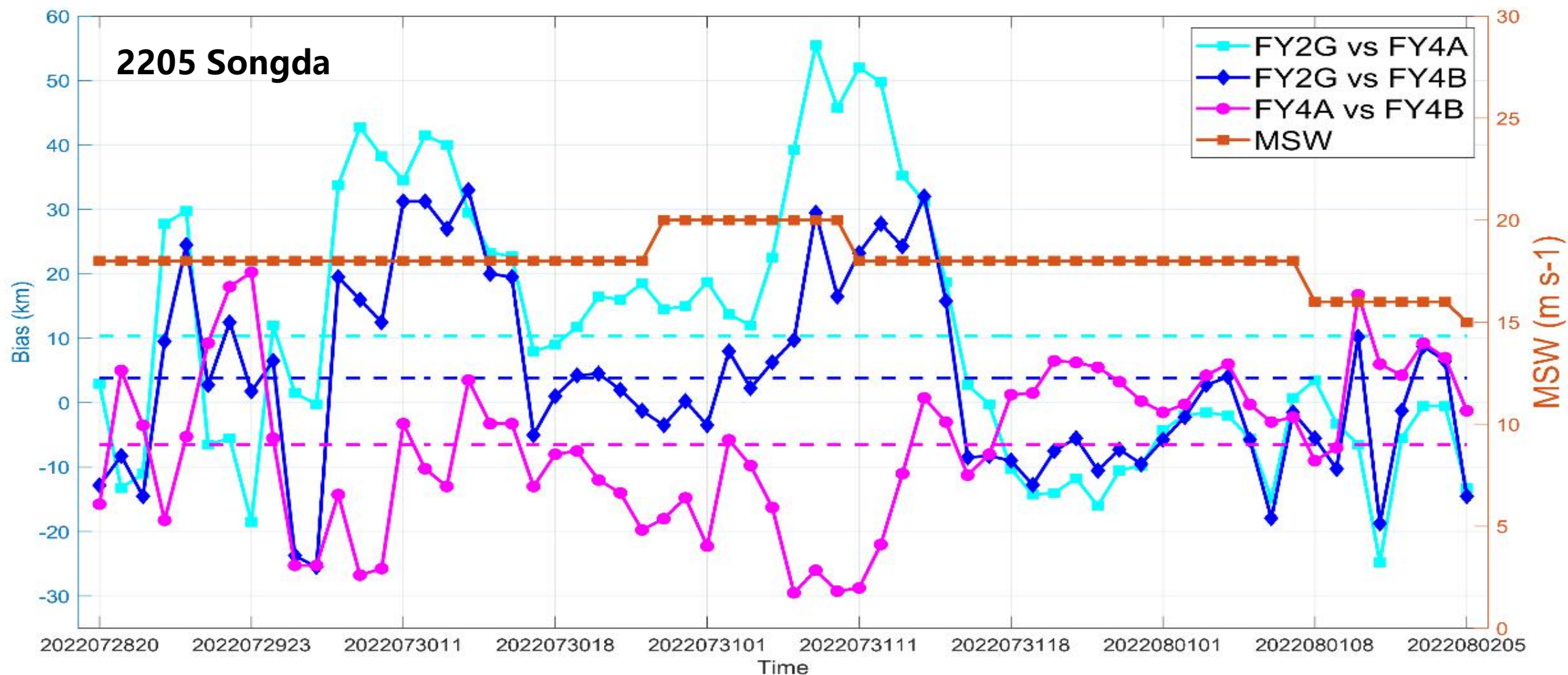
AlexNet Framework: convolutional neural networks (on-going work)

Ocean (Satellite)	TC size parameters	Estimation error (nmi)	
		MAE	RMSE
Pacific (GMS, GOE, MET, FY-2, MTS, HIM)	RMW	8.10	10.89
	R34	25.89	34.89
	R50	11.76	15.43
	R64	10.24	13.06
Atlantic (GOES, MET)	RMW	15.16	22.80
	R34	28.23	40.09
	R50	16.72	23.80
	R64	12.43	16.54
Western North Pacific (FY-2)	RMW	5.95	7.85
	R34	23.11	28.65
	R50	18.64	23.64
	R64	11.73	14.09

Model	Used data	RMW	R64	R50	R34
Knaff et al.(2011)	Scatterometer, AMSU, IR et al	/	13.00	17.80	36.50
Kossin et al.(2007)	IR	12.42	16.04	22.35	27.16
Knaff et al.(2016)	IR	/	12.00	20.00	37.00
TCSE (This study)	IR	15.16	12.43	16.72	28.23



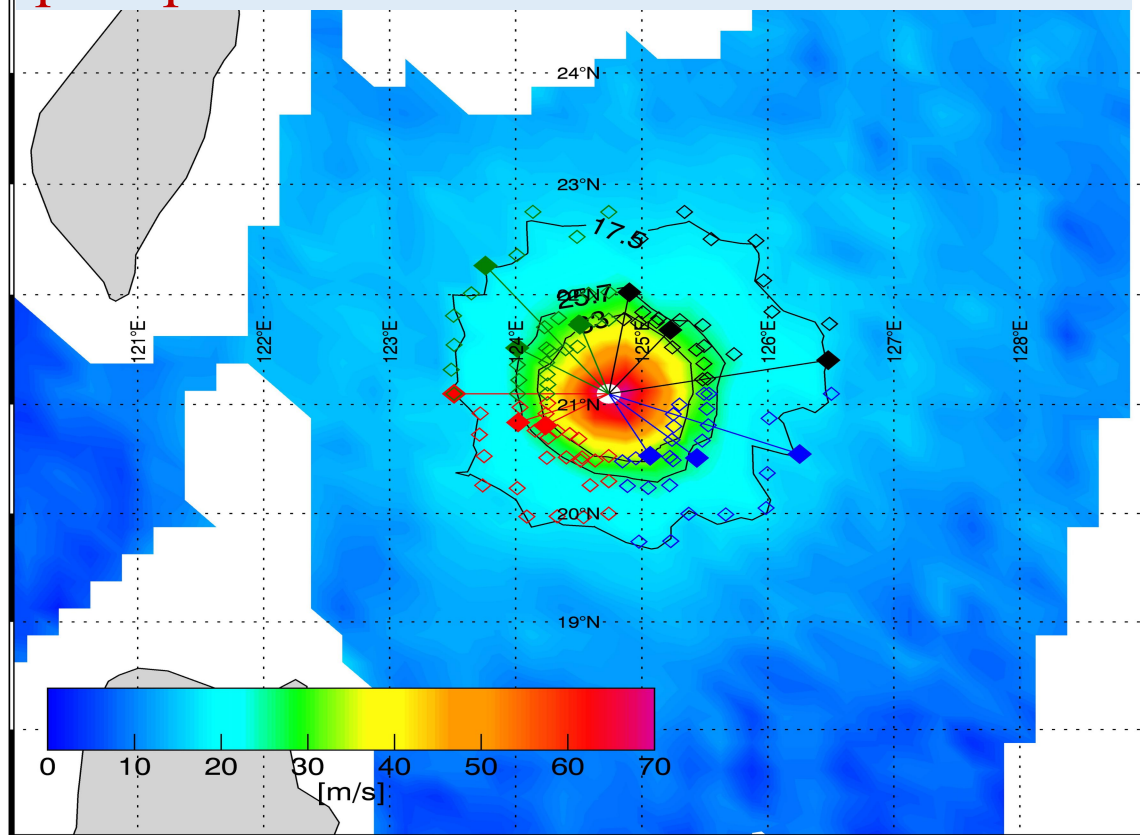
TC size estimation based on observations from different satellites (independent samples)



FY-2G和FY-4B: mean difference <5km, larger difference as compared to FY-4A

Wind field from SMAP radiometer

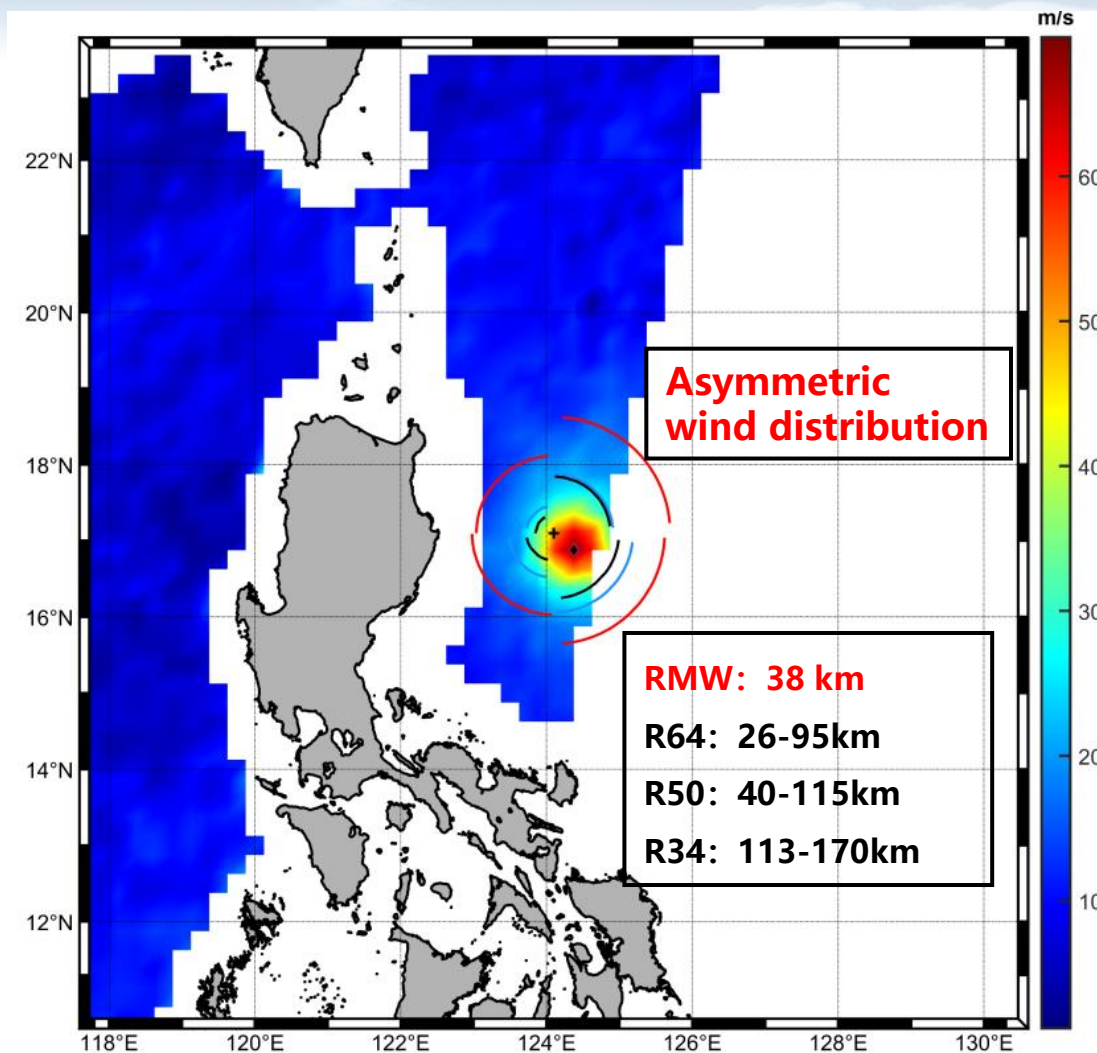
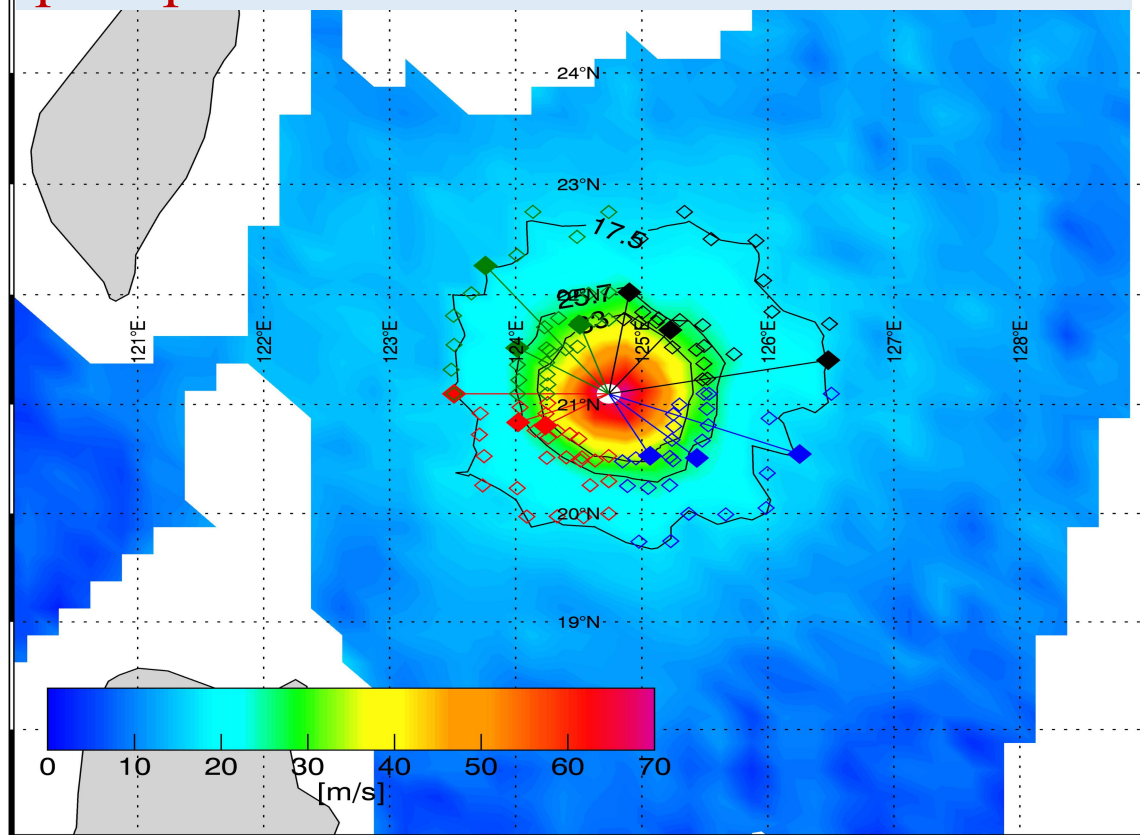
SMAP radiometer: Up to 70m/s, no precipitation contamination

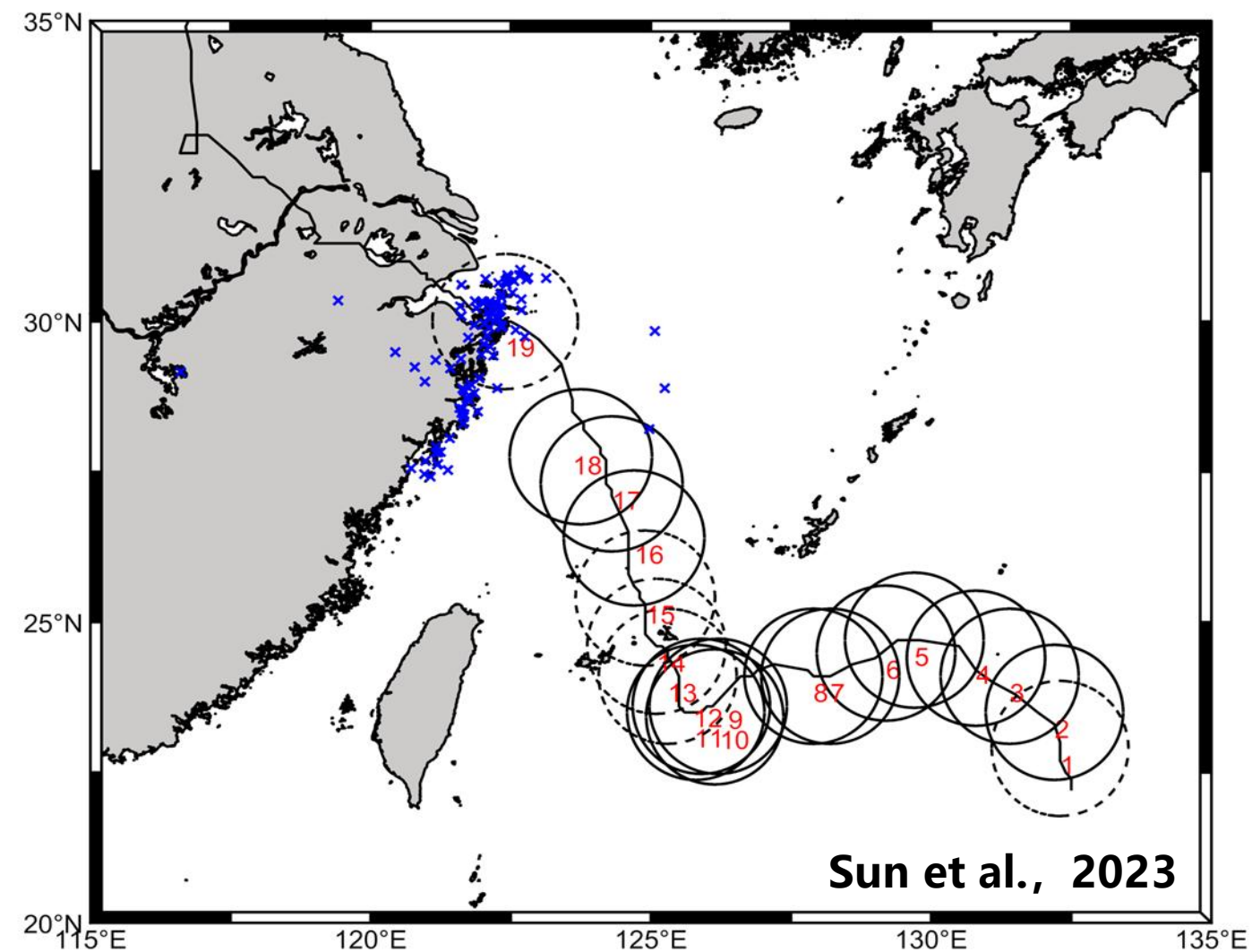


The SMAP satellite is in a near-polar orbit at an altitude of 685 km. It has an ascending node time of 6 pm and is sun-synchronous. In approximately 3 days it completes global coverage with an exact repeat cycle of 8 days. The L-band passive microwave radiometer mounted on the SMAP can be used to measure sea surface wind speed, with a spatial resolution of 40 km and a swath width of 1000km. Compared to Ku-band scatterometers (e.g., QuikSCAT), the L-band radiometer can provide more accurate measurements of high winds (~ 70 m/s) in extreme weather conditions.

Wind field from SMAP radiometer

SMAP radiometer: Up to 70m/s, no precipitation contamination

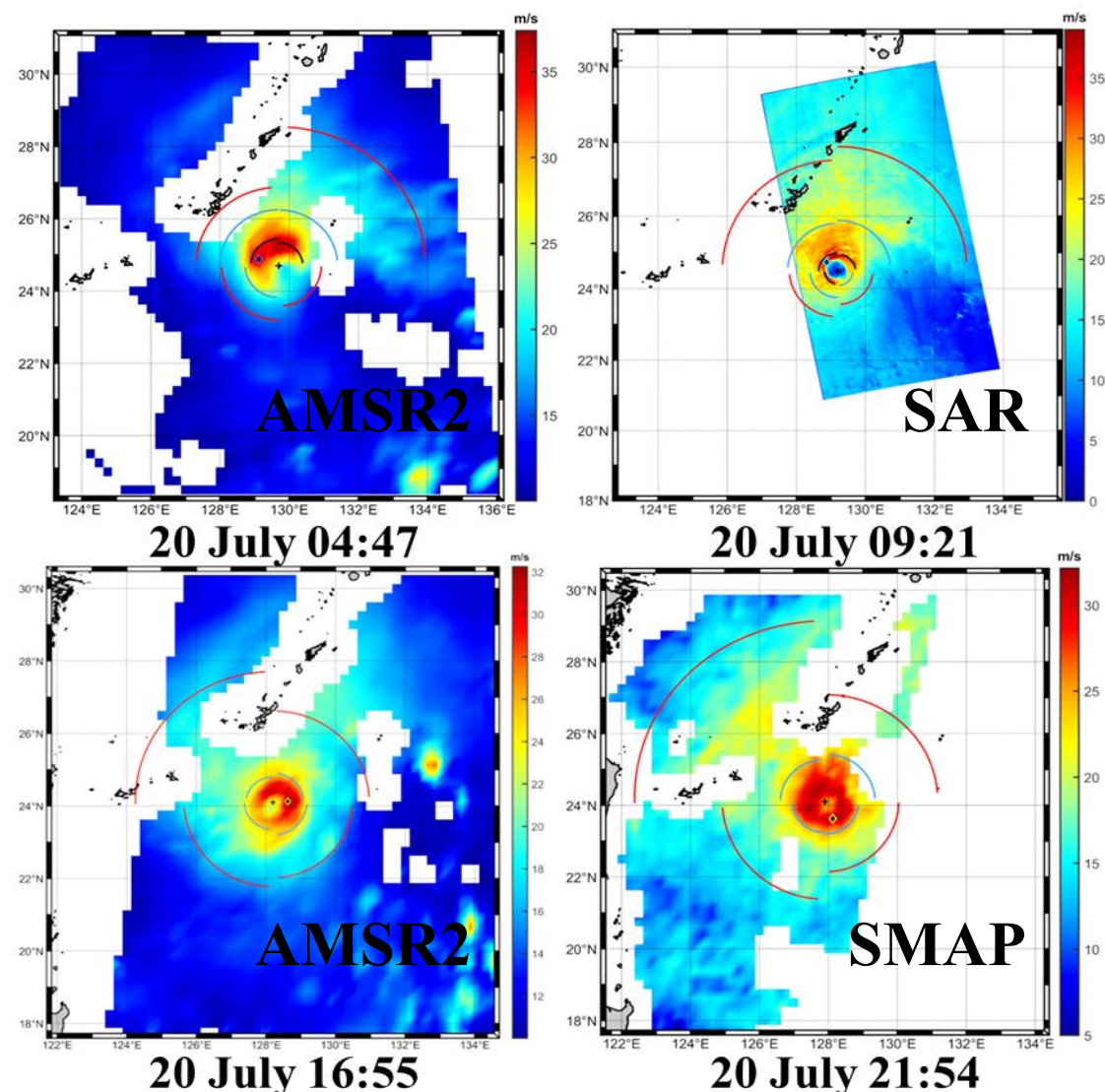
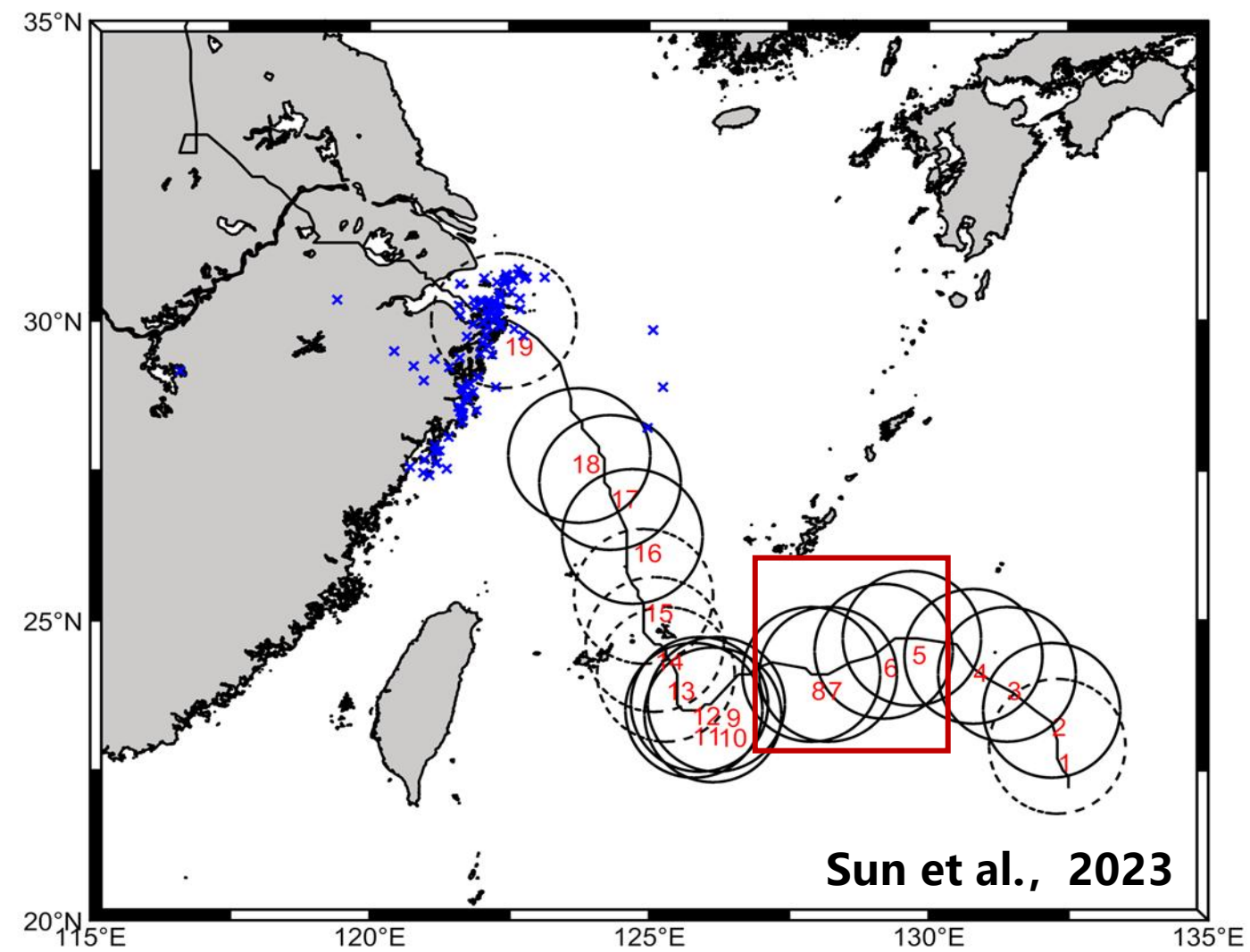




Combining observations from active and passive microwave remote sensing instruments can provide long-time series data for monitoring changes in TC wind structure

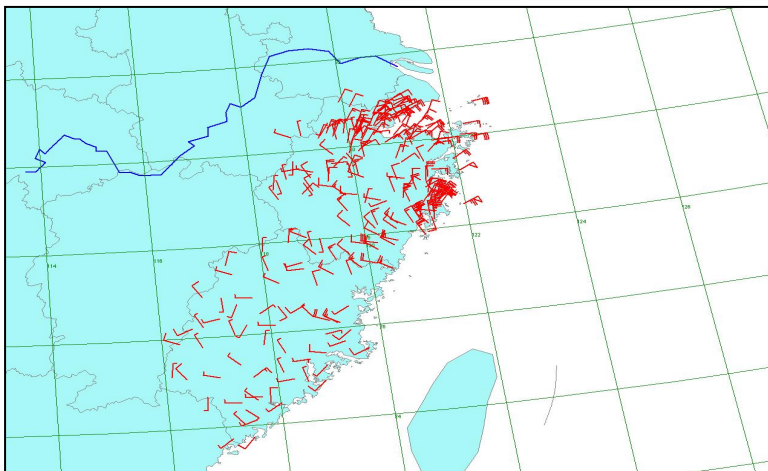
Acquisition time and microwave remote sensing instrument used for each TC wind field observation sample.

Serial Number	Instrument	Acquisition time (UTC)
(1)	SMAP	0836 UTC 18 July
(2)	AMSR2	1707 UTC 18 July
(3)	SMAP	0912 UTC 19 July
(4)	SMAP	2118 UTC 19 July
(5)	AMSR2	0447 UTC 20 July
(6)	RS-2	0921 UTC 20 July
(7)	AMSR2	1655 UTC 20 July
(8)	SMAP	2154 UTC 20 July
(9)	AMSR2	1739 UTC 21 July
(10)	SI-1A	2136 UTC 21 July
(11)	AMSR2	0435 UTC 22 July
(12)	SMAP	0924 UTC 22 July
(13)	SMAP	2130 UTC 22 July
(14)	AMSR2	0518 UTC 23 July
(15)	AMSR2	1726 UTC 23 July
(16)	SMAP	2206 UTC 23 July
(17)	AMSR2	0424 UTC 24 July
(18)	SI-1A	0954 UTC 24 July
(19)	AMSR2	0507 UTC 25 July

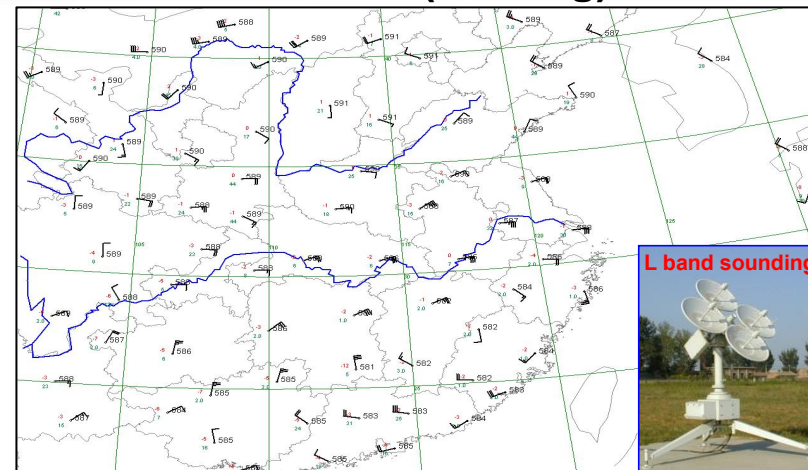


Off-shore and landfall TC

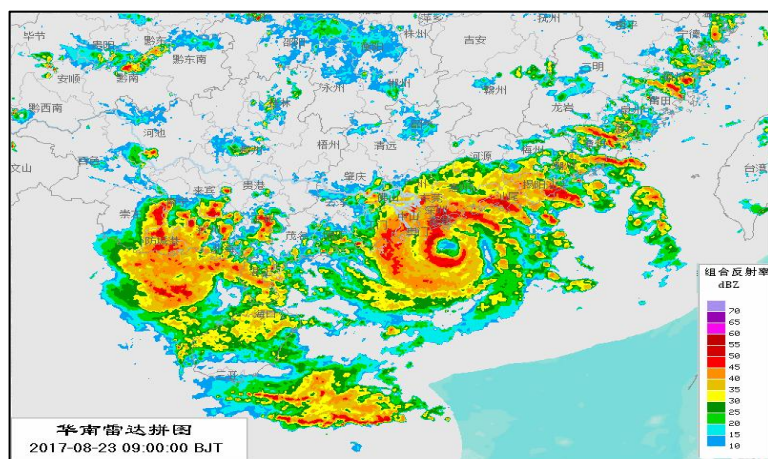
In situ (surface AWS)



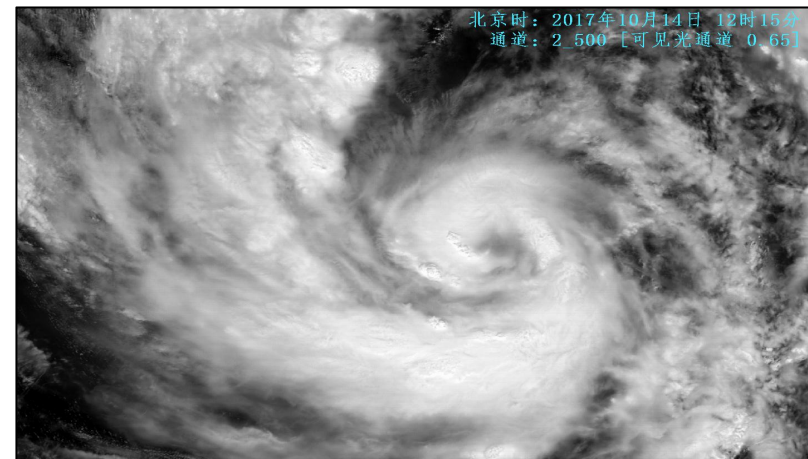
In situ (sonding)



Radar



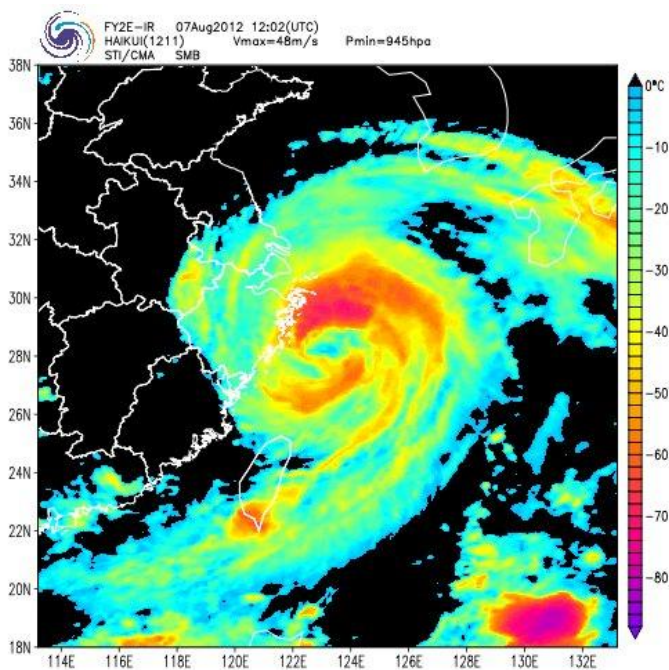
Satellite



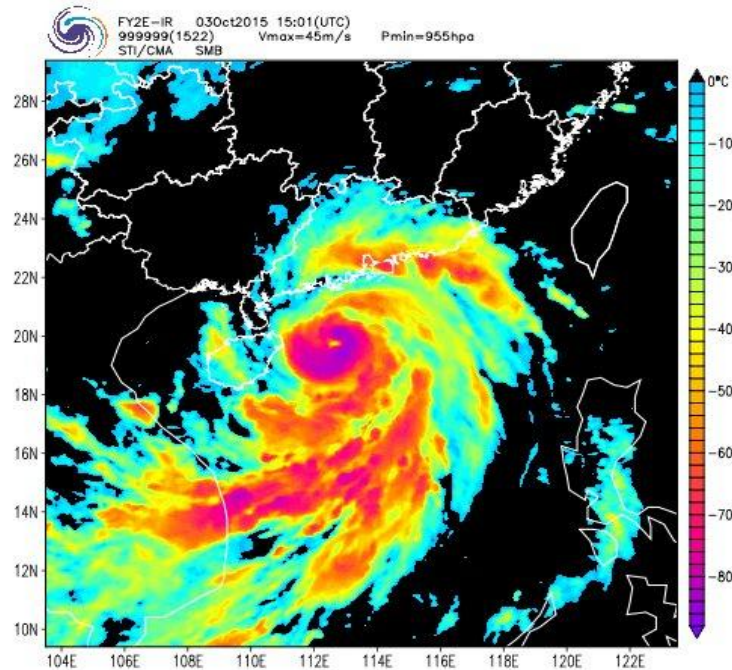
(Courtesy to Dr Xu Yinglong)



Satellite estimation vs in-site observation



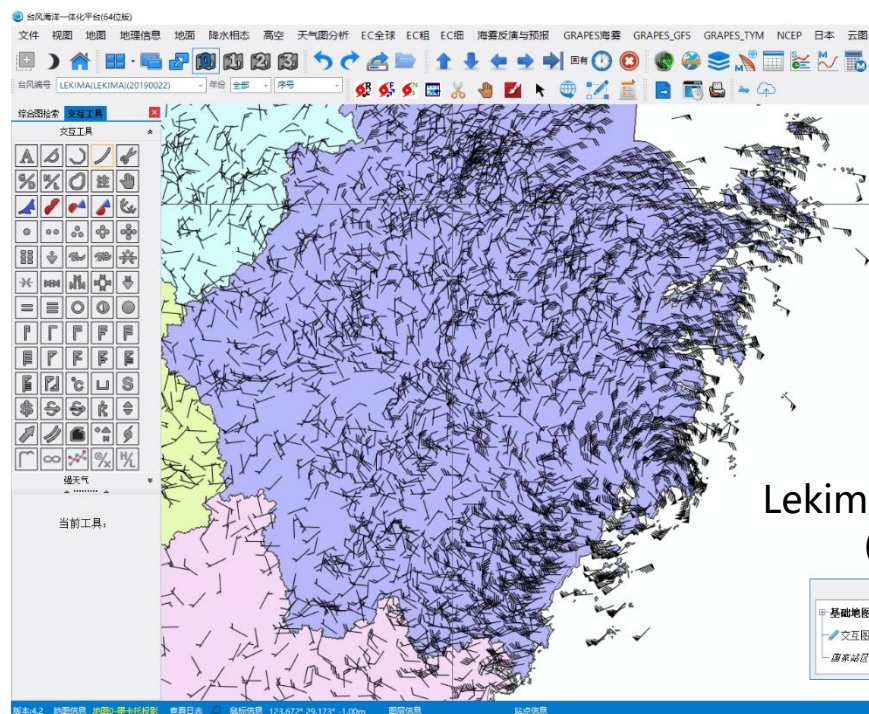
Haikui 2012 (48m/s vs 30m/s)



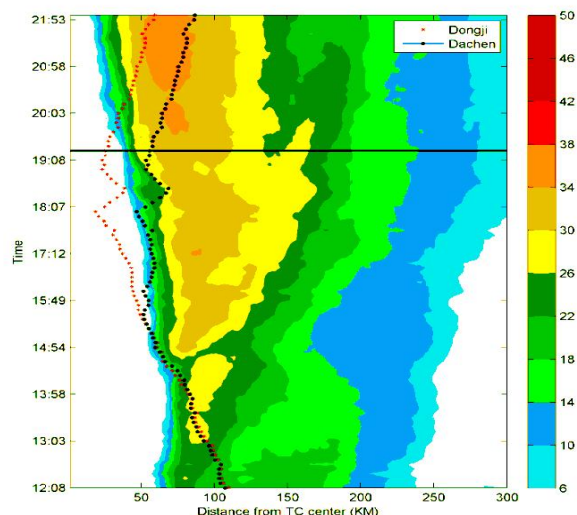
Mujigae 2015 (45m/s vs 33m/s)



Synthetic analyses with observations from wind towers, AWS, and ground-based radar



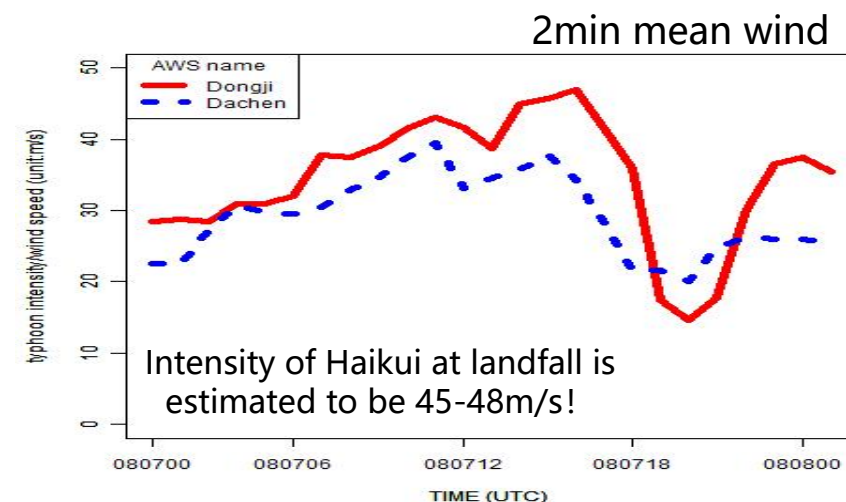
Lekima wind field (AWS)

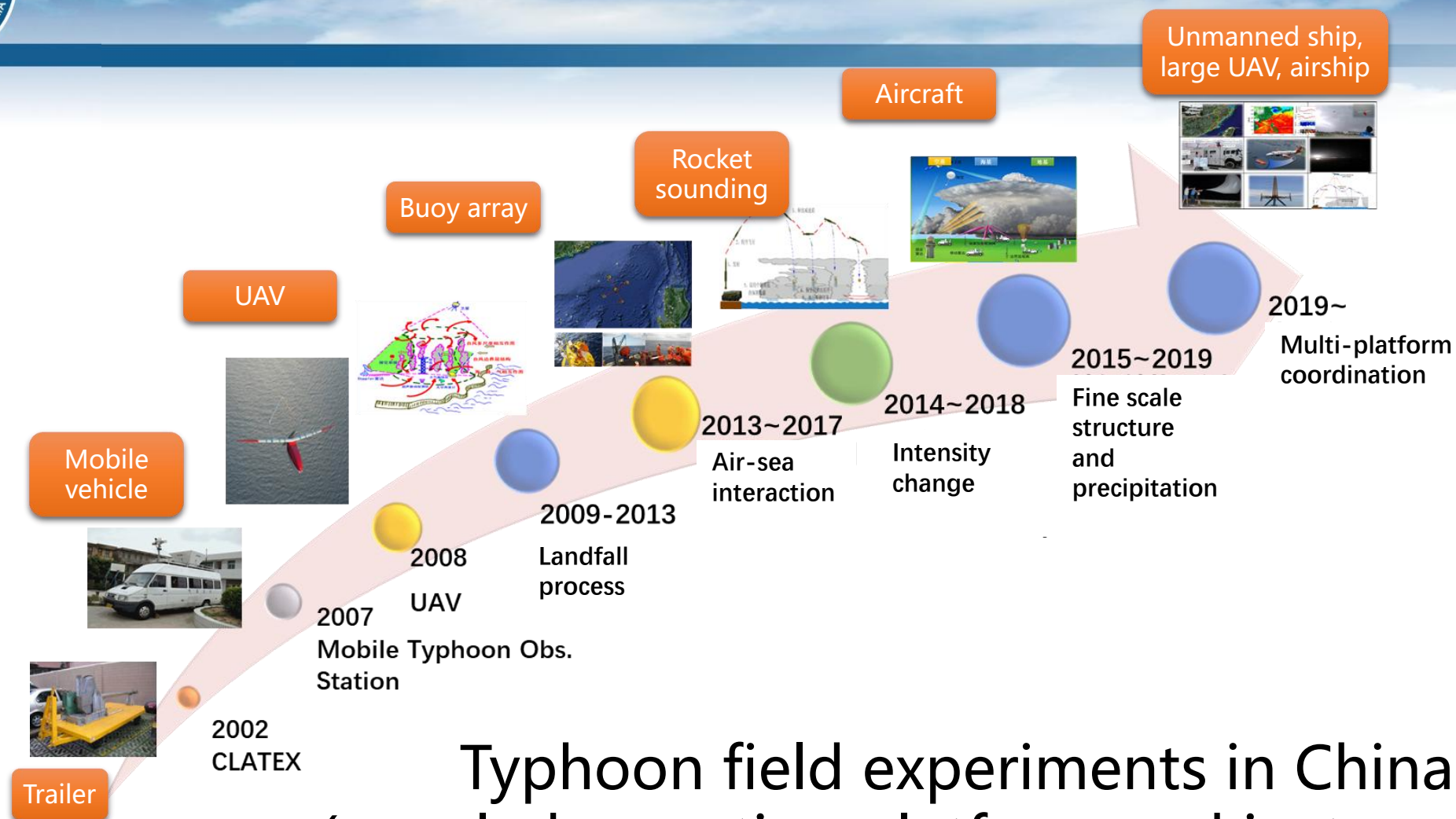


Position of two AWS stations relative to TC center (Haikui)

Conversion ratio for winds at different heights (wind tower observations)

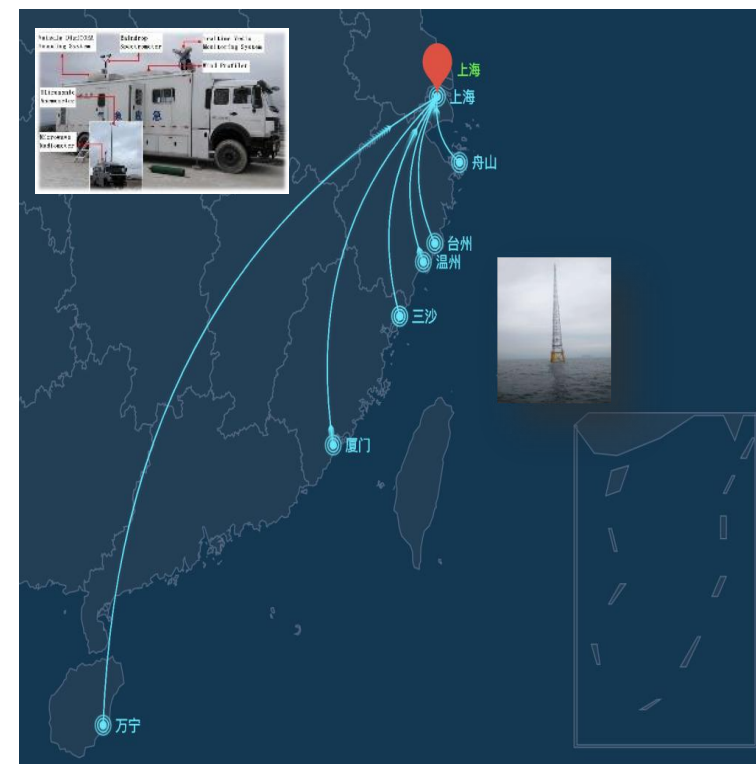
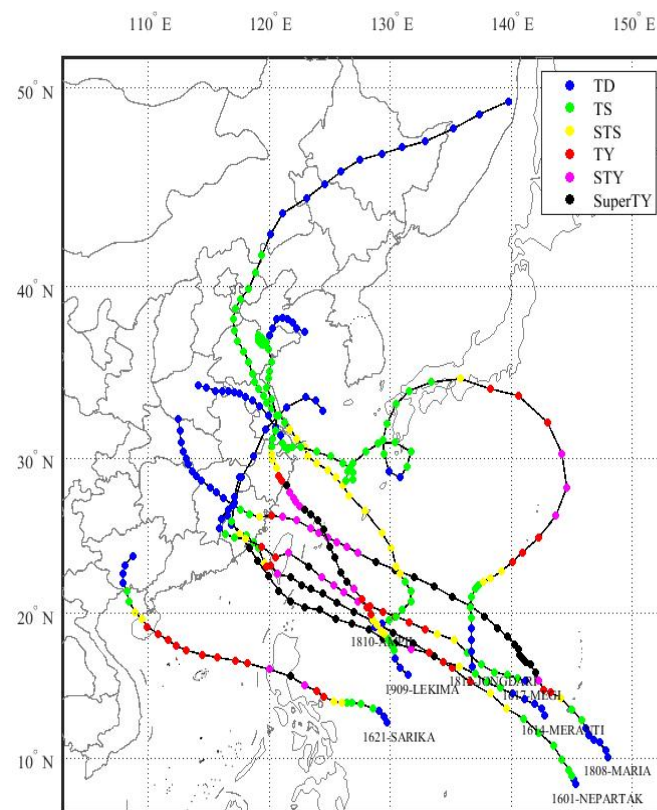
高层	低层	32 M	89 M	212 M	298 M
32 M	1	/	/	/	/
89 M	0.955	1	/	/	/
212 M	0.885	0.982	1	/	/
298 M	0.870	0.970	0.976	1	1



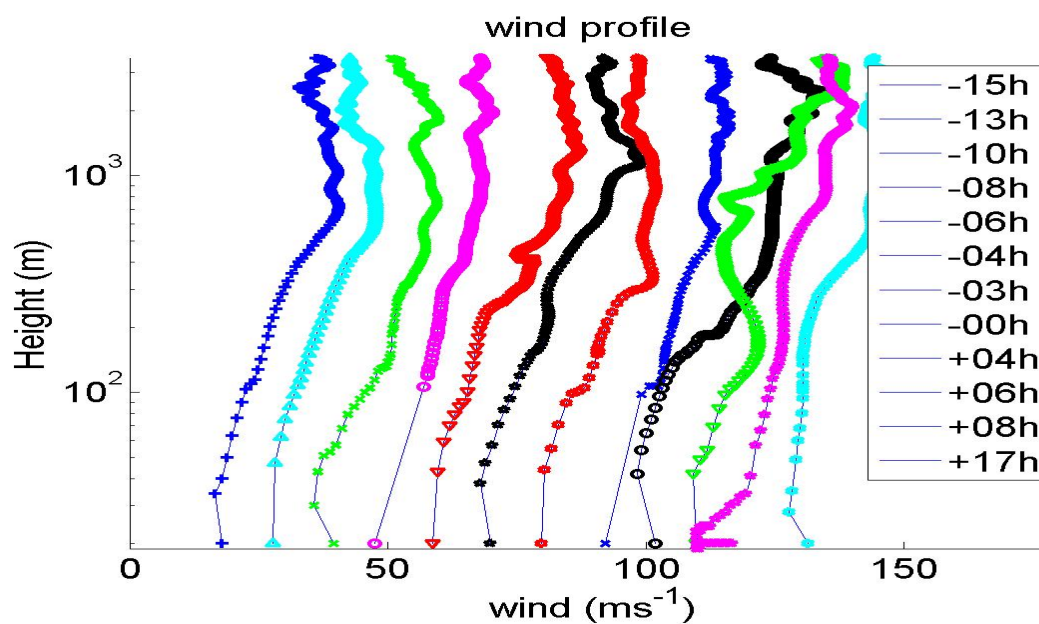


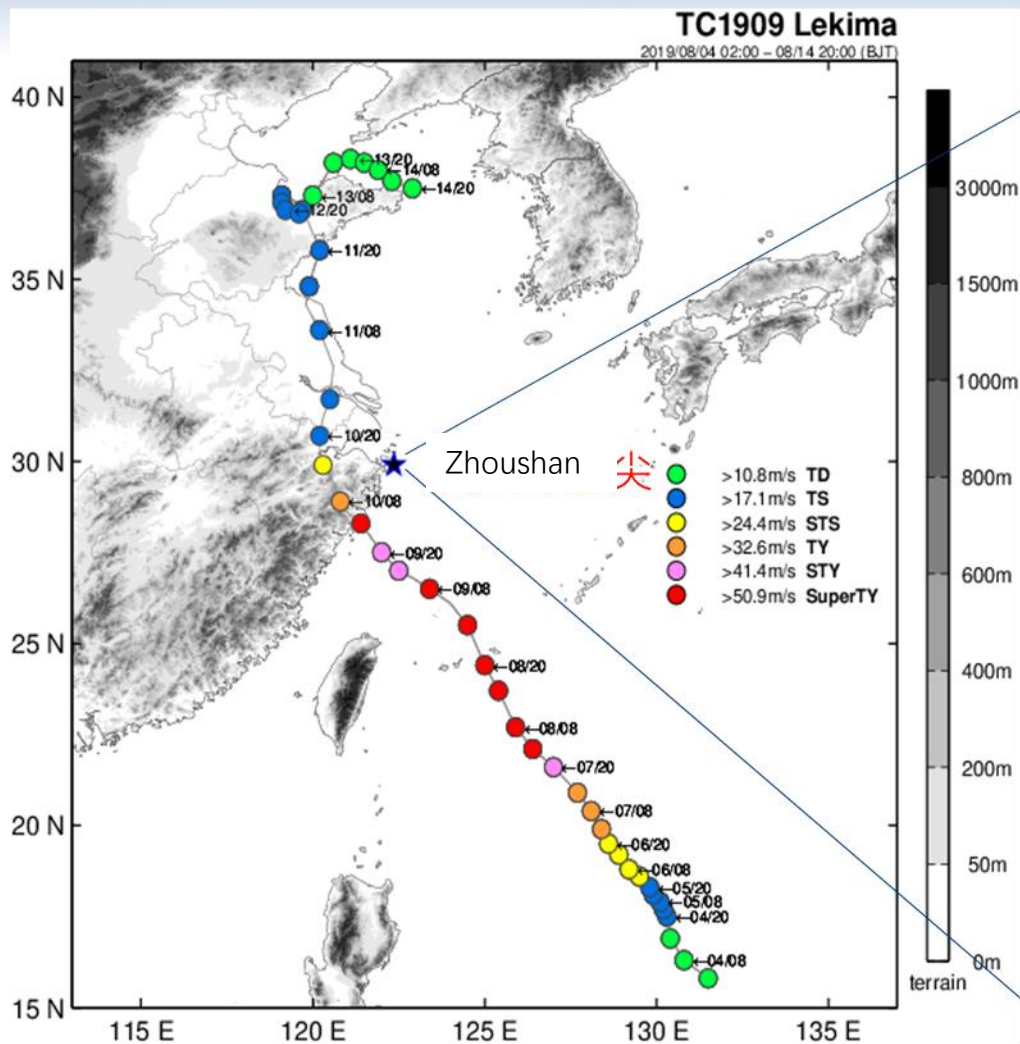
Typhoon field experiments in China (novel observation platform and instruments)

Typhoon Hunter (since 2007)

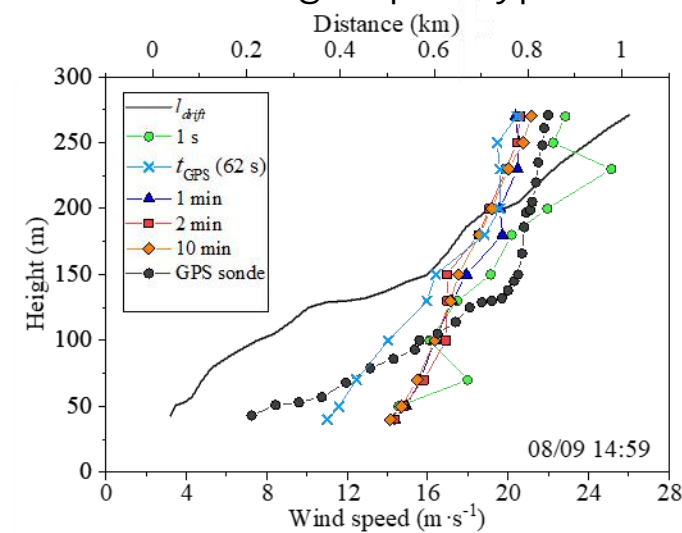
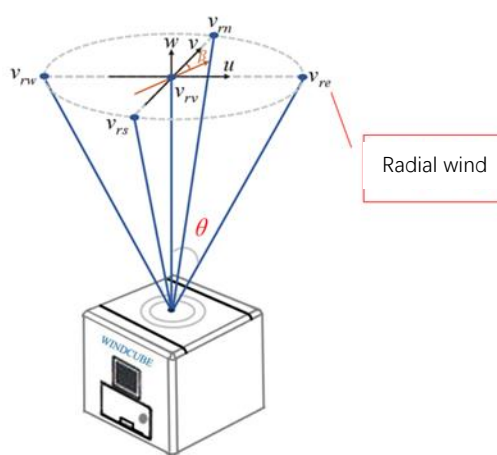


Sounding observation in SuperTy Lekima (2019)





Validation of Doppler Wind Lidar during Super Typhoon Lekima





- Bai, L., Y. Xu, J. Tang, and R. Guo, 2022a: Interagency discrepancies in tropical cyclone intensity estimates over the western North Pacific in recent years. *Atmos. Sci. Lett.*, 24, e1132.
- Bai, L. N., J. Tang, R. Guo, S. Zhang, and K. Y. Liu, 2022b: Quantifying interagency differences in intensity estimations of Super Typhoon Lekima (2019). *Front. Earth Sci.*, 16, 5-16.
- Hu, T. H., H. Yu, X. Q. Lu, 2022: A review of tropical cyclone intensity estimation methods based on satellite remote sensing. *J. Trop. Meteor.*, 38. (in Chinese)
- Lu, X. Q., H. Yu, 2013: An Objective Tropical Cyclone Intensity Estimation Model Based on Digital IR Satellite Images. *Tropical Cyclone Research and Review*. 2(4), 233-241.
- Lu, X. Q., H. Yu, X. M. Yang, and X. F. Li, 2017: Estimating tropical cyclone size in the Northwestern Pacific from geostationary satellite infrared images. *Remote Sens.*, 9, 728.
- Lu, X. Q., W. K. Wong, H. Yu, and X. M. Yang, 2022: Tropical cyclone size identification over the Western North Pacific using support vector machine and general regression neural network. *J. Meteorol. Soc. Japan*, 100, 927-941.
- Lu, X. Q., and Coauthors, 2021: Western North Pacific tropical cyclone database created by the China Meteorological Administration. *Adv. Atmos. Sci.*, 38, 690-699.
- Sun, Z. Y., and Coauthors, 2023: The extraordinarily large vortex structure of Typhoon In-fa (2021), observed by spaceborne microwave radiometer and synthetic aperture radar. *Atmospheric Research*. 292 (2023) 106837

The background of the slide is a composite image. The top half features a dark blue world map with a grid overlay. A bright, swirling hurricane-like storm is depicted over the Pacific Ocean, with a red dot and a small square frame at its center. The bottom half of the slide shows a satellite view of a large, swirling oceanic eddy or cyclone in shades of blue and white.

**Thank you for your attention !
Questions?**

THE SENIOR MANAGEMENT AND OPERATION COURSE ON TROPICAL CYCLONE MONITORING AND FORECASTING
(20 November to 1 December 2023, Guangzhou, China)

Tropical Cyclone Gale Monitoring and Forecasting Technology (Part III)

Hui YU
Shanghai Typhoon Institute/CMA



- Surface wind structure of tropical cyclones and a parametric wind field model for tropical cyclones
- Tropical cyclone intensity and size estimation techniques based on satellite observations
- **Tropical cyclone gale forecast techniques**



Numerical weather prediction technology

Statistical prediction technology

Model output statistics/downscaling technology



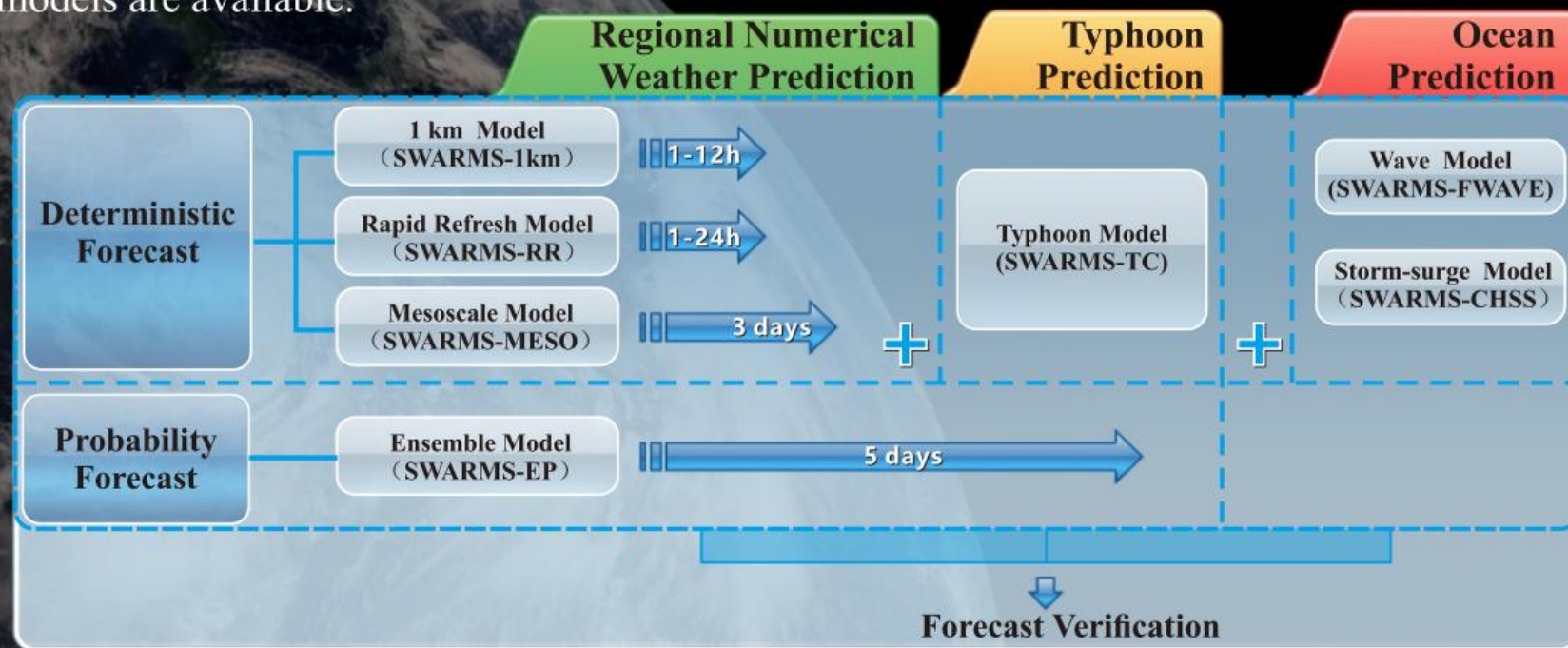
STI/CMA Tropical Cyclone Forecast Dataset for WMO Typhoon Landfall Forecast Demonstration Project (TLFDP)

Forecast guidance			Data contents	Since
NWP Model	Global Model	ECMWF-IFS, NCEP-GFS, UKMO-MetUM, JMA-GSM, KMA-GDAPS	track, intensity	2010
		CMA-GFS	track,intensity, 3-D grid data	2021
	Regional Model	GRAPES-TCM, Shanghai-TCM	track,intensity, 3-D grid data	2010
		CMA-TRAMS, HWRF, GRAPES-TYM	track, intensity	2010
Ensemble Prediction System		ECMWF-EPS, NCEP-GEFS, UKMO-EPS, MSC-CENS, JMA-GEPS	track, intensity	2015
		STI-TEDAPS	track,intensity, 3-D grid data	2018



Shanghai Weather and Risk Model System (SWARMS)

Shanghai Weather and Risk Model System is established by Shanghai Typhoon Institute of CMA and includes regional mesoscale model, regional rapid refresh model, typhoon model, mesoscale ensemble model as well as ocean model. The configuration of resolution and forecast period of each model is designed individually. To meet the demands of operational forecast, the productions from deterministic or probability forecast using different models are available.

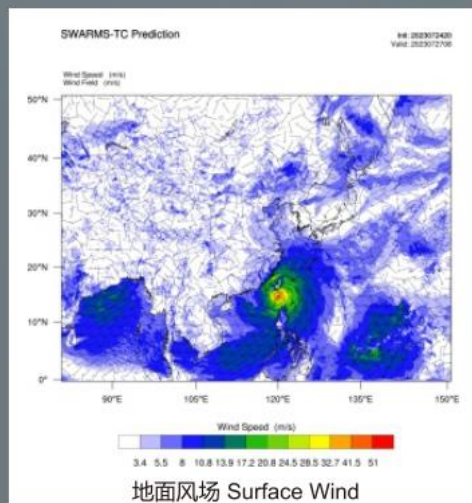
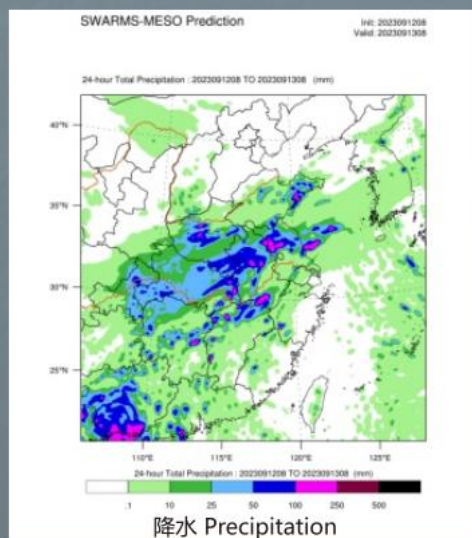


The Flow chart of Shanghai Weather and Risk Model System

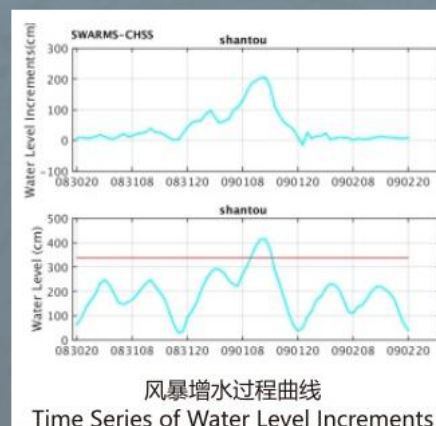
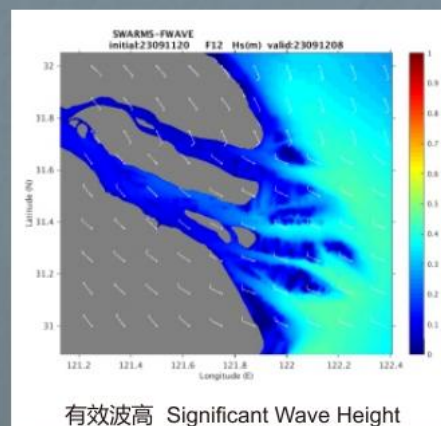


Sample products from SWARMS

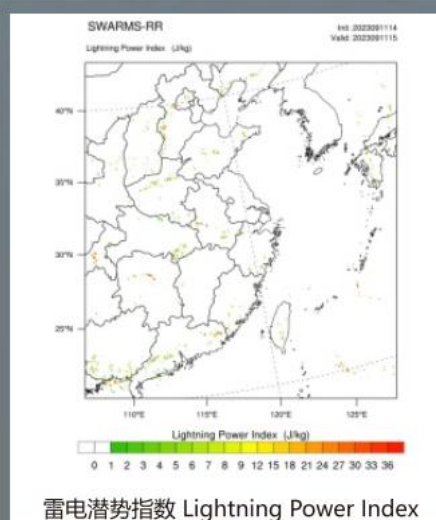
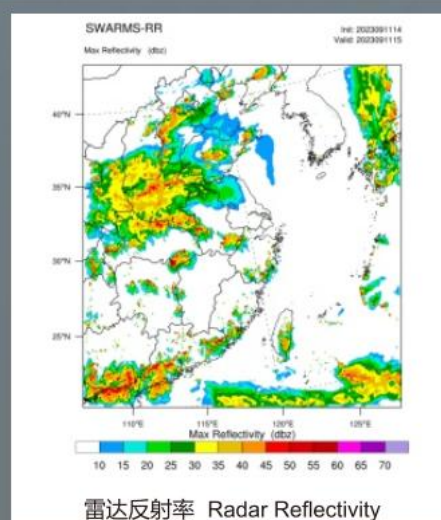
地面要素预报 Surface Element Forecast



海洋预报 Ocean Forecast

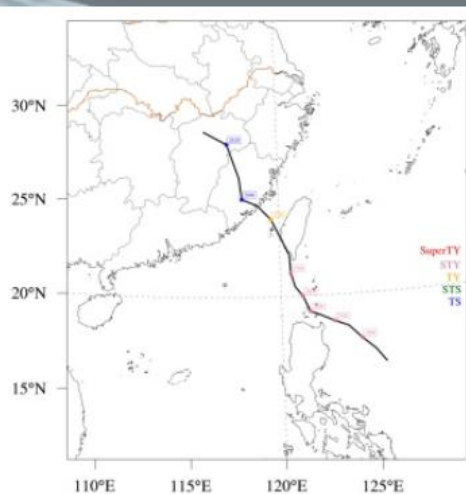


高影响天气 High-Impact Weather Forecast

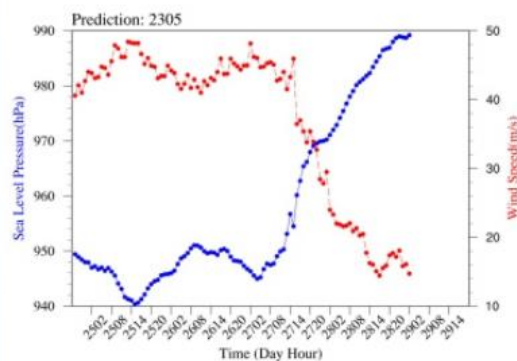


Sample products from SWARMS

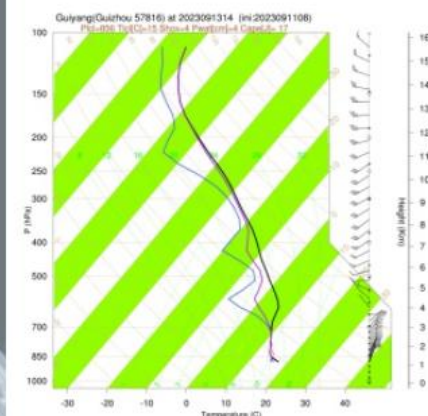
台风预报 TC Forecast



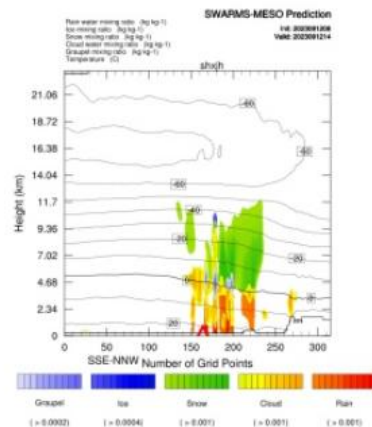
台风路径 TC track



台风强度 TC Intensity

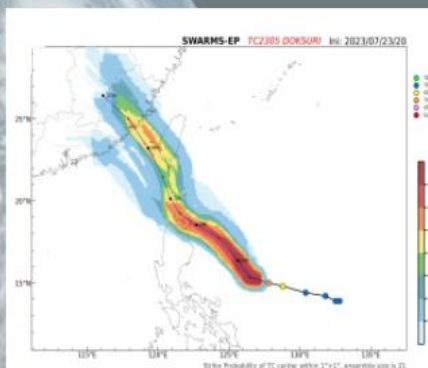


温度对数压力图 T-lnP Diagram

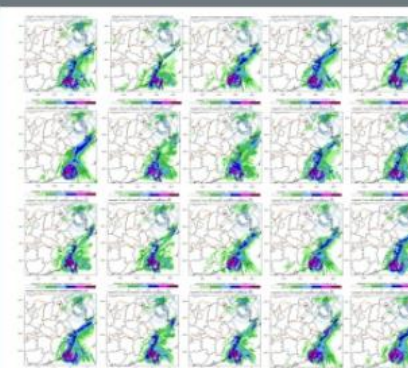


水物质垂直分布
Condensation Vertical Distribution

集合概率预报 Ensemble Forecast



路径袭击概率
TC Strike Probability

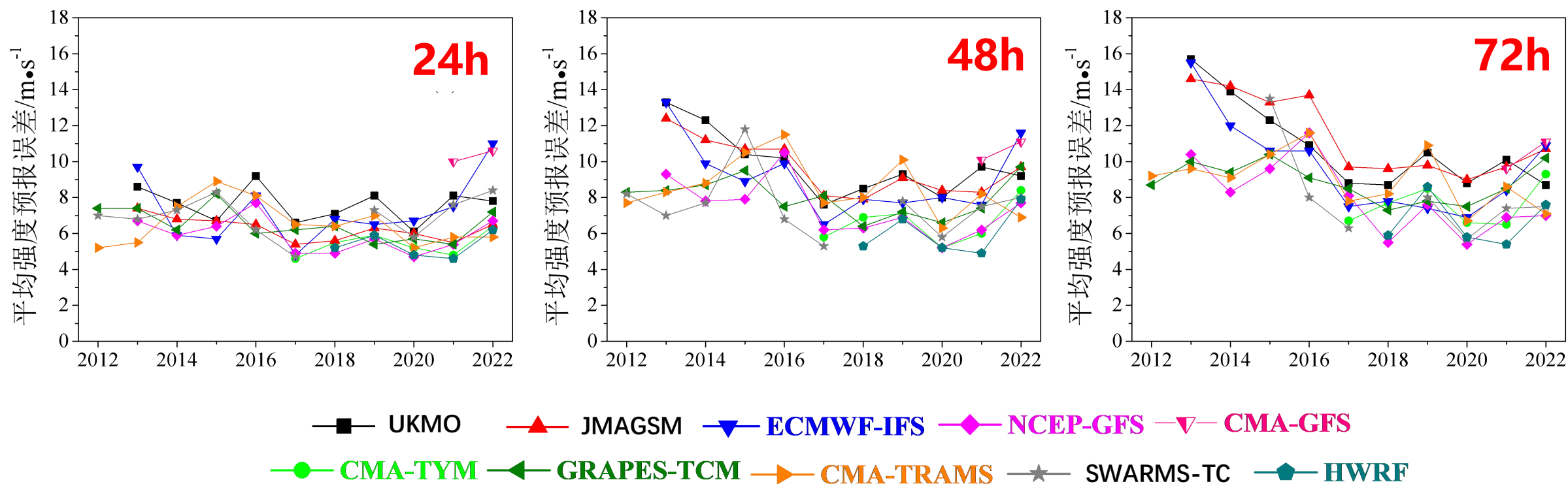


降水邮票图
Stamps of Accumulated Precipitation



Intensity forecast skill of NWP models

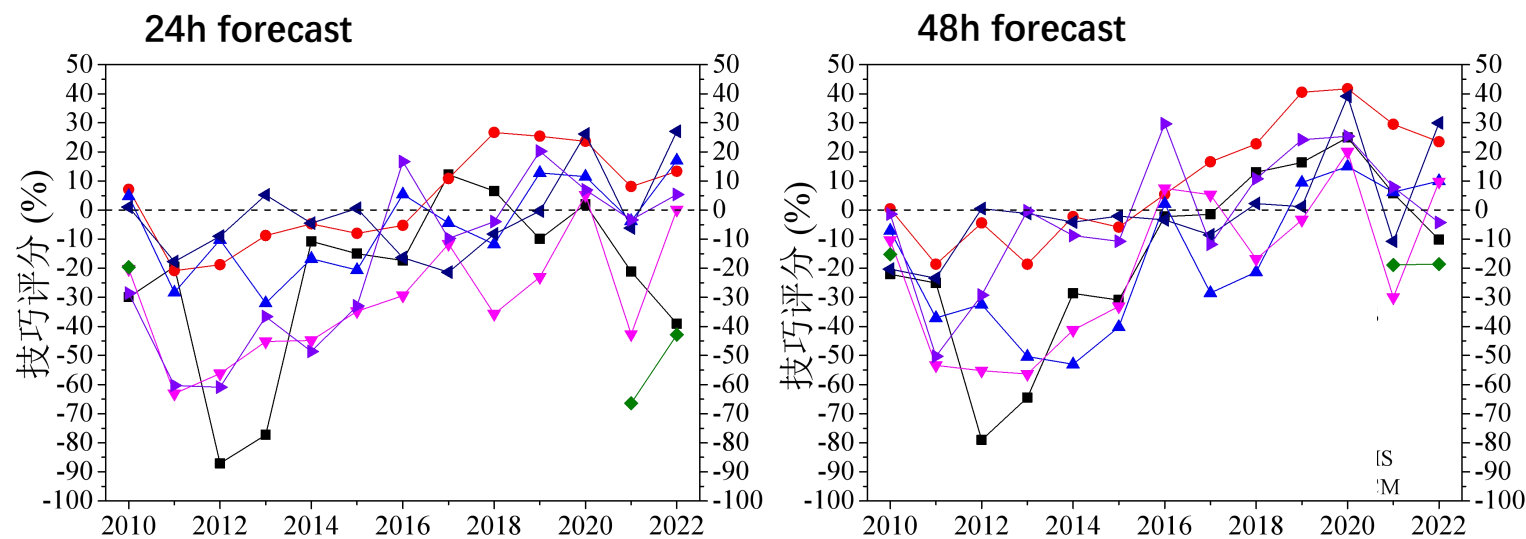
Mean absolute error of intensity forecast (m/s)





Intensity forecast skill of NWP models

Forecast skill as relative to CLIPER

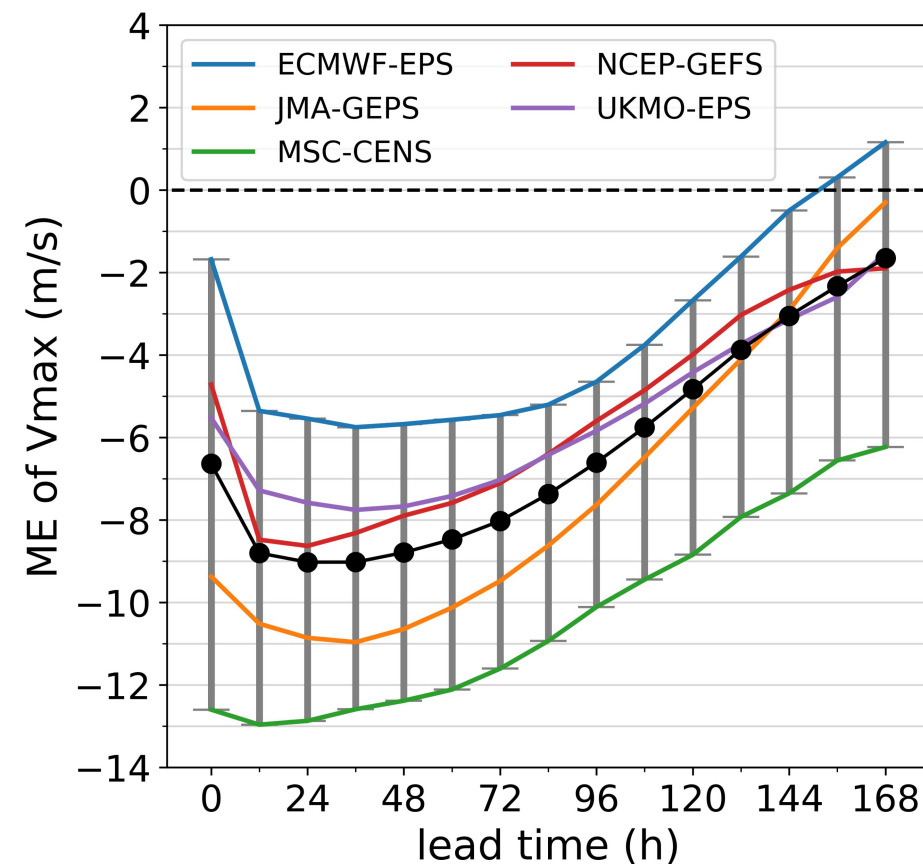




Intensity forecast skill of EPS

Evolution of EPSs during 2015-2019

Name	Horizontal resolution (km)/vertical levels	Member	Initial disturbance	Model uncertainty
ECMWF-EPS	32/91 (2015-2016.3)	51	EDA-SV	SPPT-SKEB
	18/91 (2016.3-2019)			
JMA-GEPS	40/60(2015-2017.6)	27	SV	SPPT
	40/100 (2017.6-2019)		SVs-LETKF	
MSC-CENS	66/40 (2015-2015.11)	21	EnKF	SPPT-SKEB
	50/40 (2015.11-2018.9)			
	39/45 (2018.9-2019)			
NCEP-GEFS	34/64 (2015-2019)	21	EnKF	STTP
UKMO-GEPS	50/70 (2015-2017.07)	24	ETKF	SPPT-SKEB
	30/70 (2017.7-2019)	36		
PCIF	\	20-51	历史相似	\

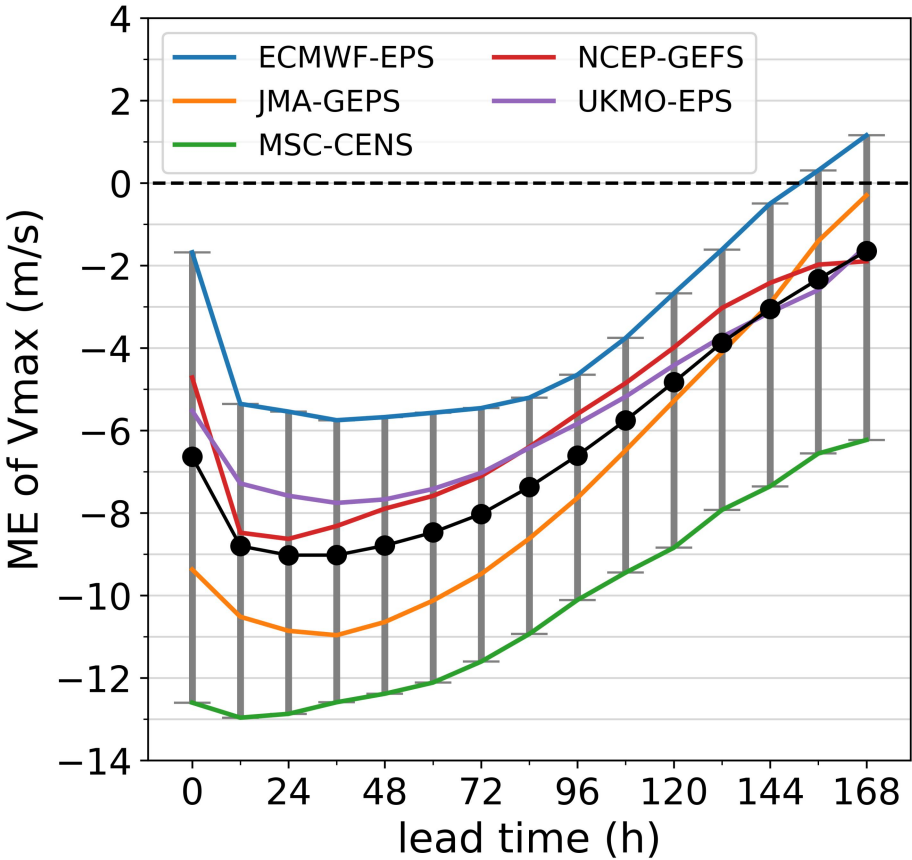


Mean errors during 2018-2019

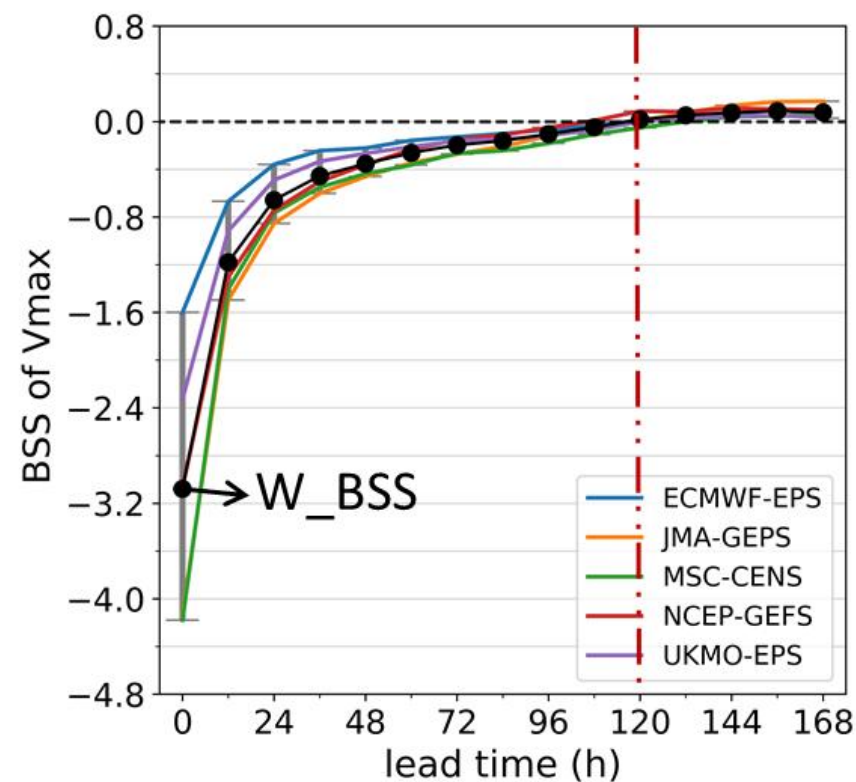
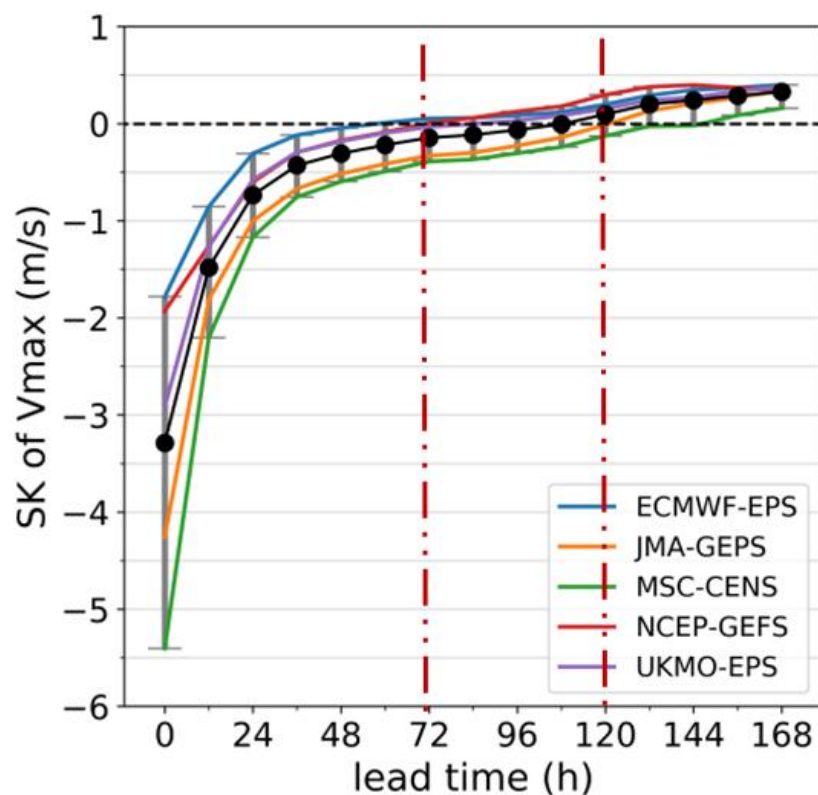


Intensity forecast skill of EPS

Evolution of EPSs during 2015-2019				
Name	Horizontal resolution (km)/vertical levels	Member	Initial disturbance	Model uncertainty
ECMWF-EPS	32/91 (2015-2016.3)	51	EDA-SV	SPPT-SKEB
	18/91 (2016.3-2019)			
JMA-GEPS	<div>All EPSs have weaker bias. Different performance among EPSs.</div>			
NCEP-GEFS				
NCEP-GEFS	34/64 (2015-2019)	21	EnKF	STTP
UKMO-GEPS	50/70 (2015-2017.07)	24	ETKF	SPPT-SKEB
	30/70 (2017.7-2019)	36		
PCIF	\	20-51	历史相似	\



Mean errors during 2018-2019

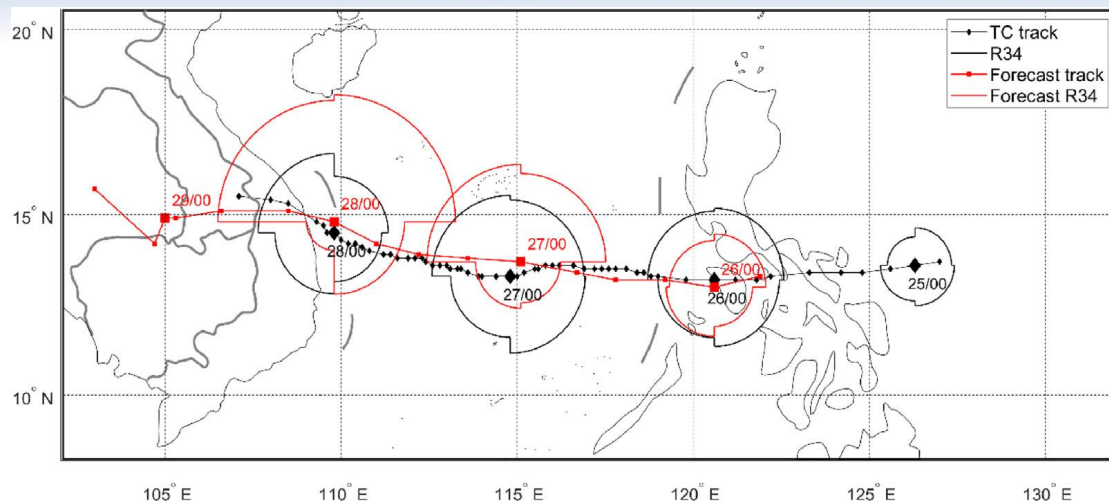


Intensity forecast skill of EPSs during 2018-2019

(L: ensemble mean; R: probability forecast)

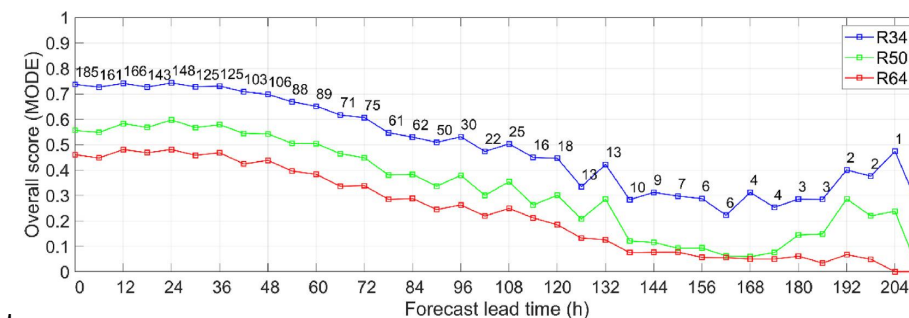
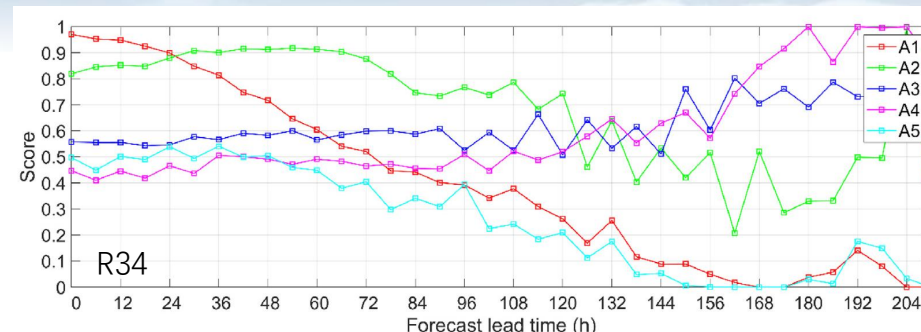
Reference method: PCIF (Chen et al. 2016)

NWP Forecast skill of characteristic wind radii



TC wind structure forecast at 18 UTC 25 Oct 2020, where the black diamond line and black circle are observed TC track and observed R34 respectively.

The red square line and red circle are TC forecast track and forecast R34 respectively.



Change of MODE scores with lead times
(the results for ECMWF-IFS)



Statistical prediction technology

CLIPER scheme: TCSP, PCIF

CLIPER + environmental factors: WIPS

Size forecast: application of empirical wind field model



TCSP (Climatology and persistency scheme)

A statistical prediction scheme for tropical cyclone intensity by setting up linear regression equations with predictors describing climatology and persistency traits of intensity change.

Used in CMA mainly as a reference scheme to evaluate the skills of other guidance.

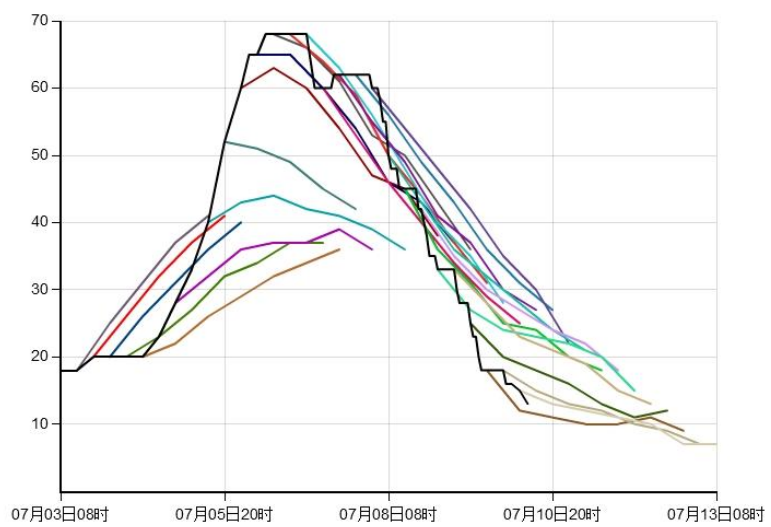


TCSP predictors (9):

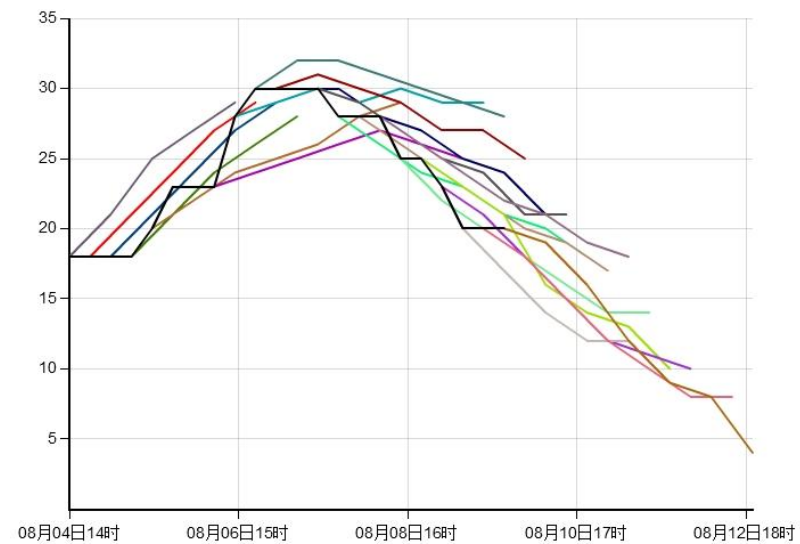
Latitude, longitude, maximum wind speed

Their changes in past 12hr and 24hr

**Monthly (May to October) stepwise regression equations
are set up every 12hr until 72hr.**



Nepartak(1601)

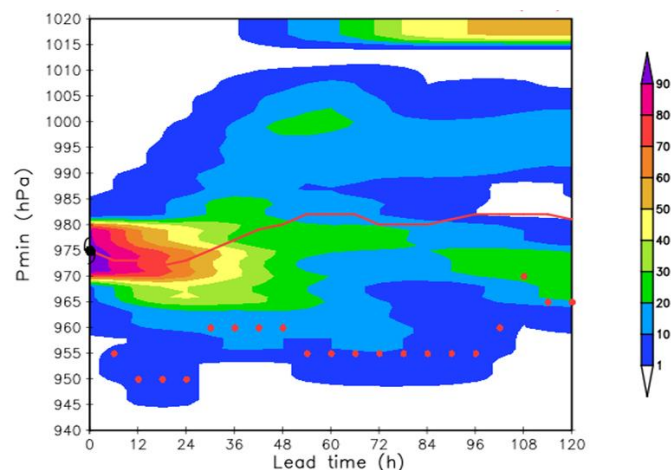


Omais(1605)



PCIF: a probabilistic climatology-based tropical cyclone intensity forecast scheme

Developed by selecting analog historic cases with given criteria for climatology and persistency predictors.



Name of predictors

The PMIN change during the last 12 h (hPa)

Minimum central pressure at initial time (hPa)

Latitude of TC location at initial time ($^{\circ}$)

Longitude of TC location at initial time ($^{\circ}$)

Direction of TC movement during the last 24 h ($^{\circ}$)

Julian day of initial time (Days)

TC lifespan (hours)

Underlying surface conditions at TC center



Procedures

Step 1: calculation of the values of the factors for the specific TC to be predicted and determining the historical sample pool to be considered

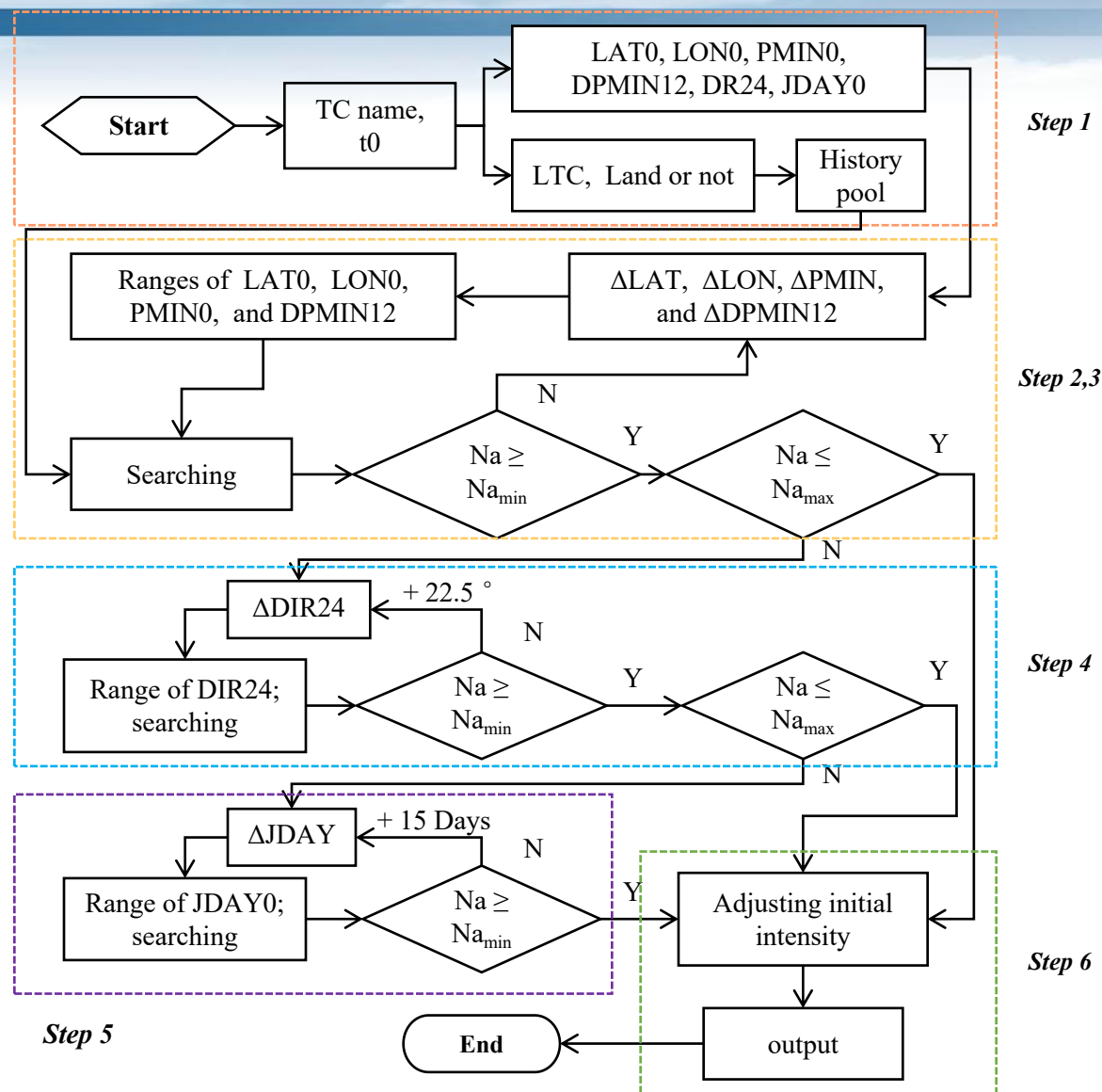
Step 2: 4 factors are considered together to select the analogous cases from the pool; A search radius is set for each factor

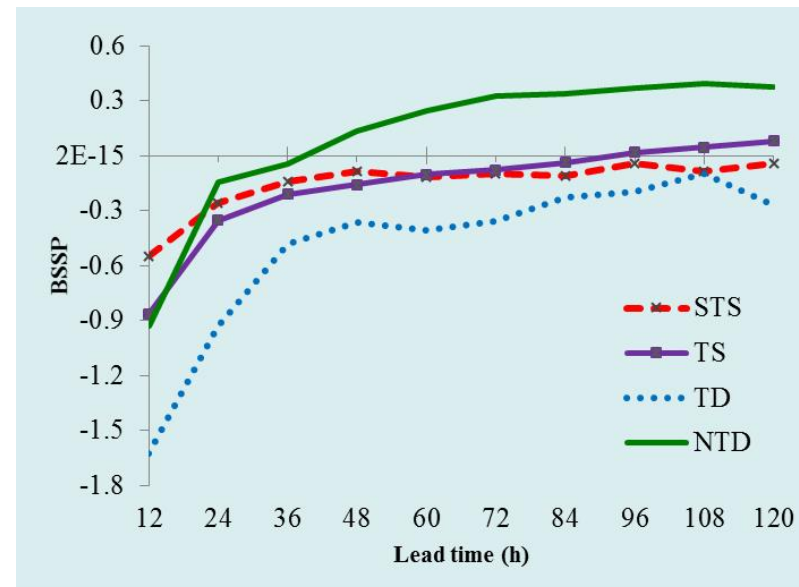
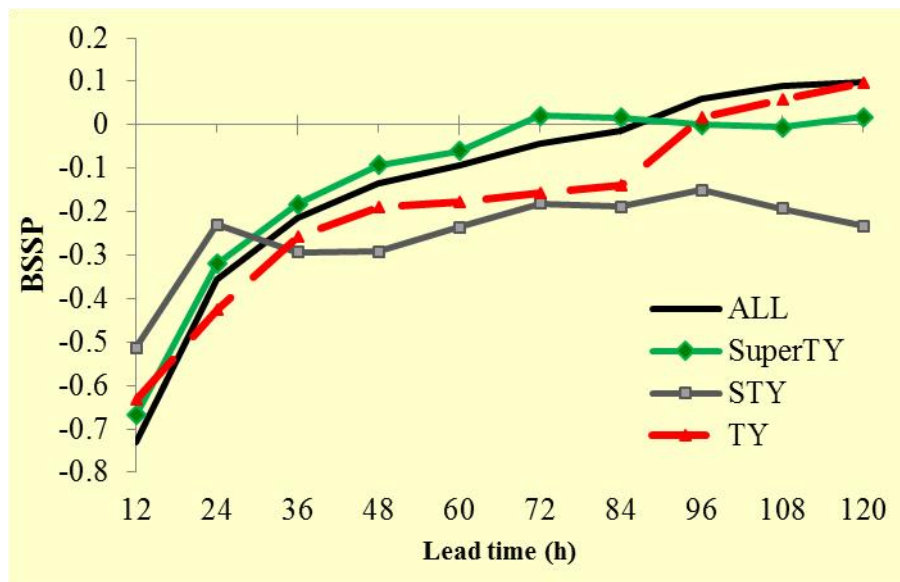
Step 3: If the number of the selected cases N_{analog} is less than N_{min} , the search radii for 4 factors are increased by half of the original search radii in turn until is reached N_{min} .

Step 4: DIR24

Step 5: JDAY

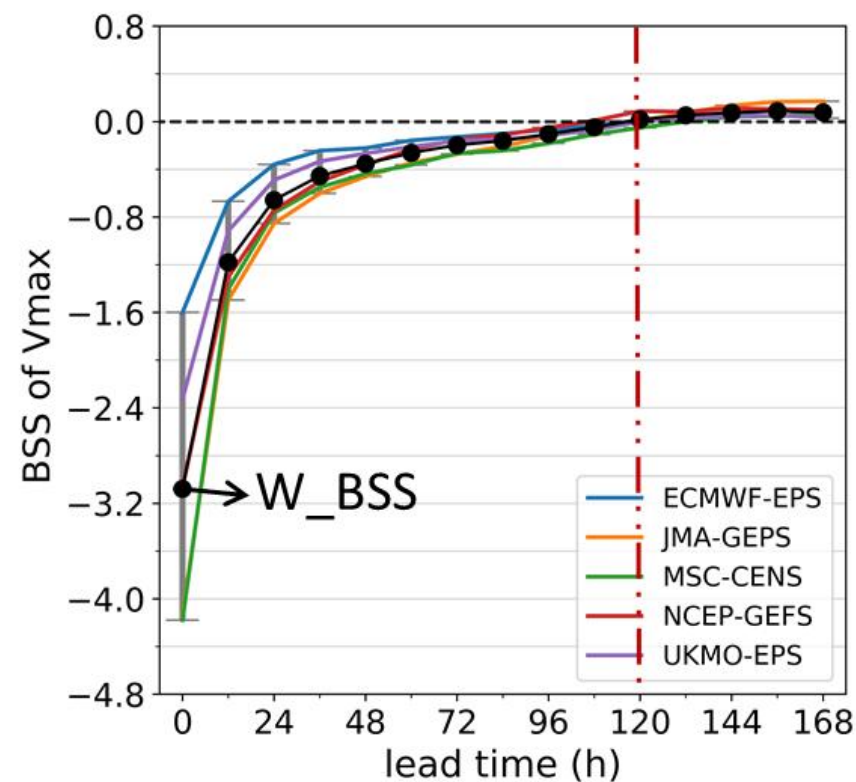
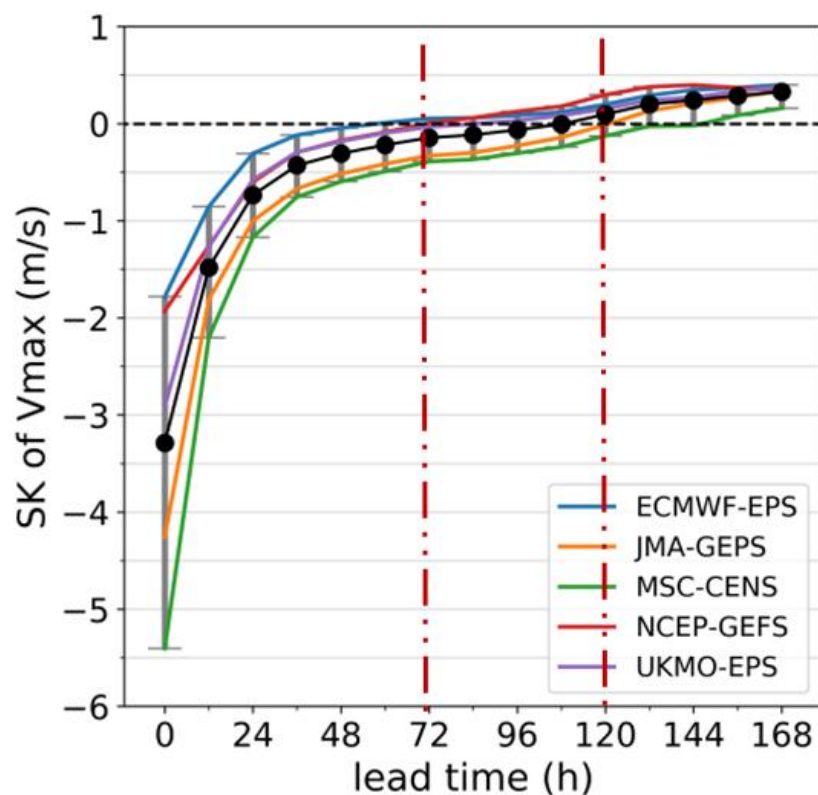
Step 6: Adjusting and outputting





Forecast skill of ECMWF-EPS as relative to PCIF (Brier Score)

The probabilistic intensity prediction of the PCIF are better than the ECMWF-EPS for lead times shorter than 72 h in general and for all lead times for the STY, STS, and TD categories.



Intensity forecast skill of EPSs during 2018-2019

(L: ensemble mean; R: probability forecast)

Reference method: PCIF (Chen et al. 2016)



WIPS

A statistical prediction scheme for tropical cyclone intensity by setting up linear regression equations with predictors describing climatology and persistency traits, synoptic features, and underlying surface conditions.

Used in CMA as an objective forecast guidance.



WIPS predictors:

(1) Latitude, longitude, maximum wind speed

Their changes in past 12hr and 24hr

(2) Synoptic situation:

EFC, VWS, vorticity, divergence, temperature difference

(3) Underlying surface condition:

Maximum potential intensity, POT, distance to land



$$\text{EFC} = -\frac{1}{r^2} \frac{\partial}{\partial r} r^2 \overline{u'_L v'_L},$$

Eddy flux convergence

u and v are the radial and azimuthal components of wind;

r is the distance from the center;

The prime means the deviation from the azimuthal mean;

L refers to the storm relative flow.

The asymmetric structures of the outflow layer associated with upper level synoptic-scale systems (e.g. trough) can produce large eddy imports of angular momentum.



Vertical wind shear:

The wind difference between 200 and 850 hPa over the storm.

Small vertical wind shear favors the intensification of a tropical cyclone, and strong vertical wind shear favors the weakening of a tropical cyclone.



$$MPI = 66.5 + 108.5e^{-0.1816 \times (30.0 - SST)}$$

Maximum potential intensity:

**Upper bound of the intensity of a tropical cyclone,
determined by SST (and environment temperature)**

Development potential:

Difference between the current intensity and MPI



Predictors for East China region

12h	24h	36h	48h	60h	72h
pdvmax12	pdvmax12	pdvmax24	dis36	pdvmax48	pdvmax60
dis0	vs	dis24	pdvmax36	vs	vs
vs	dis12	vs	vs	dis36	vx
ddis(12,0)	dis24	v-6	dlon(0,-12)	dlat(0,-6)	dlon(0,-6)
REFC		dmpi(24,12)	v-6	v-6	v-24
			dmpi(36,24)	dis48	dis72
			dlat(0,-18)	dlon(0,-6)	dis24
					dis36
					dvmax(0,-6)
					div200

Top 3: Development potential, vertical wind shear, distance to land



Predictors for South China region

12h	24h	36h	48h	60h	72h
pdvmax0	dis12	pdvmax36	pdvmax12	pdvmax36	pdvmax48
dis0	pdvmax24	ha500	dis24	dis36	dlon(0,-24)
dvmax(0, -24)	dvmax(0,-12)	vx	ha500	vx	dis-12
ha500	ha500	t	t	v-12	dlat(0,-6)
mpi	vx	dis12	dmpi(48,12)	dlon(0,-24)	dmpi(36,12)
vs		dis24	vx		dlon(0,-6)
			vs		div200
			div850		

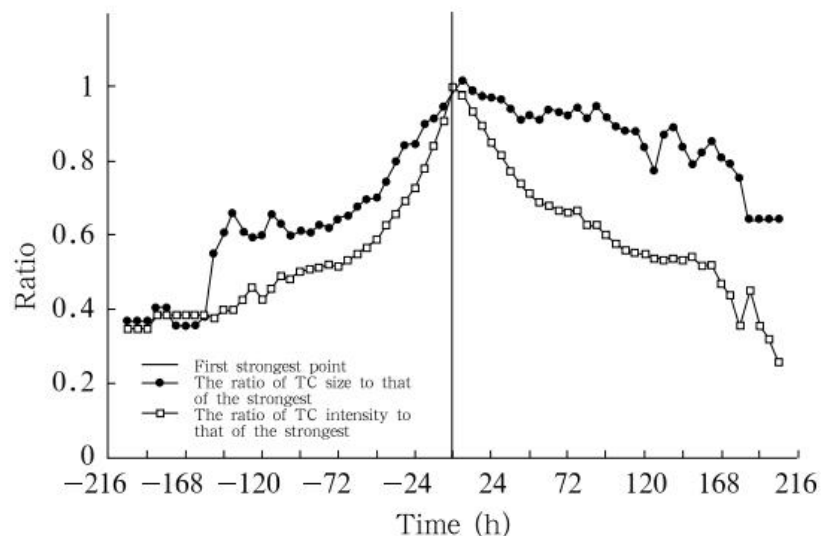
Top 3: Development potential, distance to land, 500hPa height anomaly



Predictors for Far Sea region

12h	24h	36h	48h	60h	72h
pdvmax12	pdvmax24	pdvmax36	dis-24	pdvmax48	lon0
dvmax(0,-18)	dvmax(0,-18)	dvmax(0,-12)	dvmax(0,-12)	dis-24	dis-12
dis-24	dis-24	dis-24	vmax0	mpi48	dvmax(0,-18)
vs	dmpi (24, 0)	dmpi(36,12)	lon0	dvmax(0,-12)	vor850
	vs	lon0	mpi48	lon0	mpi60
	lon0	vs	pdvmax36	mpi60	mpi72
	dvmax(0,-6)		vs	mpi36	dmpi(72,48)
			vor_lon		pdvmax60
					ddis(24,0)

Top 3: Development potential, distance to land, past intensity change



TC size can be forecast based on its strong correlation with the change of TC intensity.

Fig. 3. Composite evolution of TC size and intensity in different life stages of a TC. Zero point of the abscissa corresponds to the time when a TC reaches its maximum intensity for the first time. Negative values of the abscissa indicate hours before the zero point, and vice versa. The dotted line denotes the ratio of TC size to that at the zero point; the squared line denotes the ratio of TC intensity to that at the zero point.

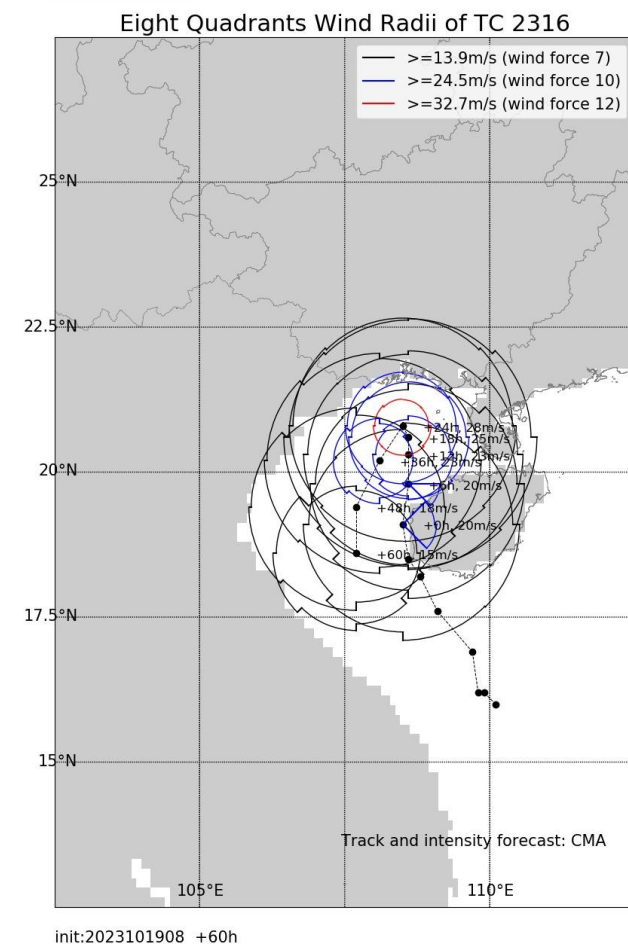
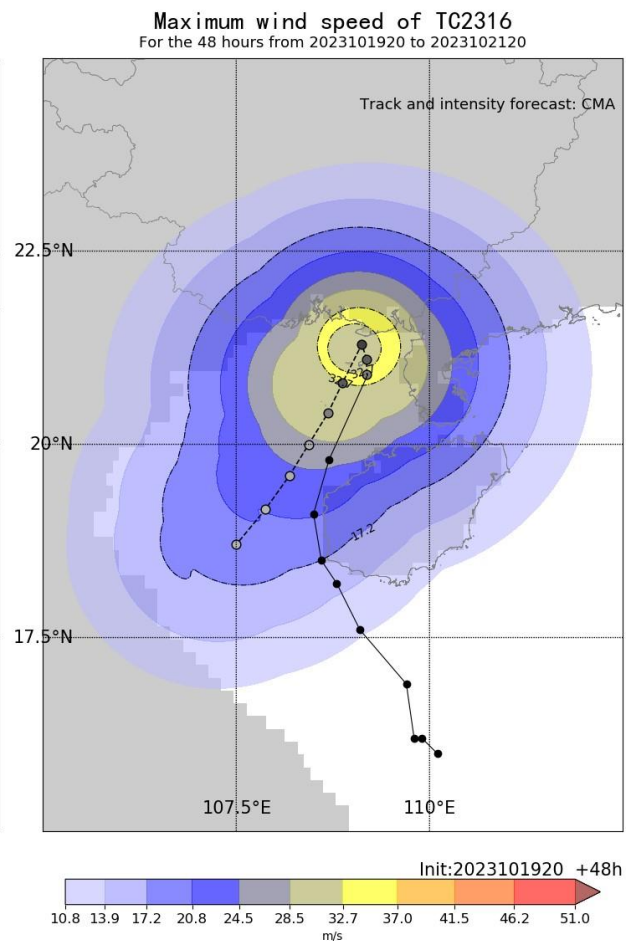
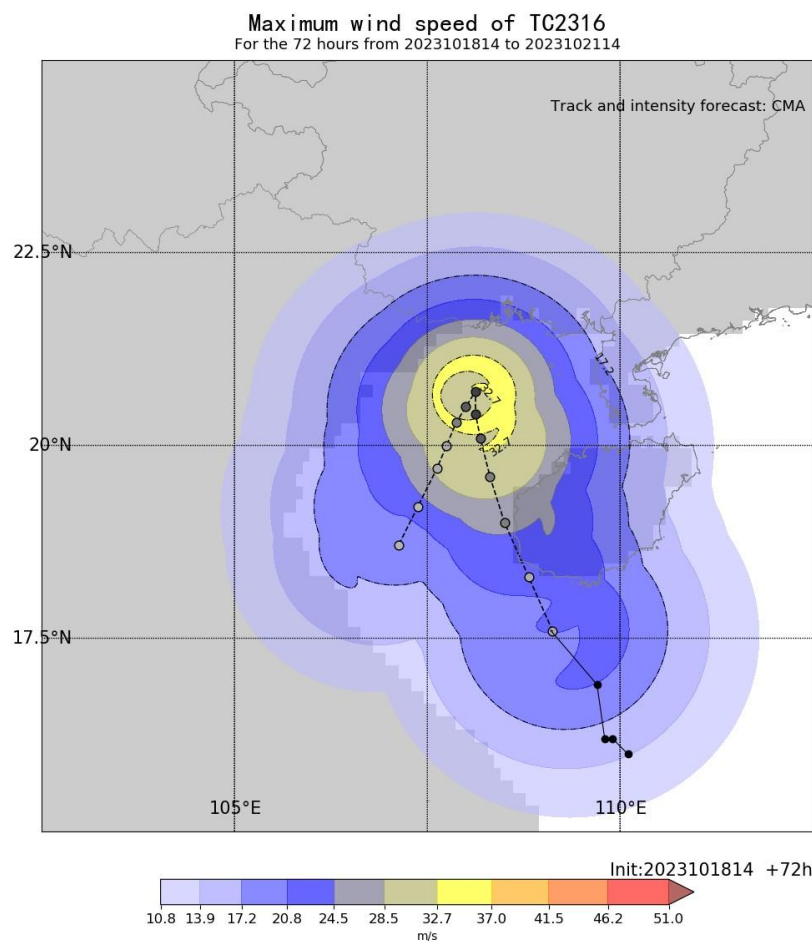
Table 3. Fitting and testing for the changes of specific wind radii and intensity (95% significance)

TC stage	Significant wind	Aging stage (h)	Correlation coefficient	Sample size (times)	Linear fitting coefficient		RMSE (km)
					<i>a</i>	<i>b</i>	
Developing stage	34 kt	6	0.1992	1322	5.844	1.698	26
		12	0.2629	1198	10.2	1.844	34
		18	0.2946	1080	14.94	1.814	39
		24	0.3265	969	19.16	1.899	44
	50 kt	6	0.2543	469	3.61	1.059	14
		12	0.3569	415	5.583	1.293	19
		18	0.4085	361	7.886	1.385	23
		24	0.4397	314	10.14	1.448	26
	64 kt	6	0.3210	283	1.724	0.7523	8
		12	0.4550	239	2.294	0.9024	11
		18	0.5449	202	2.496	0.9936	12
		24	0.5733	168	2.883	1.002	14
Weakening stage	34 kt	6	0.2468	1314	-0.662	1.826	25
		12	0.3319	1188	0.548	2.124	36
		18	0.3927	1069	2.365	2.249	43
		24	0.4229	959	3.429	2.267	49
	50 kt	6	0.2102	579	-1.317	0.852	15
		12	0.3290	524	-0.966	1.197	21
		18	0.4229	471	-0.027	1.396	25
		24	0.4669	422	1.026	1.473	29
	64 kt	6	0.2356	421	-0.5046	0.7536	11
		12	0.3496	378	0.2035	1.001	16
		18	0.4077	335	0.7439	1.037	18
		24	0.4308	298	1.438	1.065	20

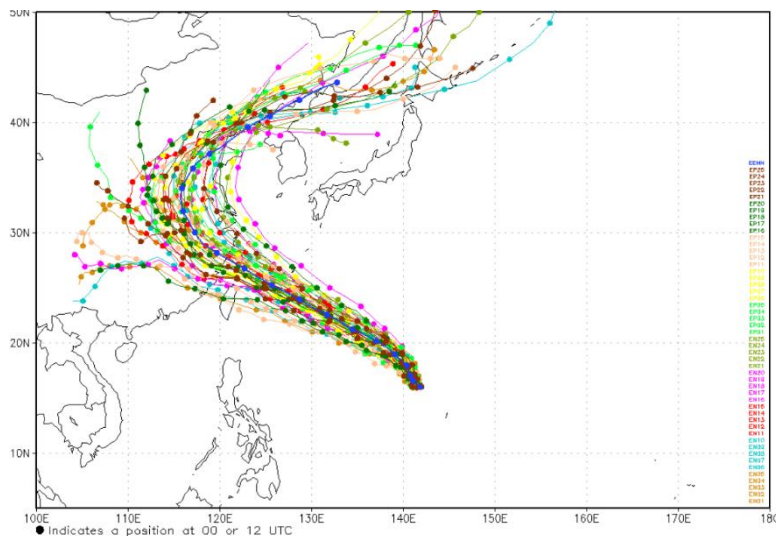
The linear fitting equation is $y = a + bx$ with y being the change of specific wind radii (km) and x the change of intensity (m s^{-1})

Application of empirical wind field model

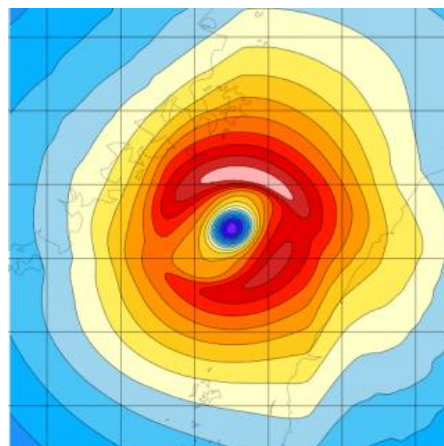
Official track and intensity forecast + STI-ETYM



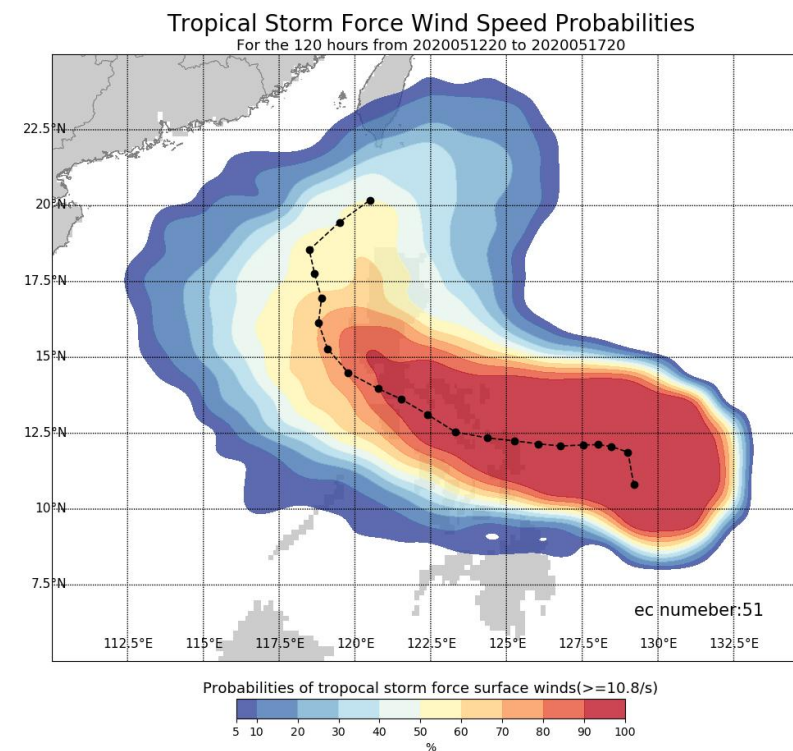
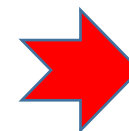
Application of empirical wind field model



Ensemble forecast

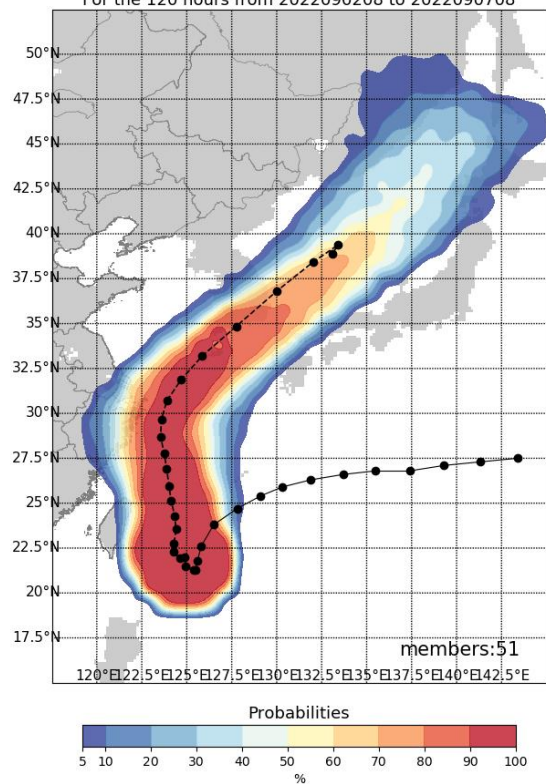


STI-ETYM

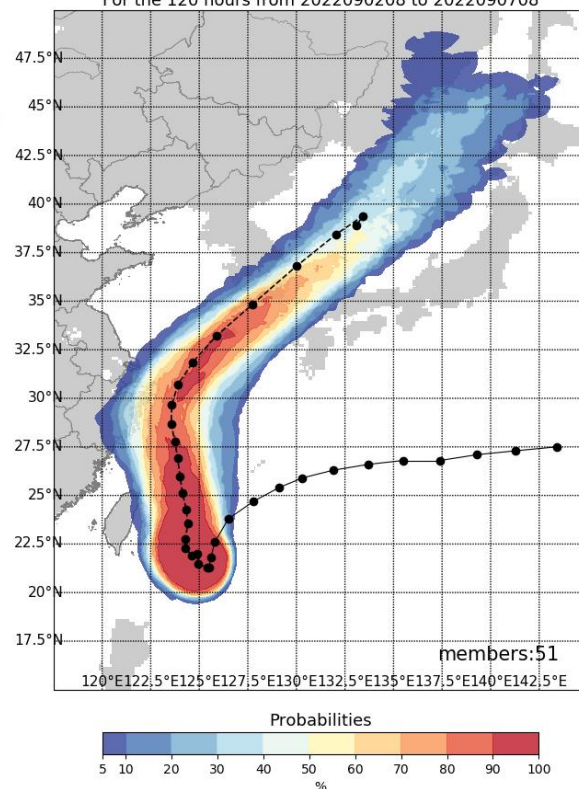


Gale forecasts: probability

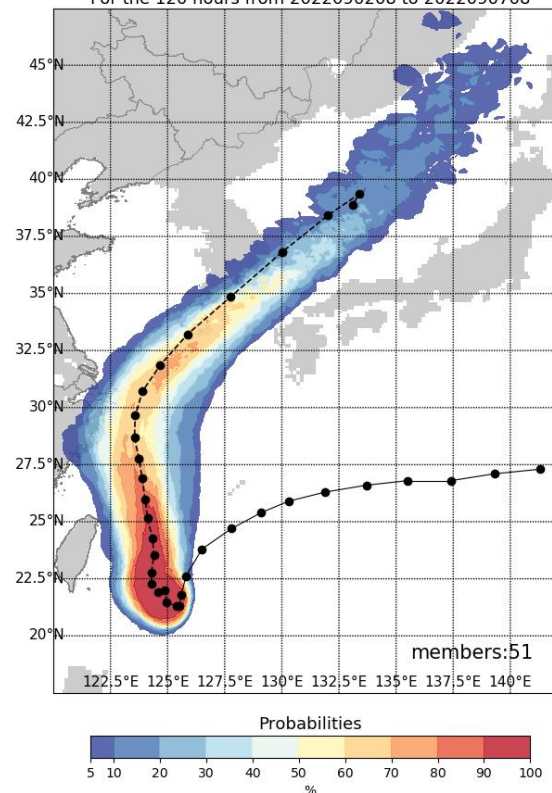
Probabilities of TC gale winds($\geq 17.2\text{m/s}$)
For the 120 hours from 2022090208 to 2022090708



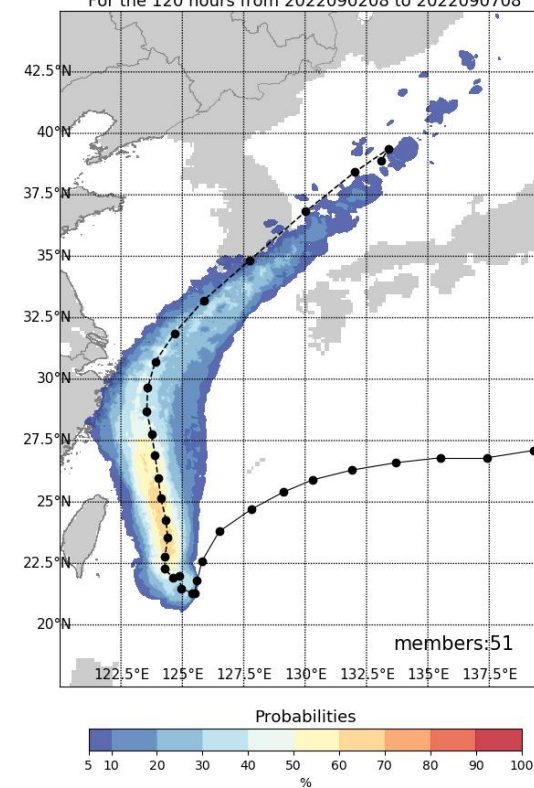
Probabilities of TC gale winds($\geq 24.5\text{m/s}$)
For the 120 hours from 2022090208 to 2022090708



Probabilities of TC gale winds($\geq 32.7\text{m/s}$)
For the 120 hours from 2022090208 to 2022090708



Probabilities of TC gale winds($\geq 41.5\text{m/s}$)
For the 120 hours from 2022090208 to 2022090708



Model output statistics/downscaling technology:

Wind forecasts in regions with complex topography



Model Output Statistics

➤ Model and data

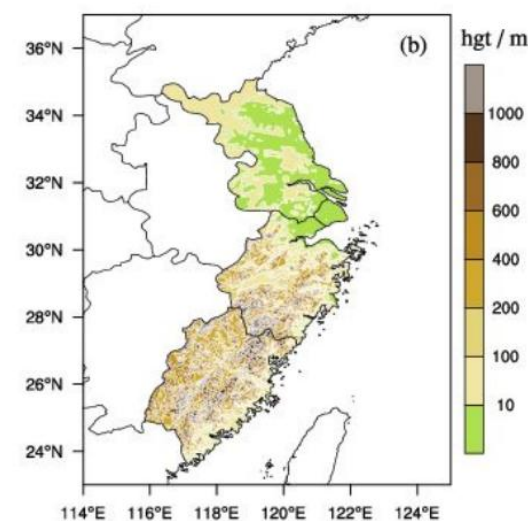
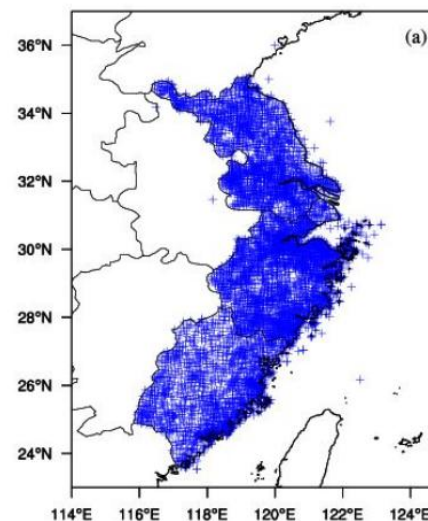
1) SWARMS-Rapid Refresh

Resolution: 3 km

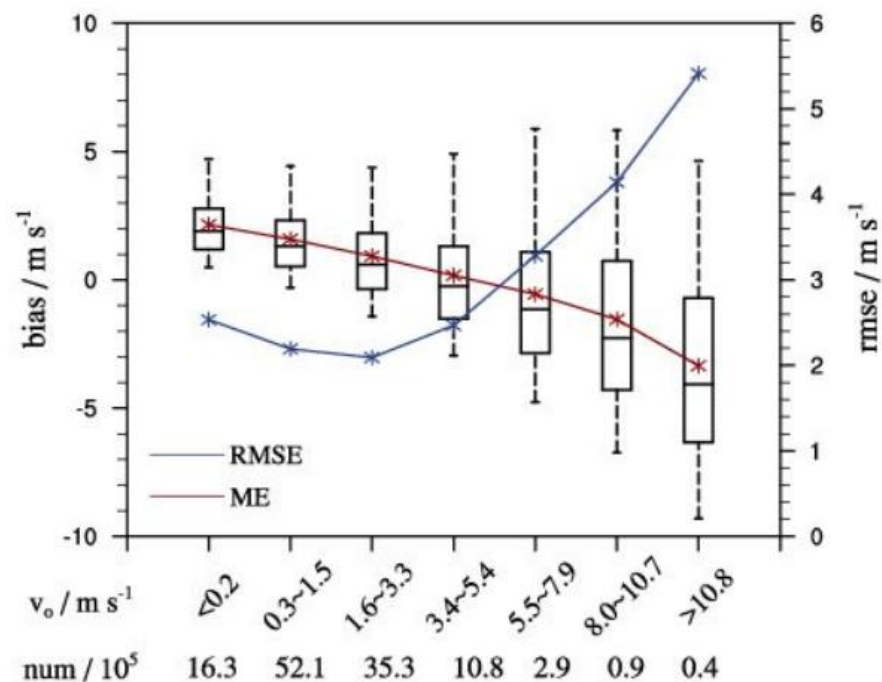
Forecast lead time: 24 hours

Duration: 2018.8 – 2019.8

2) Number of stations: ~5600 AWS

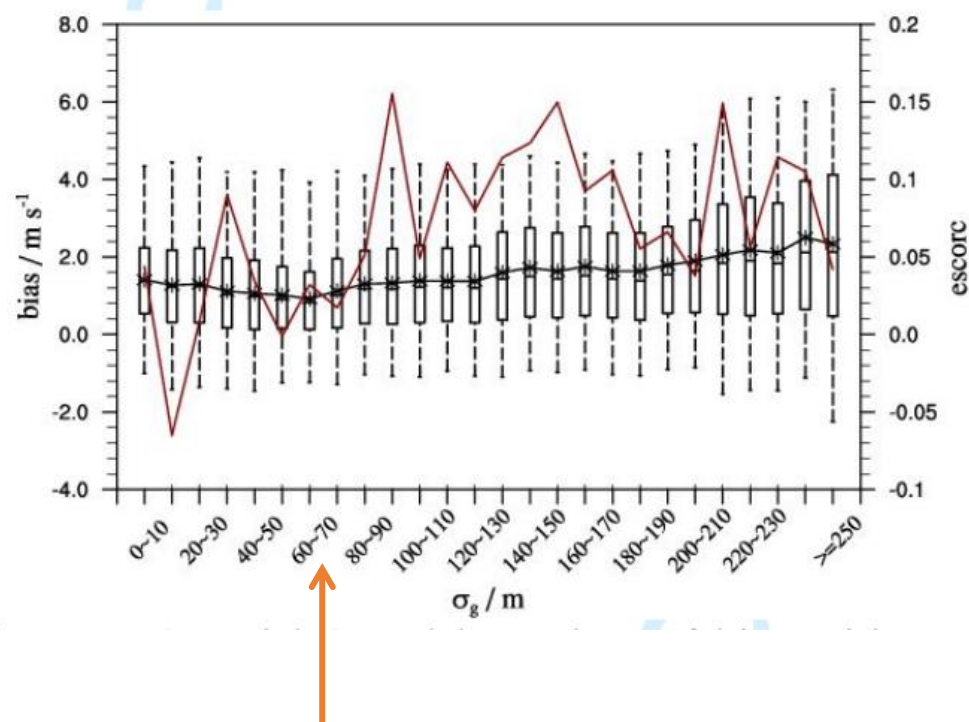


Spatial distribution of observations (blue pluses) (a) and terrain height in east china (b)



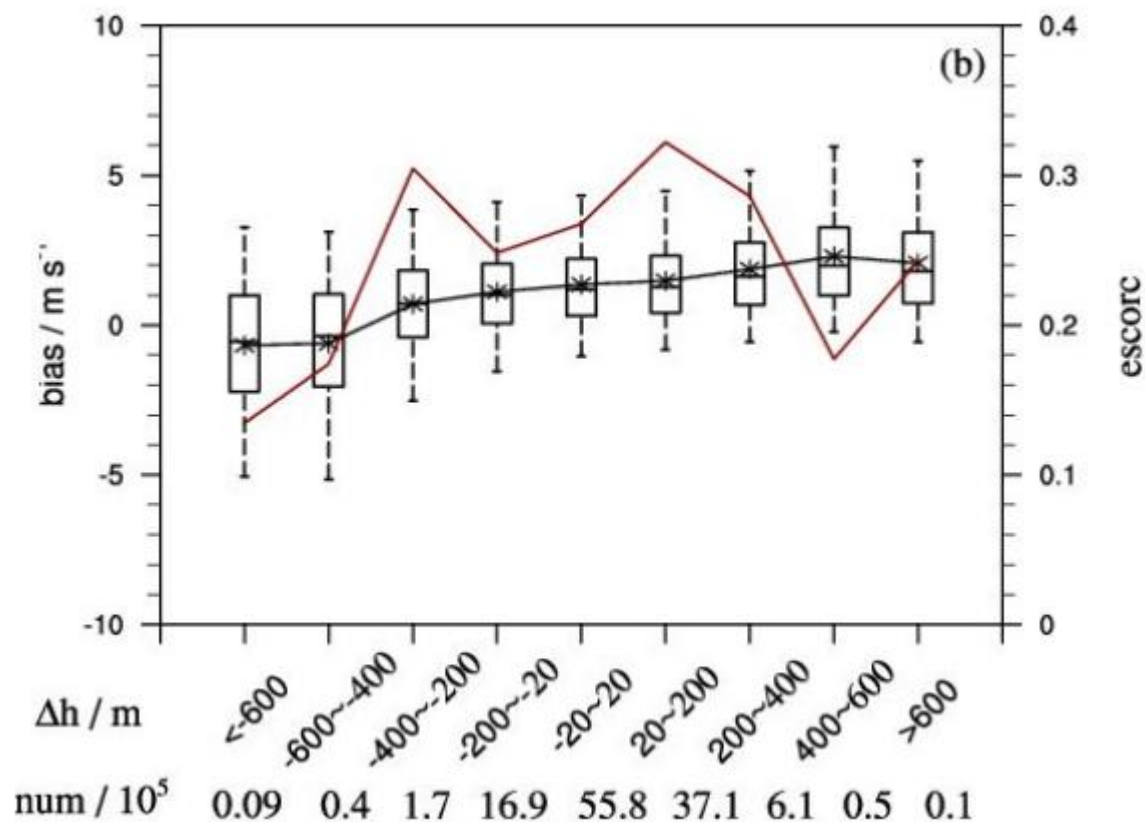
Box plots of bias for different wind velocity. The box area represents the 25th and 75th percentile values, the horizontal line inside the box is the median value, and the whiskers represent the 5th and 95th percentile values. The number of samples within different thresholds is listed below the figure.

The bias has an overall downward trend with the increase in observed wind speed, from overestimation to underestimation.



Variation in MEs (asterisks) and box plots of bias with the standard deviation of the grid-scale terrain height (σ_g). The red line is the correlation coefficients between the bias and σ_g of different thresholds.

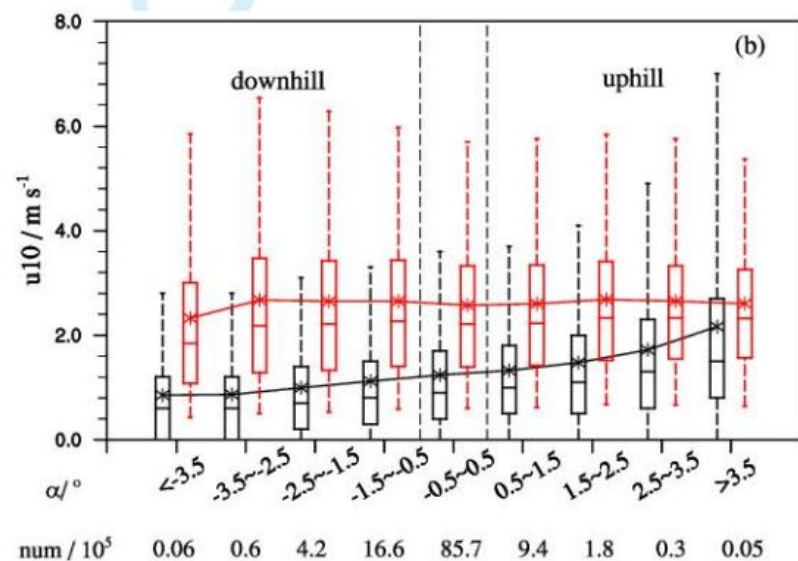
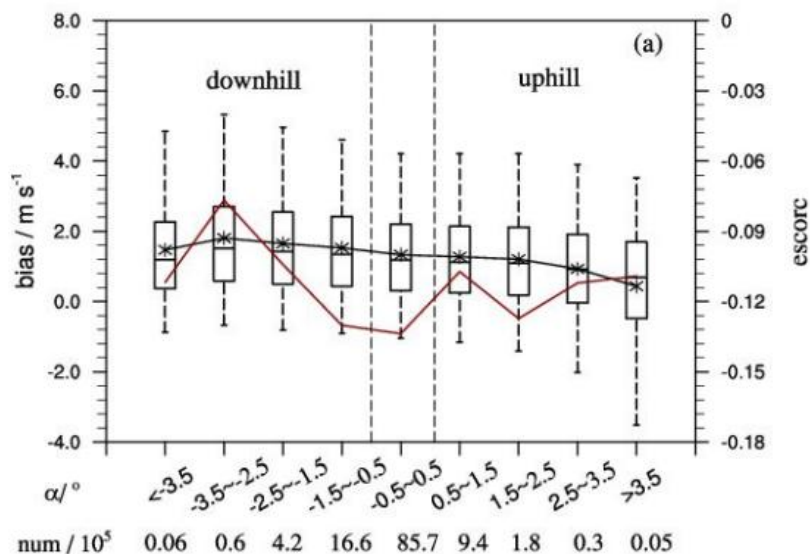
Large errors of forecast wind speed are more likely to appear over complex terrain (insufficient drag force in the model).



Variation in MEs (asterisks) and box plots for bias as grouped by the errors in model terrain height. The red lines are the correlation coefficients for different thresholds.

ME increases by 10% - 20% as the positive terrain height increases every 200 m (from (-20~20 m) to (400~600 m)), and ME increases by 20% ~ 30% as the negative terrain height difference increases every 200 m (from (-600~-400 m) to (-20~20 m)).

There are more stations with overestimated terrain height than those with underestimated terrain height.



The variation in the bias (a) and surface wind speed (b) with slope angles. The red and black boxes in (b) represent the 10-m wind speed from SWARMS-RR and observation data, respectively. The red line in (a) is the correlation coefficients between the bias and slope angles of different thresholds.



Correlation coefficients between potential predictors in MOS calibration model and bias. Linear regression coefficients in three sensitivity experiments are also listed.

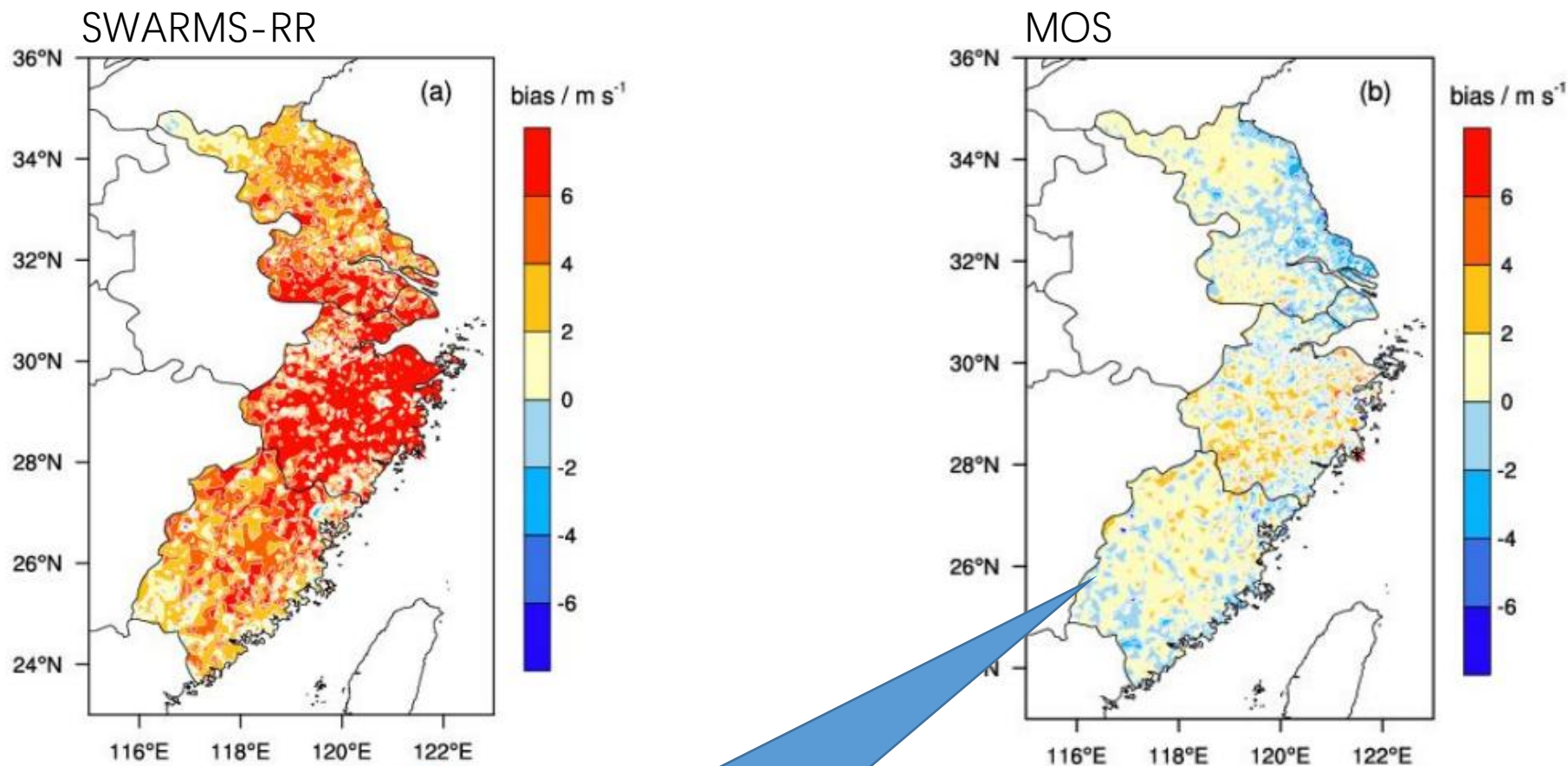
Potential predictors	Correlation coefficients	Regression coefficient (slope)			
		Exp1	Exp2	Exp3	
				$\sigma_g < 70$ m	$\sigma_g \geq 70$ m
10-m wind speed	0.7381	0.5914	0.6220	0.7219	0.5301
850 hPa wind speed	0.4728	0.0119	0.0106	0.0155	0.0104
700 hPa wind speed	0.3163	0.0025	0.0047	0.0061	0.0046
terrain height difference	0.2130		0.0026	0.0011	0.0052
sea level pressure	-0.2015	-0.0001	-0.0002	-0.0001	-0.0002
slope angle	-0.1143		-0.1083	-0.0008	-0.1095
standard deviation of the grid-scale terrain height	0.0907		0.0020	0.0008	0.0104
forecasting time	0.0826	0.0248	0.0274	0.0220	0.0273
10-m relative humidity	0.0627	0.0062	0.0071	0.0052	0.0094
latitude of station	-0.0397	-0.0370	-0.0757	-0.0510	-0.0759
10-m temperature	-0.0282	-0.0372	-0.0291	-0.0321	-0.0104
longitude of station	-0.0258	-0.1806	-0.1594	-0.1627	-0.1587



The verification results from the independent sample test: the data listed within the brackets are the improvements in three sensitivity calibration experiments compared to SWARMS-RR.

	SWARMS-RR	Exp 1	Exp 2	Exp 3
RMSE (m s^{-1})	2.48	1.49 (39.9%)	1.476 (40.5%)	1.393 (43.83%)
ME (m s^{-1})	1.55	-0.126(91.87%)	-0.08 (94.84%)	0.051 (96.71%)
max u10(m s^{-1})	38.9	15.42	19.389	25.34

A typhoon case: Lekima (2019)



Significant improvements
in wind forecasts



Dynamical downscaling

1. Single-model downscaling

Partial list of the mesoscale meteorological models (MMM)

Models	Developers
A2C	YSA Corporation
ANEMOS	Japan Weather Association
COAMPS	Naval Research Laboratory
Eta	NOAA/NCEP
FITNAH	Univ. Hanover, Germany
LOCALS	ITOCHU Techno-Solution Corporation, Japan
MEMO (MIMO)	Aristotle University, Thessaloniki, Greece
MERCURE	CEREA, France
METRAS (MITRAS)	University of Hamburg, Germany
WRF/MM5	NCAR/Penn. State Univ.
NHM	Meteorological Research Institute, Japan
OMEGA	Science Applications International Corp
RAMS	Colorado State Univ.

All MMM are based on the ensemble averaged turbulence model, while large-eddy simulation (LES) requires instantaneous values at the boundaries. (Yamada and Koike, 2011, JWEIA)

2. Multi-models downscaling

(1) Analytical Model

- Linearized Model (Jackson and Hunt, 1975)
- WAsP (Mortensen and Landberg, 1993)

2. Diagnostic Model

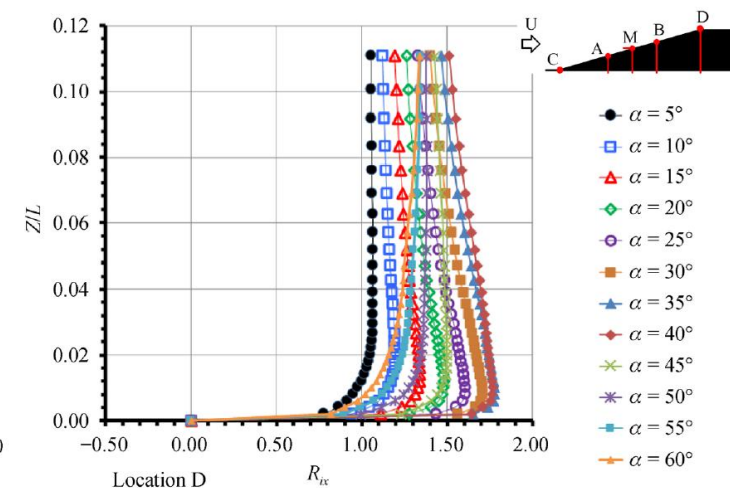
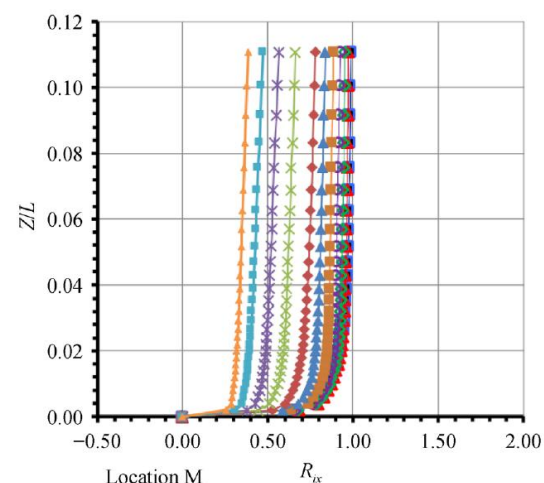
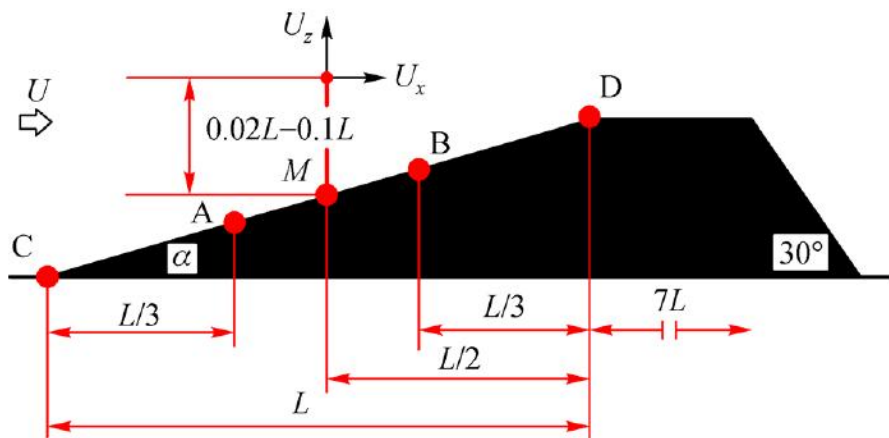
- CALMET (Scire et al, 1993)
- AERMET (US EPA, 2004)

3. Computational Fluid Dynamics (CFD)

- FLUENT
- OpenFOAM

A novel downscaling model: STIDM (the Shanghai Typhoon Institute Downscaling Model)

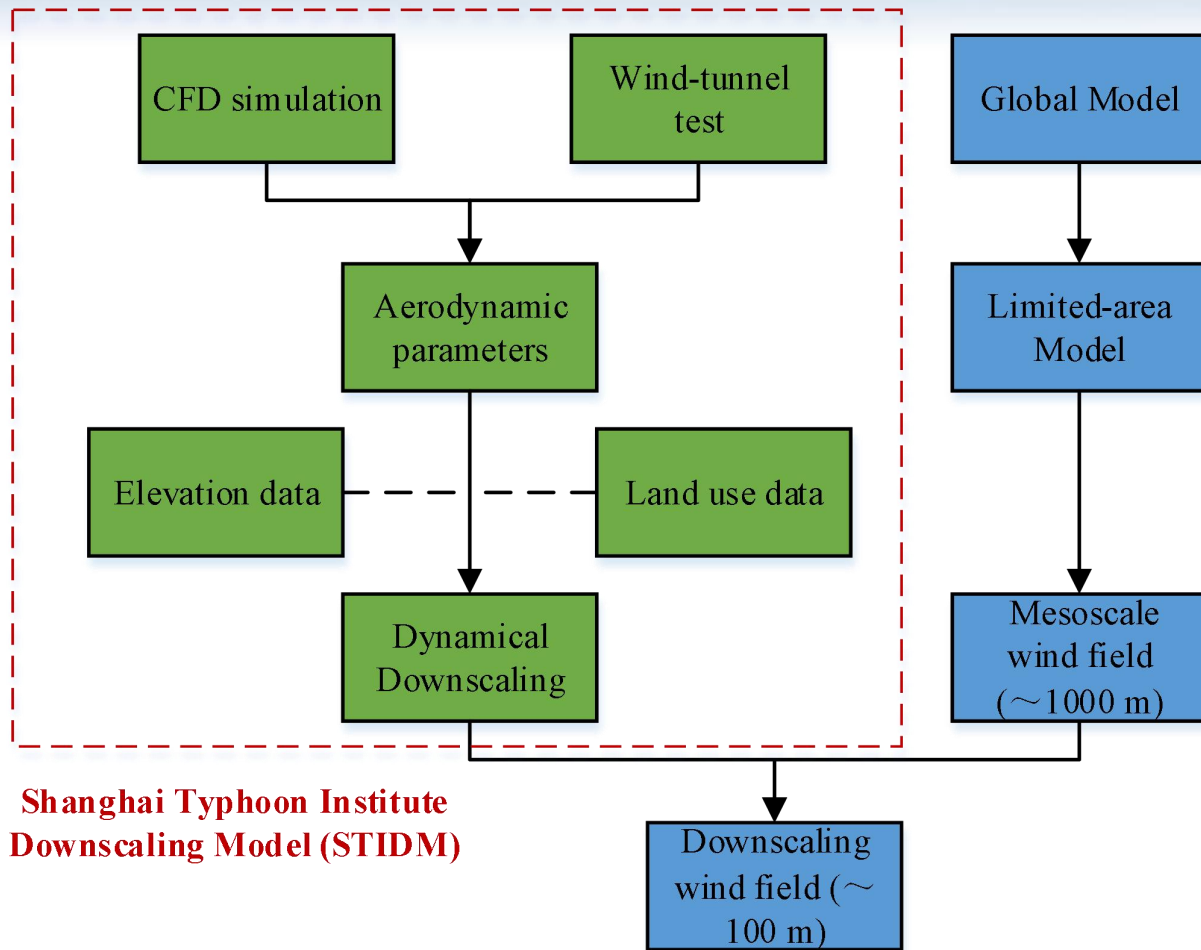
- Distributing wind speed based on aerodynamical parameters of 2D terrain (simulated offline using CFD method)
- Very high computational efficiency for large area such as that covered by a tropical cyclone (~ minutes)



The two-dimensional (2D) terrain was modeled as uphill and downhill segments with various slope angles relative to the incoming flow.

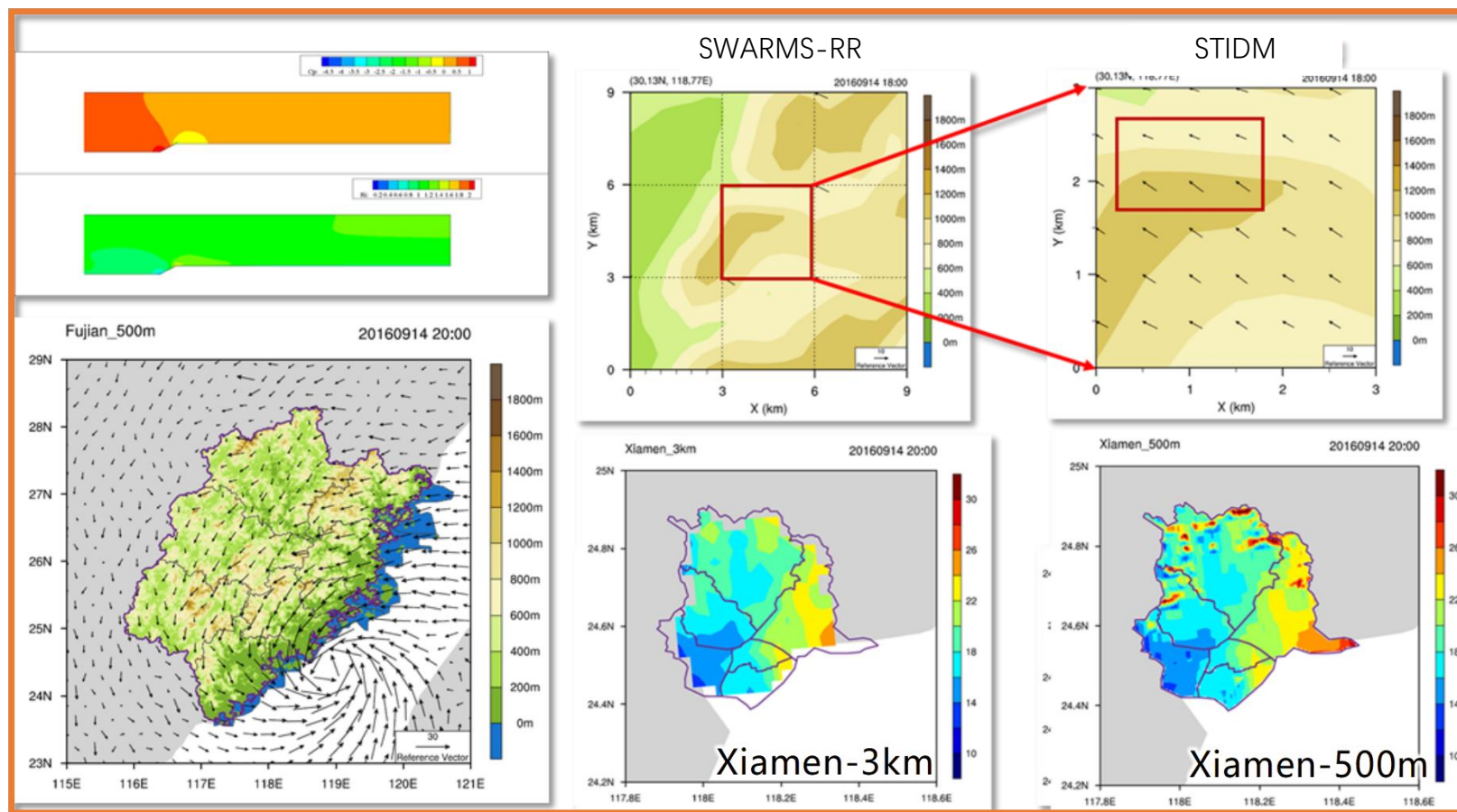
The wind speed-up ratio around the 2D terrain were simulated offline using CFD method.

Fang et al, 2019

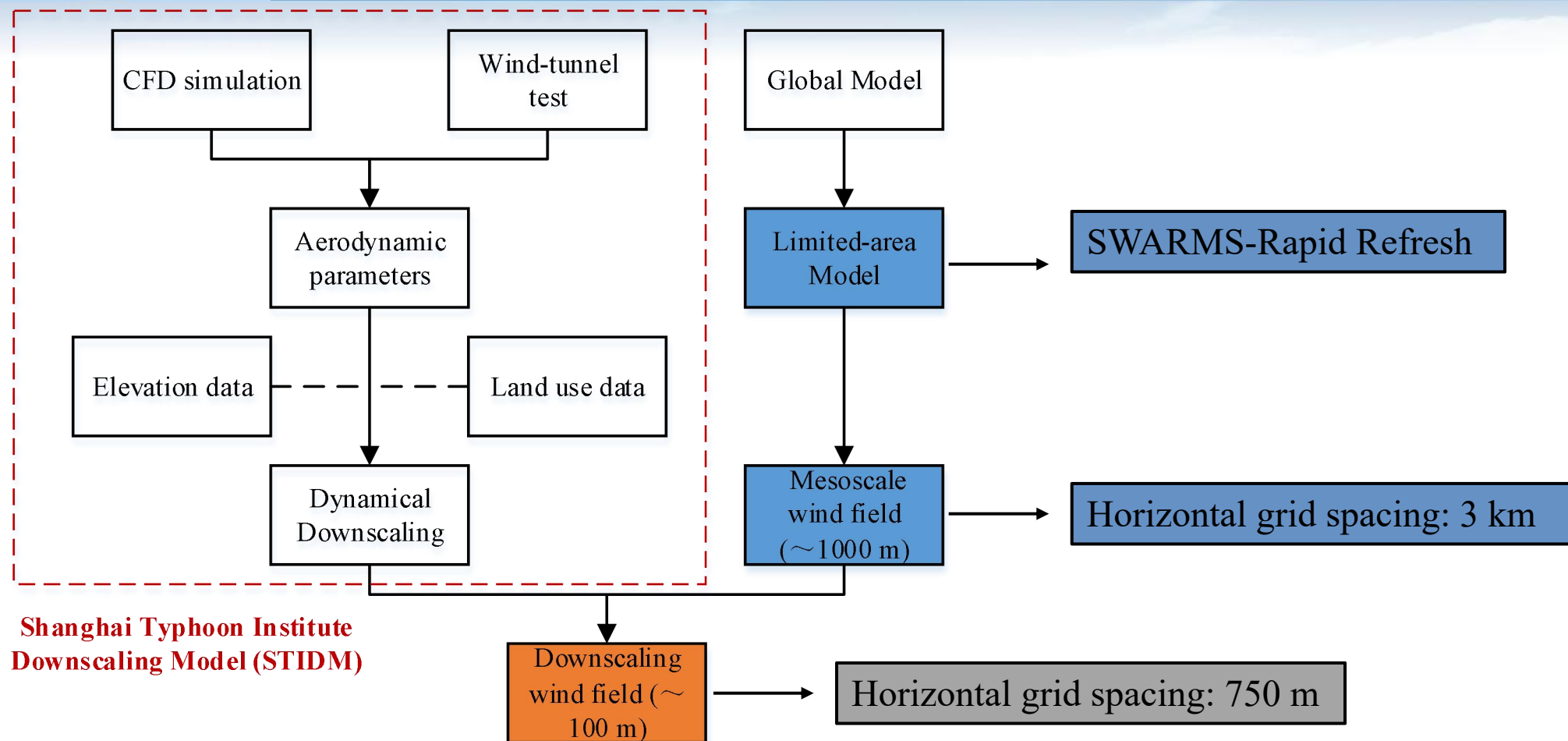


Steps of STIDM:

1. Obtain the aerodynamic parameters of the simplified terrain based on numerical simulation and wind-tunnel test;
2. Redistributing the wind speed at the corner point of a mesoscale grid within the downscaling grid based on terrain elevation data, land use type data and the aerodynamic parameters, to implement the wind field downscaling calculation.



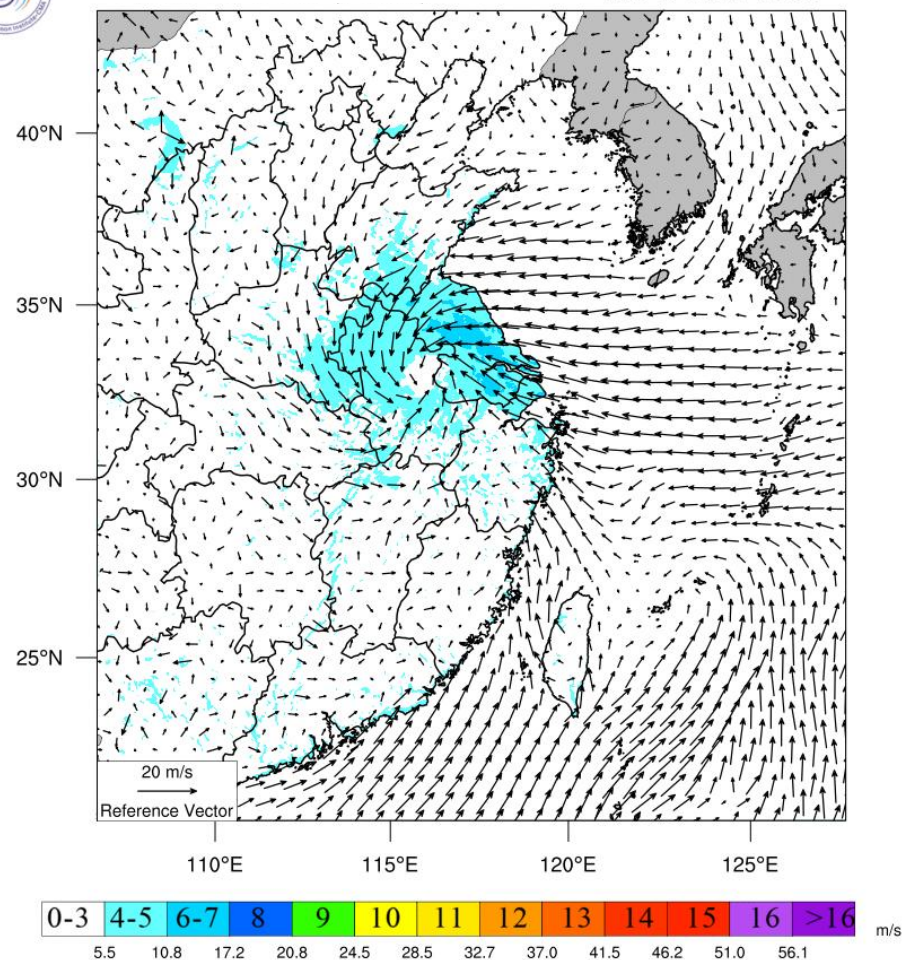
Meranti (2016) wind simulation





SWARMS-RR-STIDM (750m)

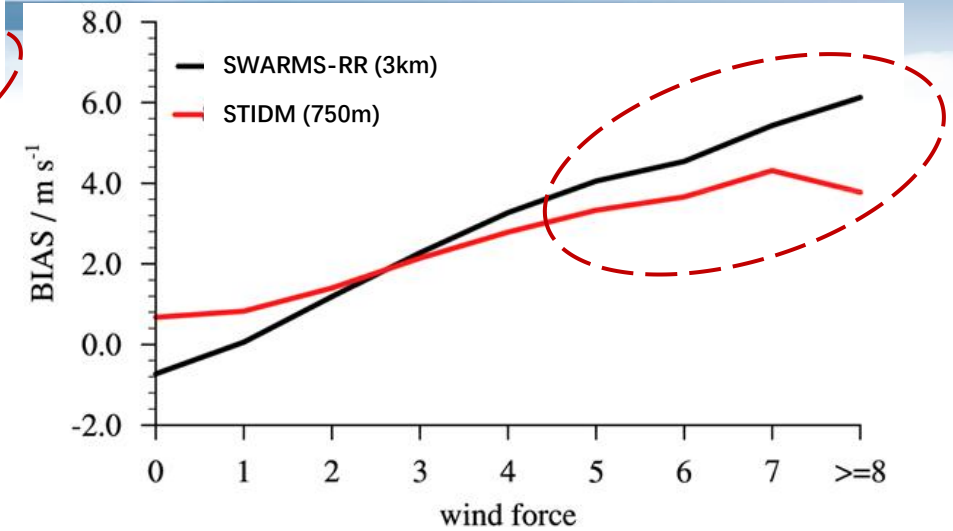
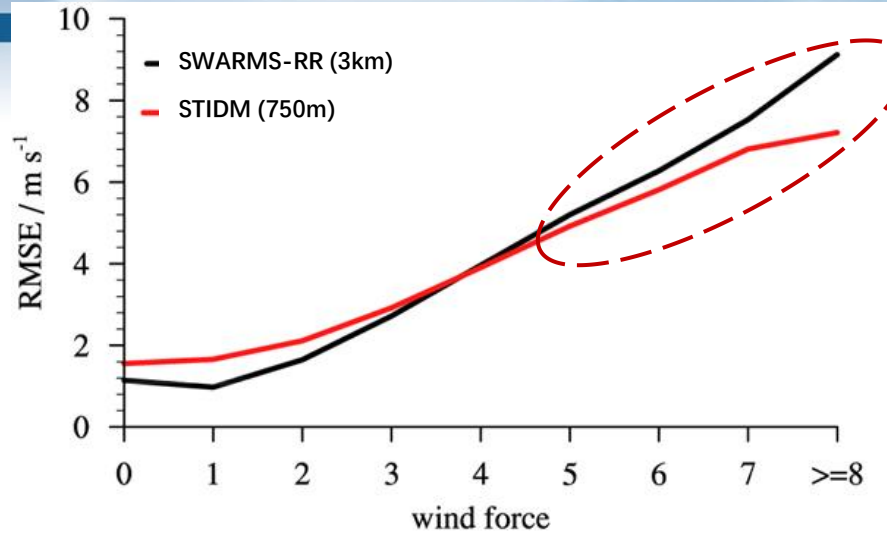
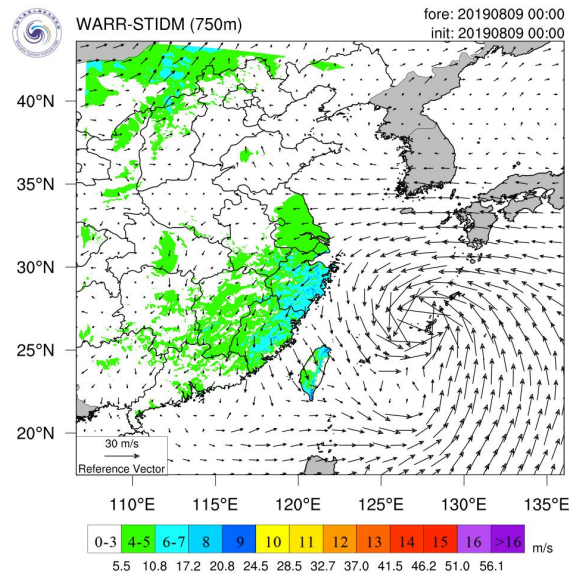
fore: 20210727 19:00
init: 20210727 19:00



Forecast wind field of In-fa (2021)

Products information

1. Horizontal resolution: **750 m**
2. Variables: u and v at 10 m
3. Forecast lead time: 24 h
4. Update frequency: hourly
5. Data interval: 1 h



(a)

SWARMS-RR (3km)

STIDM (750m)

RMSE (m s^{-1})

2.5

2.4

2.3

2.2

2.1

2.0

0-50

50-100

100-150

150-200

200-250

>=250

σ (m)

(b)

SWARMS-RR (3km)

STIDM (750m)

BIAS (m s^{-1})

2.0

1.8

1.6

1.4

1.2

1.0

0-50

50-100

100-150

150-200

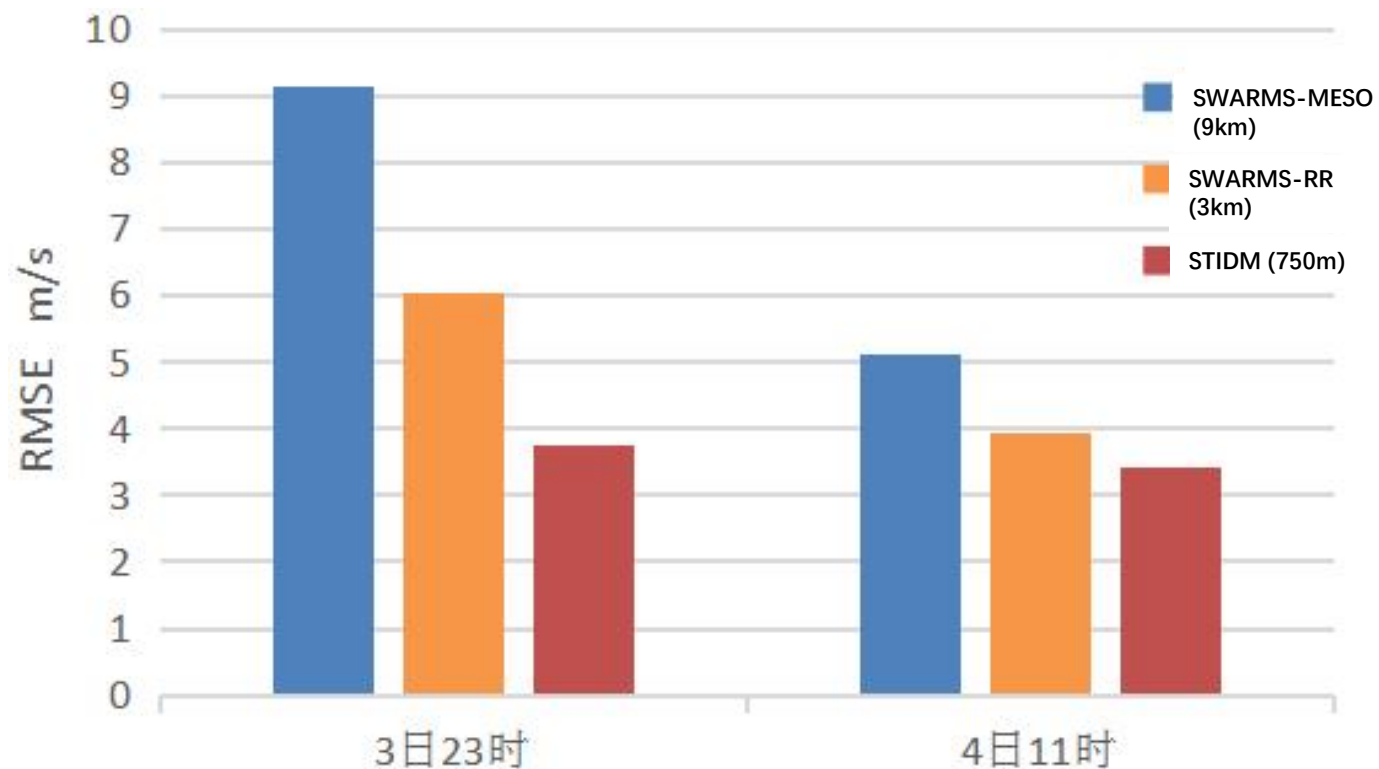
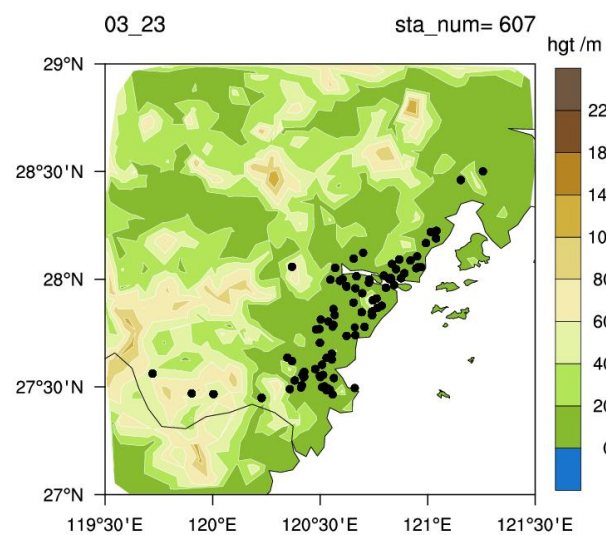
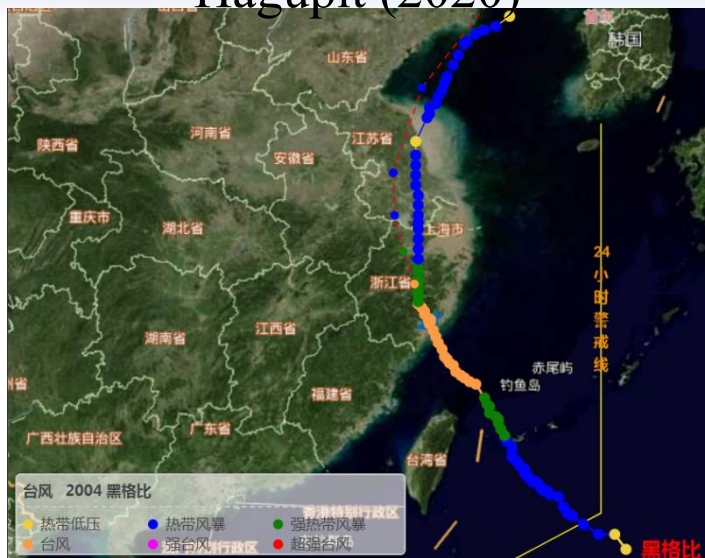
200-250

>=250

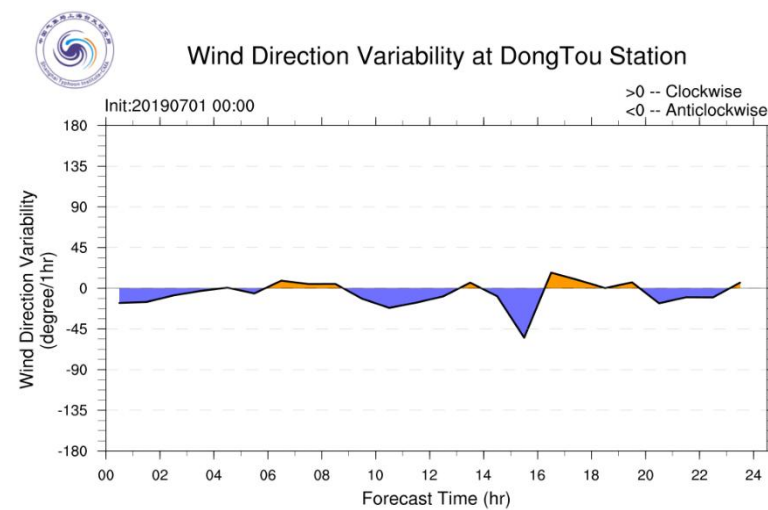
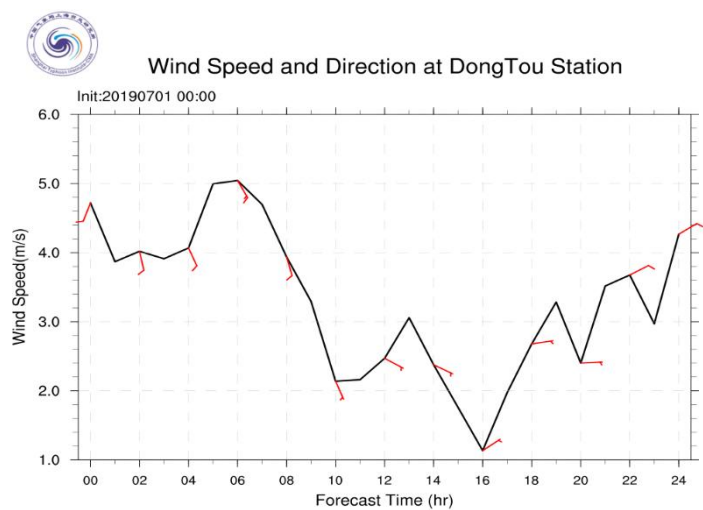
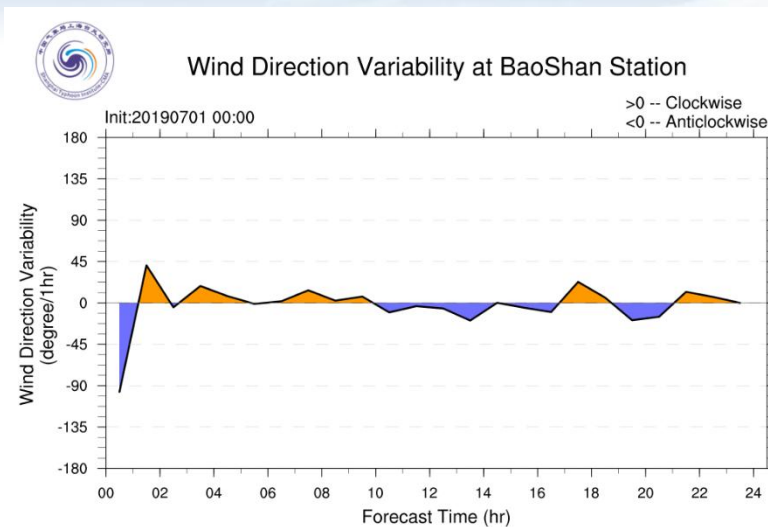
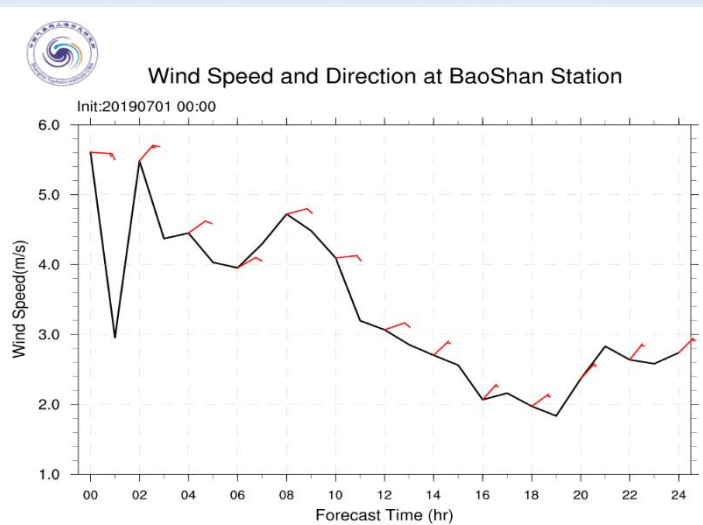
σ (m)

- STIDM shows improvements for strong winds ($> 8.0 \text{ m/s}$) and complex terrain region ($\sigma_h > 200\text{m}$)

Hagupit (2020)



AWS in mountainous region





- Chen, P. Y., H. Yu, B. Brown, G. M. Chen, and R. J. Wan, 2016b: A probabilistic climatology-based analogue intensity forecast scheme for tropical cyclones. *Q. J. R. Meteorol. Soc.*, 142, 2386-2397.
- Fang, P. Z., and co-authors, 2019: Numerical and experimental study of the aerodynamic characteristics around two-dimensional terrain with different slope angles. *Front. Earth Sci.* 2019, 13(4): 705–72.
<https://doi.org/10.1007/s11707-019-0790-8>
- Lu, X. Q., W. K. Wong, K. C. Au-Yeung, C. W. Choy, and H. Yu, 2022: Verification of tropical cyclones (TC) wind structure forecasts from global NWP models and ensemble prediction systems (EPSs). *Trop. Cyclone Res. Rev.*, 11, 88-102.
- Xin, J. J., H. Yu, and P. Y. Chen, 2021: Evaluation of tropical cyclone intensity forecasts from five global ensemble prediction systems during 2015-2019. *J. Trop. Meteorol.*, 27, 218-231.
- Xue, W. B., H. Yu, S. M. Tang, W. Huang, W. D. Jiang, X. X. Zhou, and Y. Lu, 2020: Verification on surface wind speed forecast of Shanghai Meteorological Service-WRF ADAS Rapid Refresh System (SMS-WARR) (in Chinese). *Meteor. Mon.*, 46, 1529-1542.
- Xue, W. B., H. Yu, S. M. Tang, W. Huang, 2023: Relationships between terrain features and forecasting errors of surface wind speeds in a mesoscale numerical weather prediction model. *Adv. Atmos. Sci.*

The background of the slide is a composite image. The top half features a dark blue world map with a grid overlay. A bright, swirling hurricane-like storm is depicted over the Pacific Ocean, with a red dot and a small square frame at its center. The bottom half of the slide shows a satellite view of a large, swirling oceanic eddy or cyclone in shades of blue and white.

**Thank you for your attention !
Questions?**

http://116.62.195.108/AP_demo2/Page/Home/qdyb.lj.html

